A Tool-Mounted Magnetostrictive Sensor for On-line Cure Monitoring of Polymers

By

TOM ROIDA

Diplomarbeit der Universität der Bundeswehr München

Newark, Delaware (U.S.A.)
March 31st, 2003

Supervisor:
Univ.-Prof. Dr.-Ing. Helmut Rapp
Universität der Bundeswehr München
Fakultät für Luft- und Raumfahrt
Institut für Leichtbau
85579 Neubiberg, Deutschland

Project supervisor:
Aurimas Dominauskas, PhD
University of Delaware
Center for Composite Materials
Newark, Delaware 19716, U.S.A.

ABSTRACT

The development of a tool-mounted sensor for on-line, in-situ cure monitoring of polymers is presented. *Magnetostrictive Cure Monitoring* (MCM) sensors directly measure true mechanical properties of a polymer. The magnetostrictive effect is used to excite oscillations in a small rod (40mm length), which is in contact with the polymer. During the curing process of the polymer the boundary conditions for the rod change, what has an influence on the frequency response of the sensor. A complete measurement chain is described, from properties of a polymer, the sensor, electronic signal conditioning and interface circuits, computer based data acquisition, to evaluating software.

Chapter 3 contains an overview about common and novel cure monitoring technologies. The sensors are classified and MCM sensors are integrated into this classification and especially compared to ultrasonic sensors, which are also sensitive to mechanical properties and have comparable advantages and disadvantages.

Chapter 4 contains the theoretical models, on which the design of a sensor prototype was based. The models describe the sensor behavior in a mechanical and electromagnetical way and relate mechanical properties of a polymer to the sensor output. The key element in the relation of the separate models is a *mechanical contact impedance* of the polymer. Further, some qualitative case studies are performed, which shall help to understand the sensor's behavior, and which can be seen as a plausibility check.

In chapter 5 the sensor design is presented and in chapter 6 the process of manufacturing is described. A key request for the design is that the sensor can be installed into a tool, e.g. a small experimental mold, for repetitive use. It is targeted for use in industrial manufacturing processes, but this possibility could not yet be verified. Technical drawings illustrate the sensor design.

In chapter 7 the measurement chain is explained and some sensor characteristics are given. A complete electronic signal-conditioning and interface unit is presented, which is connected to a MCM sensor and to data acquisition hardware. The unit contains amplifier circuits, a power supply, a trigger circuit, and an RMS-to-DC converter. Hence no high-speed data acquisition is necessary.

Chapter 8 deals with validation of the sensor and its model. Measurement data is compared to theoretical sensor output and measurements found in literature.

The resonant frequency and amplitude of the sensor change significantly during the whole curing process, for different kinds of polymers, and the different stages of curing can be identified. The experiments show that the sensor is highly sensitive, but repeatability and reliability need to be improved.

Chapter 9 contains a conclusion about the tool-mounted MCM sensor and some problems with the current configuration. Finally, an outlook about further research and possible improvements is given.

TABLE OF CONTENTS

1 PREFACE

First of all I would like to thank the Center for Composite Materials at the University of Delaware for inviting me. I also have to thank my advisor at the Center for Composite Materials, Dr. Aurimas Dominauskas, for realizing this project. His experience with the subject together with his efforts to carry on the development made it possible to design a cure monitoring system in six months.

Grateful I am for the support of Professor Rapp from the Institut für Leichtbau at the Universität der Bundeswehr München, who oversaw the thesis from Germany. Professor Rapp did this in spite of many administrative difficulties, caused by a student writing his master thesis in a foreign country.

I also want to thank Philip Roach and Simon Shen for their help and support. And I want to thank my wife Diana for her great, continuous support and her patience during the project.

Another important factor that contributed to the success of the project was the administrative support I had at the Center for Composite Materials. The possibilities to order materials within one day, to have parts manufactured by external companies, or to have computers with all necessary soft- and hardware were new for me. I could not yet experience this professional support at my university in Munich in Germany. Therefore, I want to thank Dr. Dirk Heider, Assistant Director of the CCM, for his financial support.

It was fascinating for me that I was in touch with so many different fields of my studies during this project. There was physics, according the sensor principle, and electrical engineering and electronics during the development of the interface circuits. On the other hand I had to deal with dynamical mechanical problems during the development of a theoretical model of the sensor. Finally, to get a basic understanding of the curing process, I had to deal with the chemical reactions of polymers and even some problems from the field of fluid dynamics. Besides these theoretical aspects I made some technical drawings of the sensor, designed a printed-circuit-board for the signal-conditioning and interface, and wrote preliminary LabVIEW software to acquire and evaluate data with a PC.

One of the consequences of this variety of activities was of course that I did not descent into many details. Nearly all problems mentioned in this work were handled with the knowledge I gained during my basic studies. On one hand this leaves much space for further research, maybe with the

consequences of some changes in the sensor design. But on the other hand this thesis covers probably all major aspects of the development of the Tool Mounted Magnetostrictive Cure Monitoring Sensor.

2 INTRODUCTION

The polymer industry is an area of great energy and drive. Over the last decades composite materials became increasingly accepted due to novel, inexpensive and high-quality manufacturing technologies, and composite materials highly depend on the mechanical properties if the polymer matrix. New products with new combinations of materials come to the market. Engineering parts ranging from tires and sophisticated extrusion profiles to injection and transfer moldings are undergoing continuous development. Engineering plastics and composites continue to make rapid headway against metals, not only in the aircraft industry but also in many low-cost applications.

The engineer requires a detailed understanding of the curing behavior of these materials in order to design the dies, molds, and processes required to form tomorrow's structural components. The rheological behavior of polymer systems is very complex and is still not fully understood. Tool-mounted sensors are needed for process control and Quality Assurance / Quality Control, and they should be able to monitor curing on-line.

MCM sensors could become a low-maintenance and fail-safe solution for that. Because of the high sensitivity, MCM sensors also have the potential to work in small experimental stations to determine cure behavior and kinetics, and therefore important characteristics of polymers.

The process of curing is very important during the manufacturing of composite materials or plastics in general. On one hand, during this process many properties of the final material will be influenced, like mechanical strength, bonding between matrix and fibers, etc. On the other hand, the development of certain parameters during the curing process is very characteristic for different stages of the chemical reactions; hence monitoring these parameters helps to understand the curing reactions. These are reasons why it is necessary to have the capability of cure monitoring, from the application of experimental analysis up to large-scale industrial manufacturing of mass products.

3 OVERVIEW OF SENSOR SYSTEMS FOR ON-LINE CURE MONITORING

There are several different measuring techniques for monitoring the curing process of polymers with the following possibilities for categorization:

- A general breakdown can be made by differentiating between off- and on-line methods, which can be performed during manufacturing. A tool-mounted magnetostrictive sensor can be used non-destructively and on-line, but a Differential Scanning Calorimetry (DSC) for example cannot be performed at a manufactured part.
- It is possible to classify the techniques as local (only effected by a small amount of resin, a "point" measurement) or as spatial. A typical spatial sensor would be an ultrasonic sensor with separate transmitter and receiver, and a sound velocity analysis. The measured sound velocity will be an average value for the entire polymer distributed between the transmitter and the receiver. On the other hand a MCM sensor performs a typical point measurement. This kind of sensor is only affected by a very small part of the surrounding resin with a radius of a few millimeters.
- Further the techniques can be grouped into the sensing principles of the sensors. In case of cure monitoring this, e.g., makes sense for optical sensors – a variety of sensors exist which are either sensitive to strain, to molecular resonance (spectroscopy), or to fluorescence of polymers. However, all these sensors make use of the capability of optical fibers to conduct light through or into a polymer without causing a significant impact on a composite part.
- Another breakdown can be made by looking at the measured properties:
  - Measuring chemical reactions:
    A typical chemical measurement technique is the DSC.
  - Measuring optical properties:
    Optical fibers are used to guide light waves into a polymer and back.
  - Measuring electrical properties:
    Sensors measuring the electrical properties of a resin are reliable and easy to build. These parameters could be electric resistance

or dielectric properties. However, the relation between these properties and the degree of curing is complicated. By-products of the chemical reaction can have a great influence on the measurement. A deep knowledge of the chemistry of the resin is necessary to interpret the data. Without this knowledge the method is very fault-prone.

- Measuring mechanical parameters:
  MCM sensors and ultrasonic sensors measure mechanical properties of the resin[1], as well as optical or magnetostrictive strain sensors.

The following chapters give an overview of common cure monitoring techniques and their advantages and disadvantages.

3.1 Measuring Chemical Reactions

Contrary to sensors that are sensitive to electrical or mechanical properties of a polymer, the following sensors are sensitive to the chemistry or to the chemical reaction itself.

The first group of sensors in these chapters belongs to thermal analysis (TA). Thermal analysis is based on the detection of changes in the heat content or enthalpy of samples. An important consequence is that at the end of the curing process, when the reaction itself slows down, the output of these sensors decreases.

The second group of chemical sensors is based on spectroscopy. Five different spectroscopy techniques were found to be used for cure monitoring – electric, nuclear magnetic and three optic (in three different spectra). It is possible to gain information about the movements of parts of the molecular chains. Because molecular group mobility is dependent on the molecular structure, there is a huge change during the curing process.

Temperature measurement

A simple temperature probe can gain valuable information on the curing process[2]. Curing is usually an exothermic reaction, and therefore related with heat release. If no active control mechanism maintains isothermal conditions,

---

1 Actually the measured parameters are electrical parameters like amplitude, frequency and phase angle of a sine wave. But as shown later, there is a strong and insusceptible relationship between these and the mechanical parameters.

2 See Twardowski: Curing in Composite Laminates.

the part temperature differs from the environment temperature. In most cases measuring just the temperature will not be enough to determine the whole curing process, but because temperature has an influence on many of the other cure measurement techniques, it can be necessary additional information.

One approach to monitor the degree of cure in an inexpensive way is to embed thermocouples into the part. They are able to determine heat flux, and it is possible to form a recurrent neural network (RNN) with these sensors. The RNN is able to "learn" a curing profile and afterwards calculate the degree of cure[3].

DSC (Differential Scanning Calorimetry)

For a Differential Scanning Calorimetry measurement a sample and a reference object are heated up (or cooled down) by a predefined program. An active controller maintains a zero temperature difference between the two objects, and the difference in the amount of energy needed is monitored. DSC can be used to determine chemical reactions (like in the case of curing), but is not limited to that. For example phase changing or atomic restructuring can also be detected.

A Sample needs to meet special conditions for a DSC Measurement (for example in seize and weight). Therefore it is in general not possible to perform it at a final part itself.

DSC is a very common technique to determine the curing behavior[4], but it is not used for on-line cure monitoring. The experiments are expensive, and for data interpretation a deep knowledge about the chemistry of polymers is necessary. However, DSC is a very common technique for characterization of polymers because of the quality of the measurements and the importance of information about energy transfer.

Although DSC gives valuable information it is sometimes necessary to combine it with other measurement techniques to fully understand the chemical reactions[5].

---

3 See Su: Monitoring the process of curing with a recurrent neural network.
4 See Panagiotis: Cure Modeling and Monitoring of Epoxy/Amine Resin Systems.
5 See Alig: Curing kinetics studied by DSC, TMDSC and dielectric rel. spectroscopy.

3.2 Measuring Optical Properties

Ultraviolet (UV) cure monitoring

Some curing agents in epoxy act as fluorophores, which means they are able to transfer invisible ultraviolet light into visible light. The curing agents change during the curing process (primary amine groups convert into tertiary ones), and herewith the amount and wavelength of the fluorescence.

Actually, intrinsic fluorescence is not a common phenomenon for polymers. Hence fluorescent probes have been developed to monitor the curing process also in acrylics, polyurethanes and epoxy resins with hardeners, which do not contain aromatic amines[6,7].

Optical spectroscopy

Optical spectroscopy can be used to identify specific components of resins. In all cases of spectroscopy a deep knowledge and a mostly complicated model is necessary to calculate the degree of cure. The following optical spectroscopy techniques have been proved to work with optical fibers and allow the determination of the degree of cure:

- Infrared Spectroscopy[7,8,9]:
  Infrared Spectroscopy and Fourier Transformed Infrared Spectroscopy (FTIR) are two of the most common cure monitoring techniques and already in wide industrial use. It is relatively easy to detect free epoxy groups, which show a significant peak.
- Raman Spectroscopy[10]:
  Raman spectroscopy makes use of light in the visible spectrum. Optical fibers transport visible light much better than infra red light; therefore the measurement system can be placed several meters away of the curing resin without technical problems.
- Near Infrared Spectroscopy[11]:
  The near-IR spectroscopy covers wavelengths between 2.5 μm and 25

---

6 See Peinado: Solvatochromic and rigidochromic fluorescent probes […] for UV-curing monitoring.
7 See Dunkers: Fiber optic flow and cure sensing […].
8 See Bartolomeo: Curing of cyanate ester resin: a novel approach based on FTIR […].
9 See Carotenuto: FT-IR Device for on-line Monitoring of Cure Reactions under Pressure.
10 See Rose: In-Situ Monitoring of Epoxy Resin using FORS.
11 See Mijovic: A study of reaction kinetics by Near-IR Spectroscopy.

μm. Compared to mid-IR spectroscopy it is still possible to use inexpensive fibers to transport light, and newest models and algorithms try to overcome problems caused by the in general less significant output compared to mid-IR spectroscopy and allow similar conclusions.

Optical refractive index monitoring

An optical fiber ends in a polymer that refracts light dependant on the degree of cure. The spectrum of the light is analyzed and a model relates this to the degree of cure, viscosity, density and components of the resin[12..15]. A weak point of this sensor family results from irregularities of the surface at the end of the optical fibers. These have an influence on the repeatability of the sensor output.

3.3 Measuring Electrical Properties

Sensors that measure electric properties are usually robust and inexpensive. This makes them a preferred choice for the industry. However, the quality of the obtained data is usually low compared to other techniques, or the systems are more fault-prone.

Direct current / ionic conductivity

One of the technically simplest possibilities for cure monitoring is a measurement of the ohmic resistance of the polymer at a direct current. Several approaches exist, either with embedded or with tool mounted sensors. Embedded sensors consist of a grid which comprises two orthogonal sets of conductive filaments, separated by one or more perform layers[16..19]. The sensors are able to detect the flow front as well as curing properties, and they can be used for health monitoring. A disadvantage of DC sensors is their

---

12 See Li Chensha: Two sorts of fiber optic sensor monitoring the cure process of composite laminate.

13 See Cusano: An optoelectronic sensor for cure monitoring in thermoset-based composites.

14 See Cusano: A Fiber optic Thermoset Cure Monitoring Sensor.

15 See Chailleux: A fibre-optic sensor for monitoring the polymer cure process.

16 See Bradley: On-line process monitoring […] utilizing SMARTweave in-situ sensing technology.

17 See Don: Large scale implementation of flow and cure sensing […]

18 See Lee: Resin transfer molding process monitoring and control.

19 See Pucic: D.C.-electrical conductivity as a method for monitoring radiation curing […].

limited ability to follow the whole curing process – the signal gets weak after the gelation. This problem can partially be overcome by doping the polymer. Another disadvantage is the sensitivity to conductive byproducts of the chemical reaction, to additives, or to conductive fibers. Tool mounted sensors can also be distorted by applying release agents to the mold – they need to be in direct electric contact with the pure polymer. In general they are very robust and insensitive to high temperatures and pressures.

Permittivity and electric spectroscopy

Additional information is available by measuring the frequency response. By measuring the electrical impedance under different frequencies or by applying FFT to transient responses the dielectric properties of the polymer can be determined. Advantages and disadvantages of this principle are similar like for DC sensors, but more information can be obtained. A complicated model is necessary to interpret the data, and small variations in the chemical content of the resin can cause big errors in the data evaluation.

Many technically different systems have been developed, e.g. with wires or with capacitor-like plates. Most of them are able to determine the relative electric permittivity ε' and the dielectric losses ε'' (real and complex part of the complex permittivity ε) over a wide frequency range. By looking at certain peaks in the frequency response, molecular groups and their mobility can be identified[20..29].

TDR (Time Domain Reflectometry)

Electric Time Domain Reflectometry (TDR) is a method of sending a high-rise (35ps) voltage step-pulse into a transmission line, and detecting reflections returning from impedance discontinuities within the transmission line. Because the sampling rate is so fast (1 THz), it is feasible to analyze electromagnetic transition events. The key attribute of the TDR method is that

---

20 See Bartolomeo: On the use of WLF equation to study resin curing by dielectric spectroscopy
21 See Maistros: Monitoring autoclave cure […]
22 See Maistros: Dielectric monitoring of cure […]
23 See Bang: Measurement of the degree of cure […] using dielectrometry.
24 See Kranbuehl: In situ Cure Monitoring […].
25 See Kranbuehl: On-line in-situ control of the resin transfer molding process.
26 See McIlhagger: The development of a dielectric system […].
27 See Kim: Dielectric cure monitoring […].
28 See Kim: Analysis of dielectric sensors for the cure monitoring […].
29 See Skordos: A dielectric sensor for measuring flow […].

it provides distributed sensing and frequency domain characterization of the surrounding dielectric medium[30,31,32]. Figure 1 shows the working principle of the sensor.

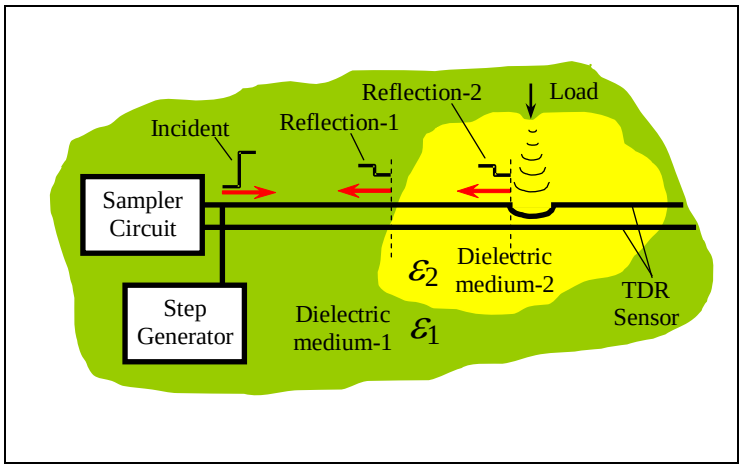

Figure 1: *Schematic representation of the operating principle of the TDR Sensor*[50,30].

3.4 Measuring Mechanical Parameters

All of the following sensor types have in common that the measured data are directly related to mechanical properties of the material. This is a very big advantage in contrast to the other types of sensors, because in many applications these properties are the interesting ones. Because only a simple model is necessary (e.g. to transform electrical to mechanical properties), a big source of potential errors is avoided.

While ultrasonic sensors measure the sound velocity and attenuation of ultrasonic waves in a polymer, vibrating needle and MCM sensors measure the complex mechanical impedance.

The significant difference between MCM sensors and vibrating needle sensors is the size, and hence the operating frequency range. Vibrating needle curemeters work at frequencies up to several hundred Hertz, and MCM sensors work between 50kHz and several MHz, depending on the construction.

---

30 See Dominauskas: TDR-Line Sensor […].
31 See Hager: Time-Domain-Reflectometry Cure Monitoring.
32 See Urabe: Cure Monitoring of Matrix Resin […]

Strain sensors

Elongation or shrinkage of the polymer can occur during a curing process. Hence it is possible to achieve curing data by measuring strain with a sensor that is placed inside the polymer. A big advantage of this family of sensors is their potential for measuring strain also after the curing process, when the part is in use, as a "smart" material. On the other hand the output is very limited and not present during the whole curing process.

Magnetostrictive Strain Sensors

A wire, which is coated with a magnetostrictive alloy, can be embedded into a composite part. Shrinkage of the polymer causes strain in the sensor wire[33]. This affects the magnetic permeability of the material, and by applying an alternating current to the wire this difference can be measured. Although this sensor technique is based on magnetostriction as well as the technique of MCM sensors, they differ significantly in the following points:

- MCM sensors work in a linear region of the B-H relation with a nearly constant μ. Magnetostrictive strain sensors are based on a nonlinear B-H relation for high strains.
- The strain that is present at the magnetostrictive material in case of MCM sensors alternates with high frequencies, caused by a magnetic field. The strain in magnetostrictive wire sensors is caused by the polymer itself and therefore alternates slowly with the curing process.

Optical Strain sensors

It is possible to measure strain with optical fibers and interferometry. One technique is called "Extrinsic Fabry-Perot Interferometry" (EFPI) and can be used during autoclave curing[34]. However, many difficulties in the application of the sensor exist, and the technology is not yet ready for industrial use. Another possibility is the use of optical fibers with a fine grating ("Fiber Bragg Grating"). Light inside the fiber core is scattered at the grating and can be correlated to the distance of the lines of the grating[35]. This distance is a function of strain. This kind of sensors is not mentioned in chapter 0, because although the measurement is optical, the sensors are not sensitive to optical properties of the polymer

---

[33] See Tayalia: Design and Optimization of Magnetostrictive Sensor for Strain Monitoring..

[34] See Katsuhiko Osaka: Strain Monitoring in Curing.

[35] See Murukeshan: Cure monitoring […] using Fiber Bragg Grating […] sensors.

Ultrasonic sensors

Several possibilities exist to excite ultrasonic waves, e.g., with piezoelectric transducers, magnetostrictive transducers or pulsed laser beams[36]. The sensors are usually designed to measure ultrasonic sound velocity and wave attenuation[37..40]. See chapter 3.5 for a direct comparison between conventional ultrasonic and MCM sensors.

Ultrasonic sensors for cure monitoring can be divided into the following groups:

- Analysis of phase, frequency and amplitude of continuous excited waves.
- Time domain analysis of reflected waves (U-TDR). (Very uncommon for cure monitoring.)
- Frequency domain analysis of generated impulses.

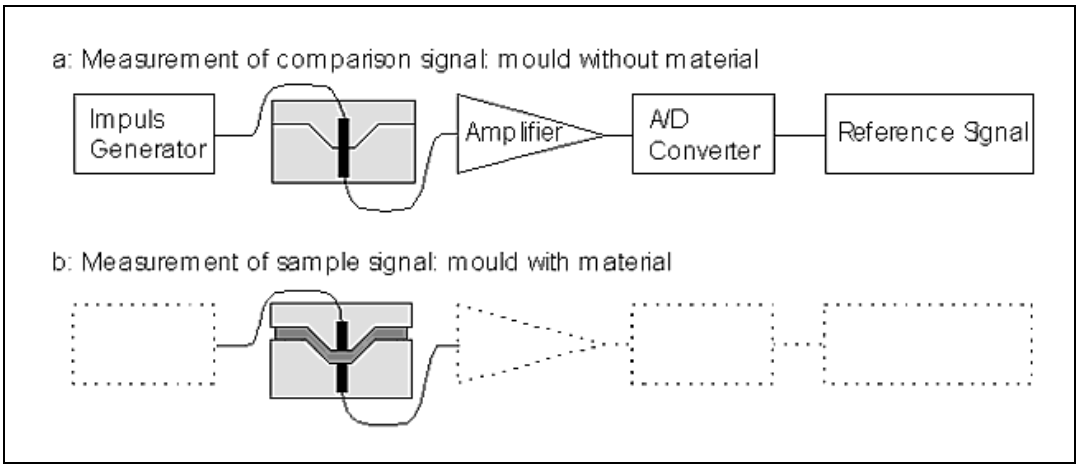

Figure 2: *Typical implementation of an ultrasonic cure monitoring sensor*[30].

Figure 2 shows a typical configuration. Most systems have a separated transmitter and receiver, but some systems also work with a combined transceiver[41].

---

36 See Fomitchov: Distributed photoacoustic system for cure monitoring […].
37 See Shepard: Ultrasonic cure monitoring […].
38 See Doering: Process monitoring […] by ultrasonic measurements […].
39 See Tabellout: The inserted piezoelectric sensor method […].
40 See Tuegel: Ultrasonic Cure Characterization of Epoxy Resins: Constitutive Modeling.
41 See Djordjevic: In-situ ultrasonic cure monitoring sensors.

Besides these sensors, which cause wave propagation inside the polymer, another technique uses a wire waveguide. It is based on wave propagation inside a small wire, embedded in a composite part[42,43].

Another approach is to embed a piezoelectric element into a composite part, but as discussed in the next chapter, this kind of sensors is not a typical ultrasonic sensor and should probably (like MCM sensors) not be counted to the family of ultrasonic sensors.

MCM and other mechanical impedance sensors

Although MCM sensors work at ultrasonic frequency ranges, they are not counted to the family of ultrasonic sensors. A reason is that ultrasonic wave propagation is not measured, and the standing wave in the magnetostrictive rod affects only the local area of the thermoset around its tip. Therefore it is possible to count the MCM sensors to the family of vibrating probes, with a mechanical impedance measurement. This kind of measurement must not necessarily be done with a magnetostrictive transducer, e.g., it can be performed with piezoelectric transducers[44] or electrodynamic transducers[45].

Although the design of MCM sensors may remind of vibrating probe sensors with electrodynamic excitation, there are some major differences. First of all, because of the magnetostrictive effect, the rod is not moved completely, that means the center of gravity remains at the same position during the vibration. This allows much faster oscillations, in the range of some 10,000 Hz up to some MHz, according to the length of the rod.

Compared to piezoelectric transducers, magnetostrictive transducers allow higher stress and strain, but with the disadvantage of a more sophisticated construction.

As shown later, the obtained data from MCM sensors is closely related to the shear-modulus of the curing polymer.

Two kinds of MCM sensors have been developed so far: Miniaturized, embedded sensors with an overall length of a few millimeters[46,47,48], and now a tool-mounted version together with this thesis.

---

42 See Dragasius: Wave-Guides Schaffen und Forschung der Diagnostischen Systeme[...].
43 See Yan Li: Monitoring the cure process […] using an ultrasonic wire waveguide technology.
44 See Fabert: Nondestructive Evaluation […] using an Inserted Piezoelectric Sensor […].
45 See Willoughby: Understanding cure with the Scanning Vibrating Needle Curemeter.
46 See Dominauskas: On-line Cure Monitoring with MCM Sensor […].

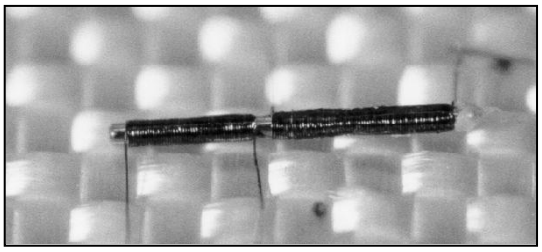

Figure 3: *Miniature MCM sensor*[46].

3.5 Comparison between Conventional Ultrasonic and MCM Sensors

Ultrasonic sensors are the strongest competitors to MCM sensors, because they also measure mechanical properties of the polymer directly. A good design allows the use in probably every hostile environment for curing. Therefore these two sensor techniques are compared in table 1. Many interesting questions cannot be answered yet for MCM sensors; hence the table contains some quotation marks.

47 See Dominauskas: Magnetostrictive Sensor for On-line Cure Monitoring of Thermosets.

48 See Dominauskas: Magnetostrictive Sensors with Variable Boundary Conditions.

Table 1: *Comparison between ultrasonic and MCM sensors.*

	Conventional ultrasonic[49]	**MCM Sensors**
Measured properties	sound velocity (longitudinal or shear) ⇓ Young's-modulus or shear-modulus with known density	mechanical contact impedance ⇓ Young's-modulus or shear-modulus with known Poisson's-ratio
Type of sensing	spatial	local
Simple model to get mechanical properties of polymer	yes	yes
Simple theoretical modeling of sensor properties	yes	no
Sensitive to the whole curing process	yes, high sensitivity	yes, highest sensitivity
Sensitive to heterogeneity of polymer (fibers or bubbles)	yes	no (minimum distance to sensor tip has to be determined)
Separated transmitter / receiver	both possible	no
Exact thickness of part necessary to know	yes	no
Tool- / mold mounting possible	yes	yes
Direct contact to polymer necessary	no	yes
Long-term use in hostile environment with high temperature / high pressure	yes, with expensive transducers	has to be determined
Non-contact measurement possible	yes, with coupler	no
Exact defined surfaces necessary	2 E.g. VARTM is not possible because of the absorbing layers at one surface.	1 Only the surface which is in contact with the sensor.

[49] "Conventional ultrasonic" means the first three sensor types listed in chapter 3.4 "ultrasonic sensors".

From the comparison between the different sensor types it can be concluded that MCM sensors open a new field of cure monitoring. They fit to needs, which up to now cannot be covered with other sensor systems, even not with ultrasonic sensors. However, MCM sensors are not a general solution for cure monitoring, because several questions are not answered yet, and in some applications it is simply necessary to have different concepts of cure monitoring, e.g. with a spatial sensing. But it could be shown that MCM sensors have the potential to spread into industrial and experimental applications

3.6 Introduction to the MCM Sensor Principle

In general, the MCM sensor consists of a magnetostrictive rod, which performs longitudinal vibrations due to a changing magnetic field. This field is created by an electric solenoid, with an excitation frequency of some 10,000 Hz.

On one end the rod is in mechanical contact with a curing polymer. This creates a certain boundary condition, which changes during the curing process. As a result the mechanical behavior of the rod changes; in fact the polymer has an influence of its resonant frequency and on the attenuation.

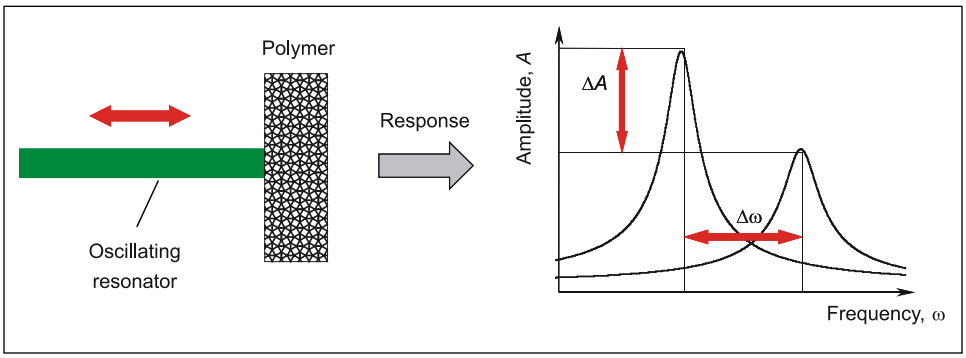

Figure 4: *Principle of MCM sensors*[50].

By performing a frequency sweep with the excitation voltage at the solenoid, the system eventually goes to resonant conditions, and the amplitude and resonant frequency are related to mechanical properties of the attached polymer.

50 See Dominauskas: On-line Cure Monitoring with MCM Sensor […].

Because of the reverse magnetostrictive effect, these parameters can be detected with a second solenoid, a “pickup” coil, which is also placed around the rod.

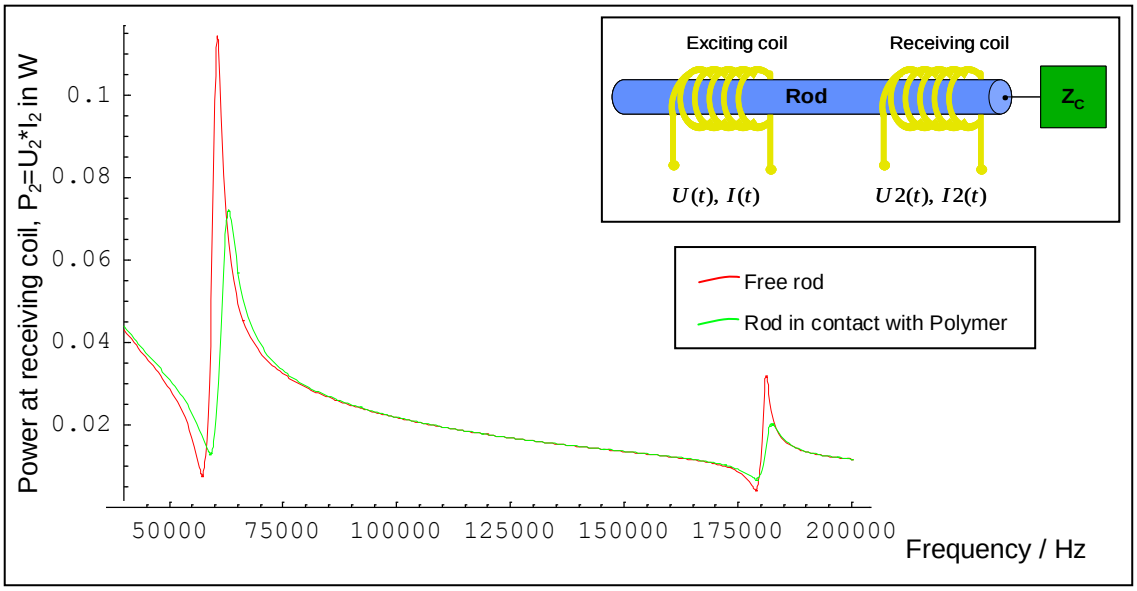

Figure 5: *Typical sensor output (power at pickup coil).*

The principle of the MCM Sensor was already proofed to be successful in a miniature version, developed by A. Dominauskas and R. Bansevicius in 1999. Dominauskas designed sensors with an overall length of a few millimeters, which can be directly embedded into a polymer.

Contrary to that, the MCM sensor, which is described in this thesis, is designed to be mounted in a mold permanently, for repetitive use. The design is targeted for industrial applications, although the reliability for that still has to be proofed. Up to now the sensor works in experimental setups with nearly all varieties of polymers with a high sensitivity during the complete curing process.

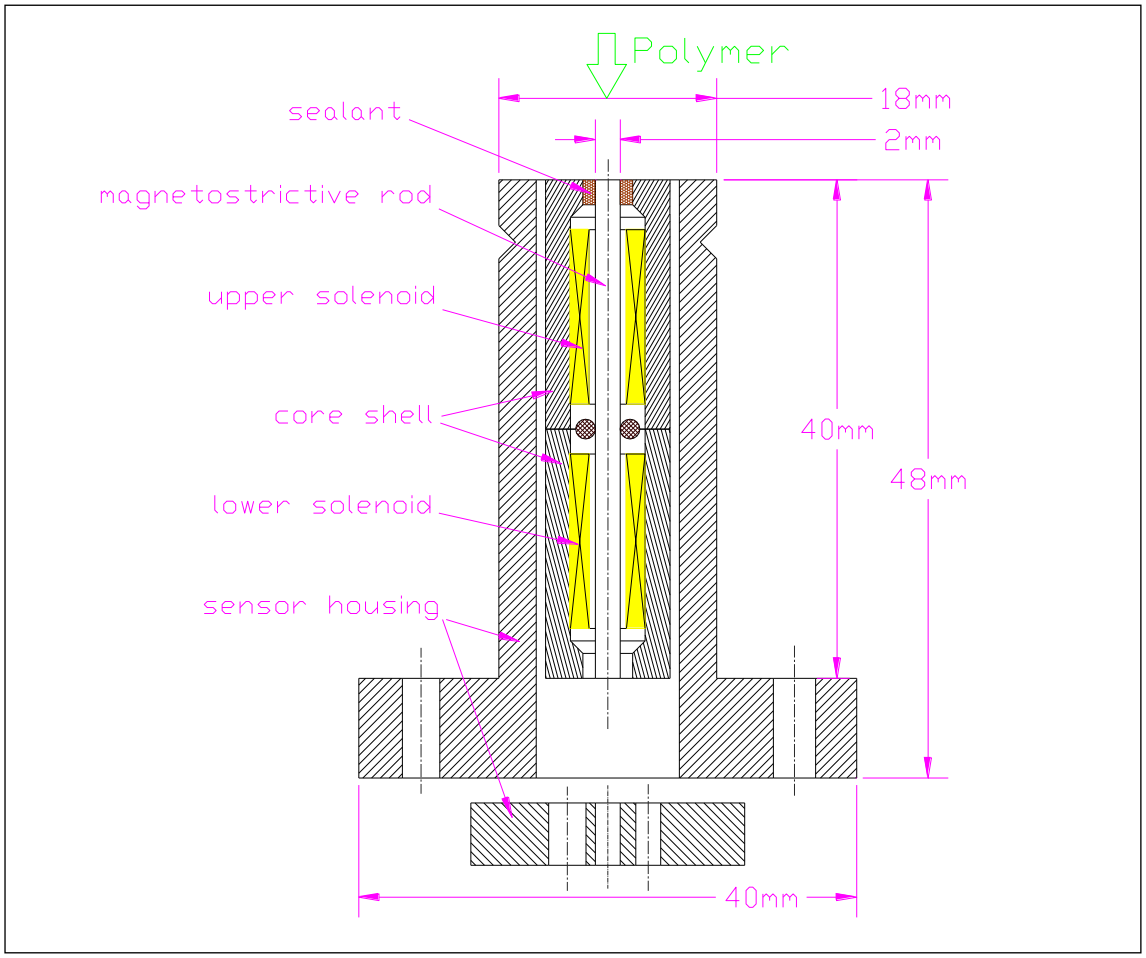

Figure 6: *Simplified drawing of the mold-mounted MCM sensor prototype.*

Figure 6 shows a simplified drawing of the MCM sensor. It consists of a housing and a core unit with the magnetostrictive material in the center. The function of the housing is to protect the core, as well as to attach the sensor to a mold. The core consists of the magnetostrictive rod and the electric coils, as well as a shell made of a high-permeability metal, to create a good magnetic flux return path. This assures that the magnetic field lines go nearly through the whole rod and therefore through both coils, and then go back through the shell. The rod itself is supported only by an elastic sealant at one tip of the rod, and by a slide bearing at the center. This allows free vibrations.

3.7 Introduction to Magnetostriction

Certain materials exhibit a micro-strain when subjected to a magnetic field. More precise, magnetostriction can be described as the deformation of a body in response to a change in its magnetization, the magnetic moment per unit

volume[51]. This is quite similar to the more famous piezoelectric effect, where an electric field causes stress and strain, respectively. From here results the expression "piezomagnetic[52]", which is sometimes used in literature besides the expression "magnetoelastic".

The magnetostrictive effect is also called *Joule* effect, after *James P. Joule* (1818-1889) who discovered this phenomenon. The *Villari* effect, also called "reverse magnetostrictive effect", describes the change in magnetization due to applied stress or strain. As shown later, both effects are strongly related with each other and therefore not further distinguished in this thesis.

Additionally, the *Wiedemann* and *Matteuci* effects are magnetostrictive effects related with torsion, and they are not further discussed in this thesis.

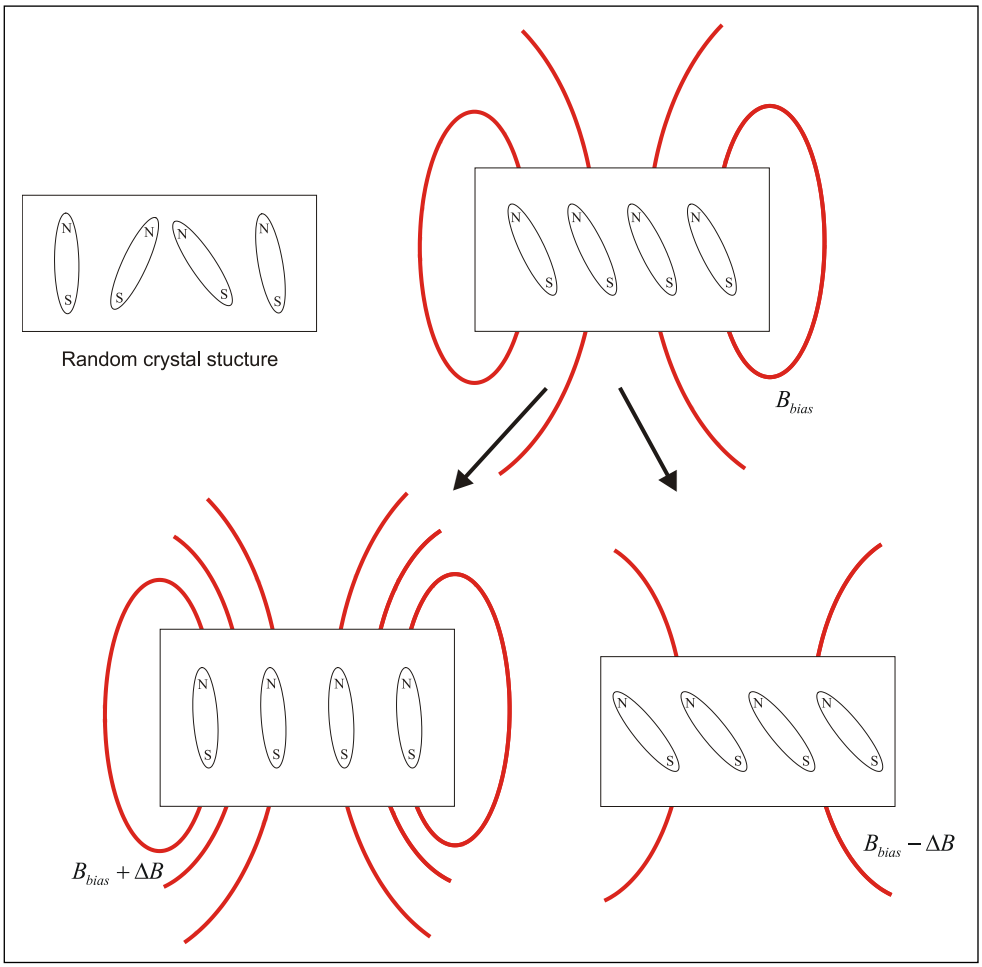

Figure 7: *Simple model of magnetostriction.*

[51] See Engdahl: Handbook of Giant Magnetostriction, p. 1

[52] "Piezo" comes from Gr. *πιέζειν* , "to press, squeeze".

Figure 7 shows a simplified model for magnetostriction. If the material is not magnetized, the magnetic elements are randomly dispersed. When a magnetic field is applied, these magnetic elements try to turn towards the field lines, until there is a certain balance between the electromagnetic force and the internal stress that is created by the rotations. If this magnetic field changes, e.g., by applying an alternating current to an excitation coil, an additional strain gets either added or subtracted from the initial biasing strain.

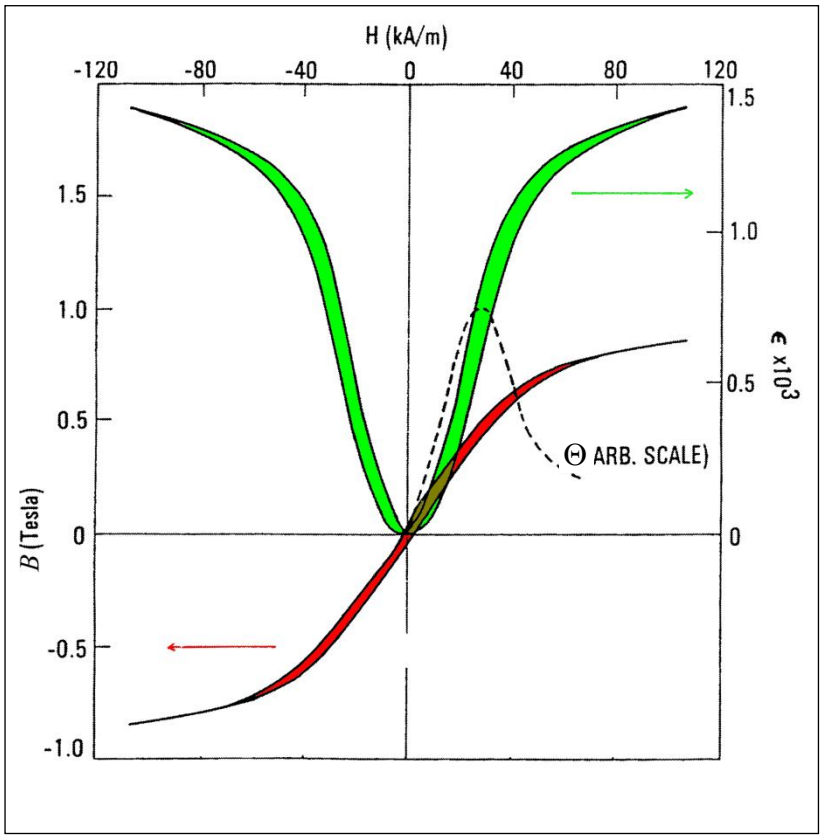

Figure 8: *Magnetization and magnetostriction of $Tb_{0.27}Dy_{0.73}Fe_{1.95}$ at 12.4MPa. The dotted line illustrates the value of Θ, which is proportional to the slope of the magnetostriction vs. magnetic field*[53].

Figure 8 shows the relation between magnetization (or magnetic flux density) B, Magnetic field strength H and the strain of the material in direction of the magnetization, for a "giant magnetostrictive" material at a certain pre-stress. While the $B-H$ curve looks typical for a (weak) magnetic material, an additional $B-\varepsilon$ curve is typical for magnetostrictive materials. It is very

[53] See Engdahl: Handbook of Giant Magnetostriction, p. 23.

significant that the strain does not change if the direction of the magnetic field changes.

Magnetostriction as a quantity is usually defined by the change in length in some direction, when a magnetic field changes from zero to saturation in that direction.

$$\frac{\Delta l}{l} = \Delta\varepsilon = \lambda \qquad (1)$$

In the case of Terfenol-D the material elongates ($\lambda > 0$), but pure nickel for example contracts. It shall be noted (and figure 8 illustrates) that a saturating magnetic field means that the linear region of magnetization is exceeded.

Several other quantities are used to describe magnetostriction, e.g. in terms of force or energy. In this thesis a magnetostrictive constant Θ is used, which can be derived from energetic relations[54]. It depends on a certain magnetic biasing and is valid for small changes of the magnetic field strength, neglecting nonlinear effects and hysteresis. With this constant it is possible to develop a linear model of magnetostriction[55], based on Hook's law (equation 2) and on the $B-H$ relationship (equation 3).

$$\sigma(x,t) = E^B \cdot \varepsilon(x,t) - \Theta \cdot B(t) \qquad (2)$$

$$H(x,t) = -\Theta \cdot \varepsilon(x,t) + \frac{1}{\mu^\varepsilon} \cdot B(t) \qquad (3)$$

With:

x	*Coordinate over rod*	*SI-Unit*	m
t	*Time*	*SI-Unit*	s
$\sigma(x,t)$	*Stress, tension*	*SI-Unit*	$Pa = N/m^2$
$\varepsilon(x,t)$	*Strain*		
E^B	*Young's-modulus at constant magnetic flux density*	*SI-Unit*	Pa
Θ	*Magnetostrictive constant*	*SI-Unit*	Pa/T
$B(t)$	*Magnetic flux density*	*SI-Unit*	T
$H(x,t)$	*Magnetic field strength*	*SI-Unit*	A/m
μ^ε	*Magnetic permeability at constant strain*	*SI-Unit*	$Vs/(Am)$

[54] See Engdahl: Handbook of G. Magnetostriction, p. 130. Engdahl uses the Greek letter "λ" for the magnetostrictive constant Θ.

[55] See Engdahl: Handbook of Giant Magnetostriction, p. 133.

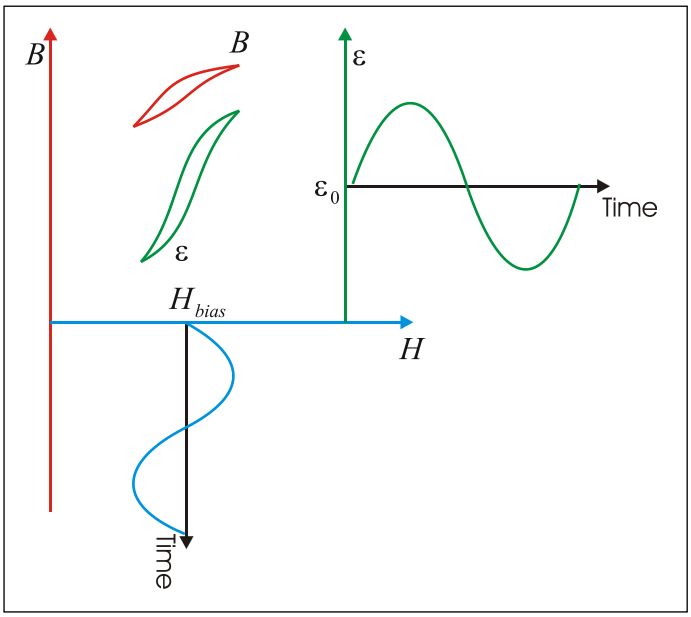

Figure 9: *Strain (blue) and magnetization (red) resulting from a sinusoidal excitation at a certain bias*[56].

As mentioned above, the equations 2 and 3 are only valid for a certain offset or biasing of the magnetic field. Therefore B and H mean only the alternating part of the overall magnetization and magnetic field strength, respectively. Figure 9 shows this relation. Further figure 8 illustrates that there is an optimum value of the bias magnetization, where Θ reaches its maximum, usually at the inflection point of the $\varepsilon - H$ curve.

$$B_{sum} = B_{bias} + B \qquad (4)$$

$$H_{sum} = H_{bias} + H \qquad (5)$$

Magnetostrictive materials

In literature materials are divided into "weak[57]", "normal" and "giant" magnetostrictive[58]. Normal magnetostrictive materials are for example Nickel and some ferromagnetic materials with a maximum strain λ between -100 and +100 microns ($\mu m/m$).

---

56 See Angus: Nickel-based magnetostrictive alloys […].

57 Actually many magnetic materials like Iron or some steels show (weak) magnetostriction. This sometimes causes unwanted effects like a hum in transformers.

58 The Excel-file "comparison of material data.xls" on the CD-Rom contains a table with magnetostrictive materials and their physical properties. The data were collected from manufacturers.

In the 1960's some military applications required the improvement of high-intensity ultrasonic transducers (e.g. for sonar). This led to the development of the "giant" magnetostrictive materials, which are specially grown rare-earth crystals. These outperform every known piezoelectric material; the strain can exceed 2000 microns.

Rare-earth materials are generally fragile and therefore difficult to machine. A rod in the required dimensions for the MCM sensor has to be grinded. Although the material is in general working at higher temperatures, the magnetostrictive properties would decrease down to 50%; therefore the material would have to be thermally aged to maintain stability.

Magnetostriction not only depends on the chemical content of the material but also on the thermal history. Magnetostrictive metals should be annealed for optimum performance to reduce internal stresses.

4 THEORETICAL MODELS

The whole theory that is related to the MCM sensor consists of three separate models.

The first model describes the magnetostrictive phenomena and the mechanical behavior of the rod. One boundary condition to this model is a complex contact impedance Z_c at one tip of the rod, and the solutions given to the differential equation are dependant of Z_c, which is not further specified.

The second model relates mechanical properties of a polymer with a contact impedance. It describes the polymer when it is already in a pure solid state and has developed a certain Young's-modulus. Therefore Z_c becomes the interface between the first and the second model. The model does not describe the curing process, and therefore it cannot predict a degree of cure, at least if the degree of cure is not defined directly by mechanical properties[59]. Further it does not analyze the change of properties over the time.

The third model describes an approximation of both the first and the second model. The resonant frequency and the amplitude are approximated by functions of the complex contact impedance, and with the second model a Young's-modulus is calculated. This approximation is necessary to relate the sensor output on-line to the values of the contact impedance. The measurement software in can do this real-time, only with a quick calculation.

4.1 The MCM Sensor Model

The following model describes the macroscopic mechanical behavior of a magnetostrictive rod, and the electric impedance of solenoids, which are wound around it.

Two linear, one-dimensional approaches are possible for modeling the magnetostrictive material[60], with lumped or with distributed parameters. In the first case this would be a network of discrete components like springs, dampers and masses. It works well for low frequencies when the wavelengths are much larger than the length of the rod. But when wave propagation occurs inside the material due to its distributed mass, this approach is not recommended. In the case of the MCM sensor resonant phenomena of the rod itself are under consideration, hence a model with distributed parameters is used.

---

59 See appendix II: Glossary.

60 Besides this several other models can be found in literature, linear and nonlinear. See Engdahl: "Handbook of Giant Magnetostrictive Materials", p. 127 et sqq.

Two equations (equations 2 and 3) describe the magnetostrictive effect of the rod in a linear way:

$$\sigma(x,t) = E^B \cdot \varepsilon(x,t) - \Theta \cdot B(t)$$

$$H(x,t) = -\Theta \cdot \varepsilon(x,t) + \frac{1}{\mu^\varepsilon} \cdot B(t)$$

With:

σ	Stress, tension
E_R	Young's-modulus of the rod, here actually the value of the Young's-modulus at a constant magnetic flux density
ε	Strain
Θ	"Classical" magnetostrictive constant
B	Magnetic flux density, or magnetization
H	Magnetic field strength
μ	Magnetic permeability, $\mu = \mu_0 \mu_r$, when the strain is kept constant

The first equation is derived from Hook's law, a relation between stress and strain. With an additional term this is extended by a relation to the magnetic flux density multiplied by a material constant. This material constant describes in general how much stress or strain can be generated by a certain magnetic field, and it can be derived theoretically from energy and work considerations[61].

Assumptions for the MCM sensor model

1. Only steady-state oscillations are under consideration, no time domain transients.

Because of the ideal elastic case described by Hook's law, some other assumptions have to be made:

2. No mechanical losses occur in the magnetostrictive rod.
3. Stress and strain do not exceed linear regions.

[61] See Engdahl: "Handbook of Giant Magnetostrictive Materials", p. 130

Other assumptions have to be made to allow a one-dimensional treatment of the problem:

4. The diameter of the rod is small compared to the wavelength in the rod[62]: $l/d \geq 10$.
5. No bending of the rod occurs.
6. Plane sections remain plane. The material is rigid at the surface that is in contact with the polymer.

Further assumptions help to keep the electromagnetic relations simple:

7. Effects of magnetostriction are linear, and no hysteresis effects occur.
8. The magnetic circuit is ideal with no losses and an ideal magnetic flux return path.
9. No dissipative losses occur in the solenoids, and no eddy-currents occur in the rod.
10. The thickness of the coil is thin compared to other dimensions (the inner diameter equals the outer diameter).
11. The diameter of the rod equals the diameter of the solenoids.

The last assumption allows excluding the receiving coil from the differential equation:

12. The output power at the receiving coil is low compared to the mechanical power and to the electrical power in the excitation coil.

4.1.1 Mathematical Derivation

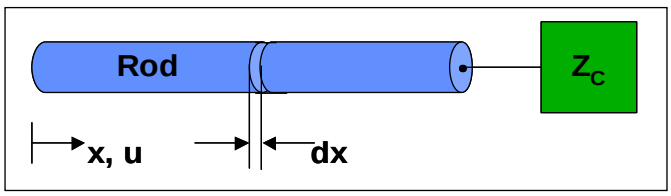

Figure 10: *Magnetostrictive rod and mechanical contact impedance* Z_c *at* $x = l_{Rod}$.

62 See Vadel: Magnetostrictive Sensor with variable boundary condition […].

Differential equation for rod

The differential equation for longitudinal wave propagation in an elastic material[63] is fundamental for modeling the magnetostrictive rod[64]. Starting point for the derivation of this equation is Newton's Second Law, reduced to a one-dimensional problem:

$$\frac{\partial \sigma(x,t)}{\partial x} = \rho_R \frac{\partial^2 u(x,t)}{\partial t^2} \qquad (6)$$

With:

x Length-variable
u Displacement of a cross-sectional area of the rod
ρ_R Density of the magnetostrictive rod

Strain:

Strain is defined as:

$$\varepsilon(x,t) = \frac{\partial u(x,t)}{\partial x} \qquad (7)$$

Stress

The following equation (2) is designated as the *first magnetostrictive equation*. It is based on a linear model of magnetostriction. The classical stress-strain relationship (Hook's law) is extended by a magnetostrictive relation. Hence the following expression describes an association between mechanical and electromagnetical properties of the system:

$$\sigma(x,t) = E_R \cdot \varepsilon(x,t) - \Theta \cdot B(t)$$

This equation can be applied to equation 6, then substituting strain with equation 7 gives:

$$E_R \frac{\partial^2 u(x,t)}{\partial x^2} - \Theta \frac{\partial B(t)}{\partial x} = \rho_R \frac{\partial^2 u(x,t)}{\partial t^2} \qquad (8)$$

---

63 The model of the MCM Sensor is mainly based on equations from G. Engdahl "Handbook of Giant Magnetostrictive Materials", p. 143 et sqq.

64 This chapter exists as a MATHEMATICA file "Theoretical model 1"with the same equations and additionally plots, simple case studies and a unit verification. Additionally these Mathematica notebooks are on the CD-Rom as PDF documents.

B is independent from the length variable x because only a longitudinal component is assumed and because $div(B) = 0$ according to Maxwell. This gives:

$$\frac{\partial^2 u(x,t)}{\partial x^2} = \frac{\rho_R}{E_R} \frac{\partial^2 u(x,t)}{\partial t^2} \qquad (9)$$

This is a very important result. It shows that the same differential equation is valid for both magnetostrictive and non-magnetostrictive materials. Hence the same solutions are valid – solutions of standing waves and wave propagation in the rod, respectively.

Solution for the differential equation

The displacement is assumed to be a function of the position (of a *dx* element) multiplied by a function of time:

$$u(x,t) = X(x)T(t) \qquad (10)$$

With a function of the variable *x*:

$$X(x) = a_1 \cos(K x) + a_2 \sin(K x) \qquad (11)$$

With:

K Wave Number:

$$K = \frac{\omega}{c_R} = \omega \sqrt{\frac{\rho_R}{E_R}} \qquad (12)$$

a_1, a_2 Complex amplitude coefficients

And a function of time:

$$T(t) = e^{i\omega t} \qquad (13)$$

With:

ω Angular frequency, $\omega = 2\pi f$

Velocity

The velocity of an element of the rod is defined as:

$$v(x,t) = \frac{\partial u(x,t)}{\partial t} \qquad (14)$$

Relation between magnetic flux density B and properties of a solenoid

Based on *Faraday's law* the following equation is valid for an *ideal solenoid*:

$$B(t) = \frac{U(t)}{i\,\omega\,N\,A} \qquad (15)$$

With:

B Magnetic flux density in the rod
N Number of turns of the solenoid
A Cross-sectional area of the solenoid

Please note that the magnetic flux density is primarily related to the voltage, not to the current going through the solenoid! Actually a constant magnetic field for biasing the magnetostrictive rod is excluded from this model. Therefore *B* and *H* mean just the alternating components[65].

Voltage drop function

The voltage drop at the solenoid has to be a sinusoidal function when the system is in a steady state. Therefore the time function $T = e^{i\omega t}$ is also used for the voltage. However, there may be a phase shift between the displacement and the voltage.

$$U(t) = Ud\,e^{i\omega t} \qquad (16)$$

With:

Ud Complex amplitude of the voltage function

Boundary conditions for amplitude coefficients *a1* and *a2*

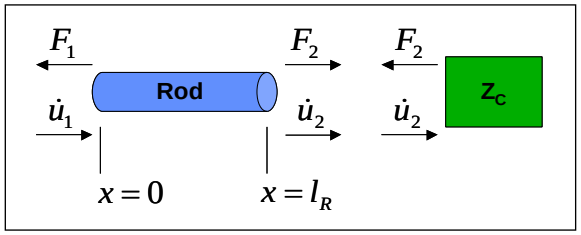

Figure 11: *Boundary conditions.*

[65] See chapter 2.2: Introduction to magnetostriction.

First boundary condition (determining coefficient a2)

No stress occurs at the free end of rod (x=0), at all times:

$$\sigma(0,t)=0 \qquad (17)$$

Solving this for coefficient a2 gives:

$$a_2 = -\frac{i\,c_R\,Ud\,\Theta}{A E_R\,N\,\omega} \qquad (18)$$

Second boundary condition (determining coefficient a1)

It is assumed that the sealant as well as the polymer is in contact with the rod only at the end of the rod. Therefore overall mechanical impedance Z_c is defined as a second boundary condition:

$$-Z_c = A_c\,\frac{\sigma(l_R,t)}{v(l_R,t)} \qquad (19)$$

With:

Z_C Complex mechanical contact impedance of polymer and sealant, SI unit $\frac{N\,s}{m} = \frac{kg}{s}$

A_C Contact area

Solving this for coefficient a_1 and applying equation 18 gives:

$$a_1 = Ud\,\Theta\,\frac{c_R\,(i\,c_R\,Z_c\sin(\frac{l_R\,\omega}{c_R}) + A_c\,E_R\cos(\frac{l_R\,\omega}{c_R}) - A_c\,E_R)}{A_c\,E_R\,N\,\omega^2\,(i\,A_c\,E_R\sin(\frac{l_R\,\omega}{c_R}) + c_R\,Z_c\cos(\frac{l_R\,\omega}{c_R}))} \qquad (20)$$

Magnetic field strength H

The magnetic field strength has to be calculated, because it is related to the electric current going through the solenoid.

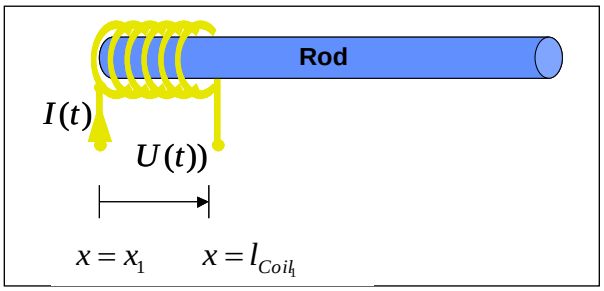

Figure 12: *Magnetostrictive rod and one coil.*

The following equation is designated as the *second magnetostrictive equation* (3). The classical relationship between magnetic field strength and flux density ($B = \mu H$) is extended by the strain:

$$H(x,t) = \frac{B(t)}{\mu_R} - \Theta\,\varepsilon(x,t)$$

With:

H Magnetic field strength, SI unit A/m

Contrary to the flux density, the field strength varies in between the rod. Therefore H has to be integrated over the length of the coil[66]. In the following consideration the solenoid is placed at the free end of the rod, with a yet unknown length l_{Coil_1} :

$$Hq(t) = \int_{x_1}^{l_{Coil_1}+x_1} \frac{H(x,t)}{l_{Coil_1}}\,dx \qquad (21)$$

With:

Hq Average magnetic field strength in the solenoid
l_{Coil_1} Length of the solenoid
x_1 Location of the coil

The current I is proportional to the (average) magnetic field strength:

$$I(t) = \frac{Hq(t)\,l_{Rod}}{N} / K_1 \qquad (22)$$

With:

I Current through solenoid.

66 See chapter 9.2: Problems.

K_1 A combined factor of geometry factor and field factor of the coil. For $K_1 = 1$ the equation describes an ideal solenoid.

One very important consequence of equations 21 and 22 is that the length and especially the position of the coils are relevant. If the receiving coil for example is placed at a node of strain[67], the signal gets cancelled out[68]. On the other hand, by measuring the signal with a high impedance voltage probe it is still visible.

Electric impedance

The electric impedance of the excitation coil can finally be calculated:

$$Z = \frac{U(t)}{I(t)} \qquad (23)$$

Power

The electric power (including the magnetostrictive power) can be calculated as:

$$P(t) = U(t)I(t) \qquad (24)$$

P is complex – the real part is the active power, the complex part is the reactive power.

This is the *effective* (time independent) apparent power:

$$Pa = \frac{1}{2}|U(t)||I(t)| \qquad (25)$$

[67] See Figure 16. Nodes of strain are present for all higher modes of oscillation than the first one.

[68] This could be verified in preliminary experiments.

Model of the electric circuit

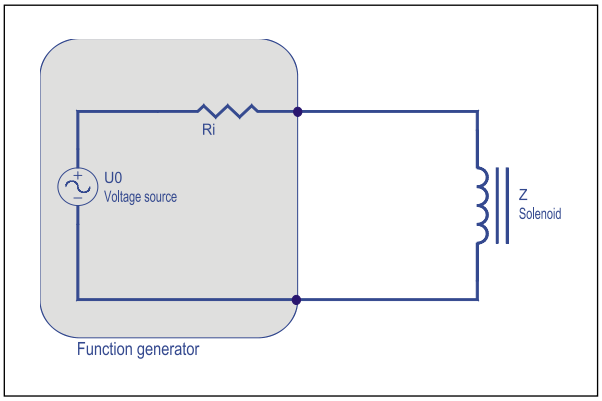

Figure 13: *Simple electric circuit to determine the voltage drop at the solenoid.*

The Voltage drop at the solenoid depends on the internal resistance of the voltage source (a function generator), and on the current. Applying Kirchhoff's law gives:

$$U_0(t) = I(t)(R_i + Z) \qquad (26)$$

With:

$U_0(t)$ Internal voltage source of the function generator
R_i Internal resistance of the function generator

Equation 26 can be solved for the actual voltage at the solenoid after inserting equation 23 into it, and herewith equations 20 and 18 can be solved for a displacement amplitude of the oscillation.

Model of the receiving coil

Please note that the effect of a receiving coil is not mentioned in the equations above. Therefore they are only valid for low power consumption at the receiving coil because all energy that is leaving the system has to be supplied through the excitation coil.

Again Faraday's law is used to determine the voltage, here at the receiving coil:

$$U_2(t) = i\omega N_2 AB(t) \qquad (27)$$

Applying equation 15 shows that the voltage of the receiving coil is related to the voltage of exciting coil:

$$U_2(t) = \frac{N_2}{N} U(t) \qquad (28)$$

This is the same equation like for a transformer. It shows that the output voltage at the receiving coil is directly proportional to the input voltage at the excitation coil. If an ideal voltage source were used for excitation the output voltage would not change because of a magnetostrictive effect! Therefore the magnetostrictive effect can here only be measured because of the internal resistance of the voltage source.

The current can be calculated like in equation 22:

$$I_2(t) = \frac{Hq_2(t)\, l_{Coil_2}}{N_2} K_2 \qquad (29)$$

With:

N_2 Number of turns of the receiving coil
l_{Coil_2} Length of the receiving coil
K_2 A factor to express losses in the coil

Like in equation 21 the average field strength can be calculated:

$$Hq_2(t) = \int_{x_2}^{x_2 + l_{Coil2}} \frac{H(x,t)}{l_{Coil_2}} dx \qquad (30)$$

Now the power output of the receiving coil is calculated:

$$P_2(t) = U_2(t)\, I_2(t) \qquad (31)$$

And the effective power is:

$$Pa_2 = \frac{1}{2} \left| U_2(t) \right| \left| I_2(t) \right| \qquad (32)$$

Applying all equations from above to equation 32 gives a very long and complex formula[69], because several trigonometric functions are involved (see equation 20). However, the effective power is proportional to the following variables:

$$P_2 \propto K_2 {U_0}^2 \qquad (33)$$

[69] See Mathematica file “Theoretical Model 1.nb” on the CD-Rom.

4.1.2 Studies of System Behavior

Curves in this chapter were created with the theoretical model and the input quantities are closely related to the properties of the real MCM sensor.

For a first analysis of the sensor model the mechanical behavior of the rod is under consideration. The amplitudes a_1 and a_2 of the displacement can be calculated with equations 20 and 18.

The amplitude a_1 (coefficient for the cosine part) for zero impedance (both ends free) degrades to:

$$\lim_{Z_c \to 0} a_1 = \frac{i\, c_R\, Ud\, \Theta \tan(\frac{l_{Rod}\, \omega}{2\, c_R})}{A E_R\, N\, \omega^2} \qquad (34)$$

The amplitude a_2 (coefficient for the sine part) does not depend on the impedance. It stays:

$$a_2 = \frac{i\, c_R\, Ud\, \Theta}{A E_R\, N\, \omega^2} \qquad (18)$$

Both amplitudes are mainly imaginary, that means that there is a 90° phase lag between the excitation voltage Ud and the displacement. However, certain values of Z_c can change this phase angle.

The phase angle between the ideal voltage source of the function generator and the excitation solenoid gets added to this. Figure 15 shows that in this case the phase lag can be up to 180 degrees. Another important conclusion can be drawn by comparing figures 14 and 15: Although a the function generator can be modeled with an internal resistance the assumptions of the ideal electro-magnetical and magneto-mechanical coupling cause always a hard phase jump at the resonant frequencies. For sure this is not the case for the real system.

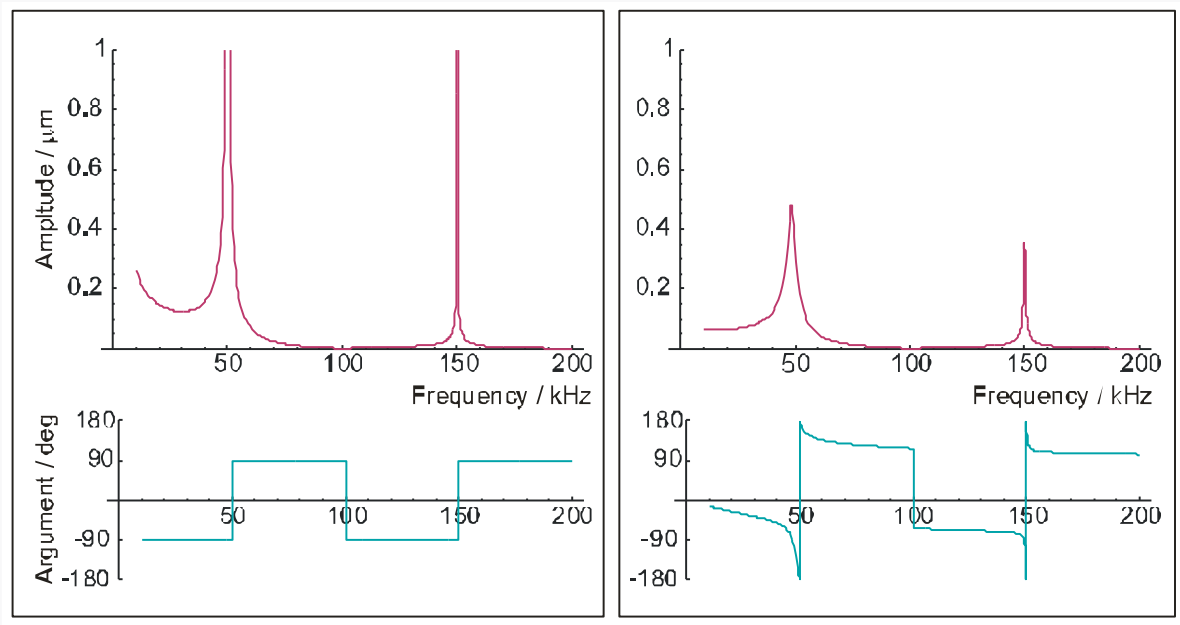

Amplitude & Phase angle of displacement

Figure 14: *Ideal voltage source.* ***Figure 15:*** $R_i = 50\Omega$.

In case of its first mode of free oscillations, for

$$\omega \to 2\pi\left(\frac{c_R}{2l_{Rod}}\right)$$

the argument of the tangent becomes π, hence a_1 goes towards complex infinity.

In case of its second mode of free oscillations, for

$$\omega \to 2\pi\left(\frac{2c_R}{2l_{Rod}}\right)$$

the amplitude a_1 becomes zero.

The amplitude a_1 becomes exactly zero for all even modes of free oscillation. This anti-resonant effect can be explained with the two magnetostrictive equations 2 and 3. Figure 16 shows that in all modes the displacement is always symmetric to $u = 0$ (in accordance with the fact that the center of gravity remains constant). At the same time the stress is asymmetric to $\sigma = 0$ for odd modes, but symmetric for even modes. Because it is assumed that the magnetic flux density B is constant over the length of the rod this magnetic

field cannot cause an imbalance between stress and strain, and therefore it cannot excite these oscillations[70].

[70] For a clamped rod all modes show an asymmetric stress distribution. Hence all resonant modes can be excited.

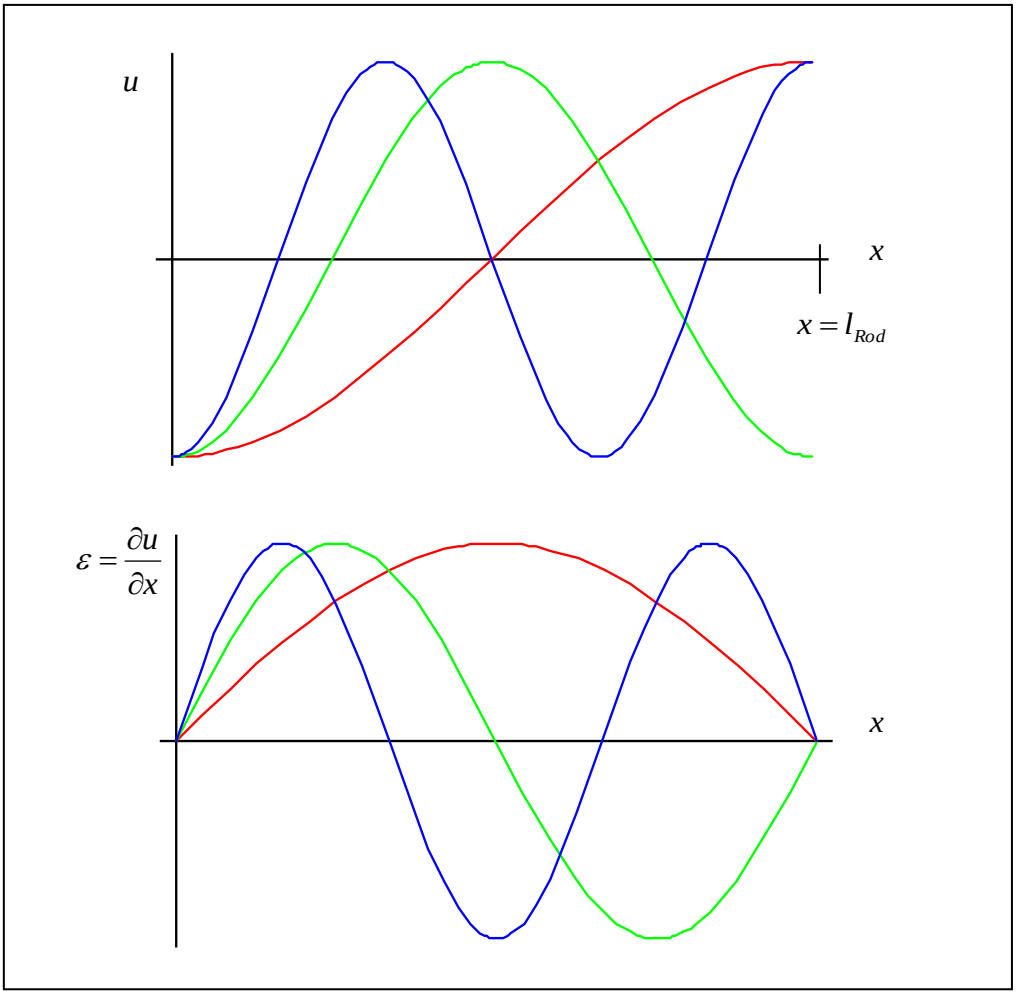

Figure 16: *Stress and displacement for free modes of oscillation. Red: First mode; green: Second mode; blue: third mode. For even modes both stress and strain are symmetric to* $u = 0$ *and* $\sigma = 0$*, respectively.*

Now another case shall be under consideration, when the contact impedance goes towards infinity or complex infinity:

$$\lim_{Z_c \to \infty} a1 = \lim_{Z_c \to i\infty} a1 = \frac{i c_R U d \Theta}{A E_R N \omega^2} \tan\left(\frac{l_{Rod}\,\omega}{c_R}\right) \qquad (35)$$

In both cases the expression degrades to the same simple formula, now with resonant frequencies for a rod with a fixed support at one end.

4.1.3 Influence of Mechanical Contact Impedance ZC

The behavior of the oscillating system is comparable to simple mechanical systems, for example a rod without magnetostrictive properties, and an ideal force, damper, or mass at one end. However, not every phenomenon can be explained with such a simple “spring-mass-damper” model.

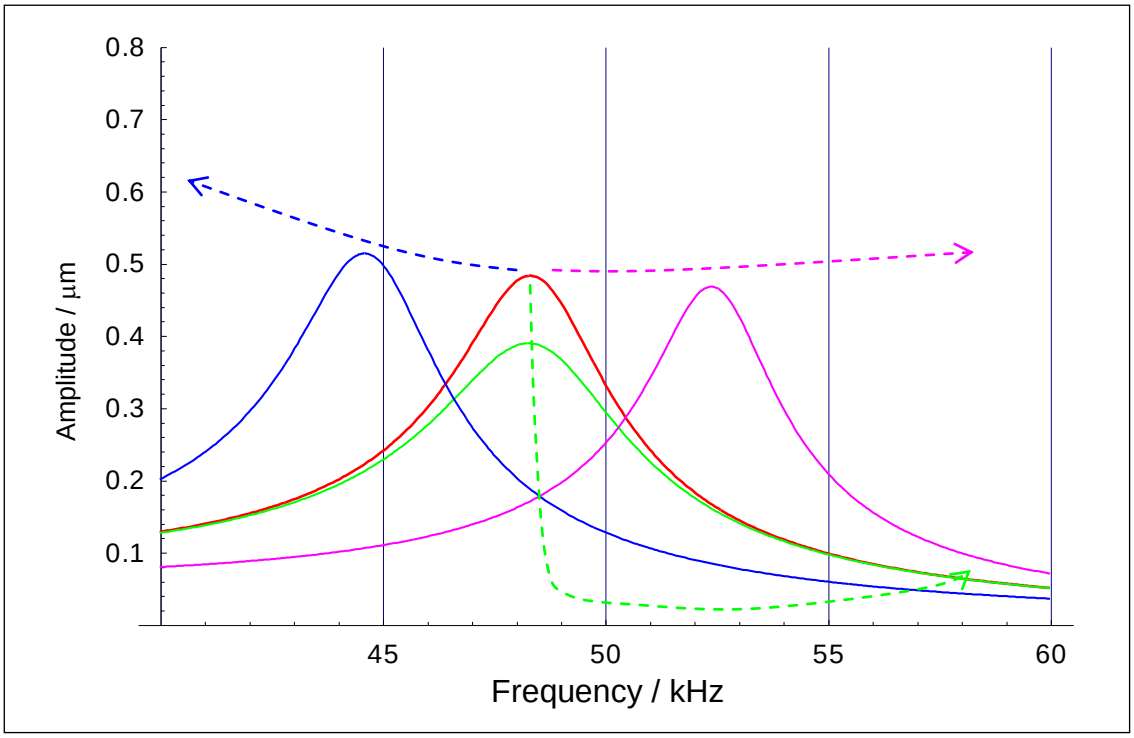

Plot 17: *Frequency response of the rod in dependence of the impedance* Z_c. *By increasing the impedance, the red curve moves towards one of the other curves.*

(red):	$Z_C = 0$
(green):	$Z_C = 15 Ns/m$
(blue):	$Z_C \approx i160 Ns/m$
(pink):	$Z_C \approx -i160 Ns/m$

Plot 17 shows the behavior of the oscillating system for low discrete values of the contact impedance Z_C. The red curve shows the frequency response of a free system, driven with a 10V function generator and an internal resistance of 50Ω (therefore the amplitude does not rise to infinity at the resonant frequency). The green curve shows the response to a pure mechanical resistance, like an ideal damper. The blue and the pink curve show the response of the system according to inertia and to capacitive impedance component, respectively. The arrows show the direction of the peak movement for increasing impedance terms.

Cured Epoxy for example could have an impedance of about $(10 - i15) Ns/m$ at about 50kHz and its curve would be somewhere in between the curves of figure 17.

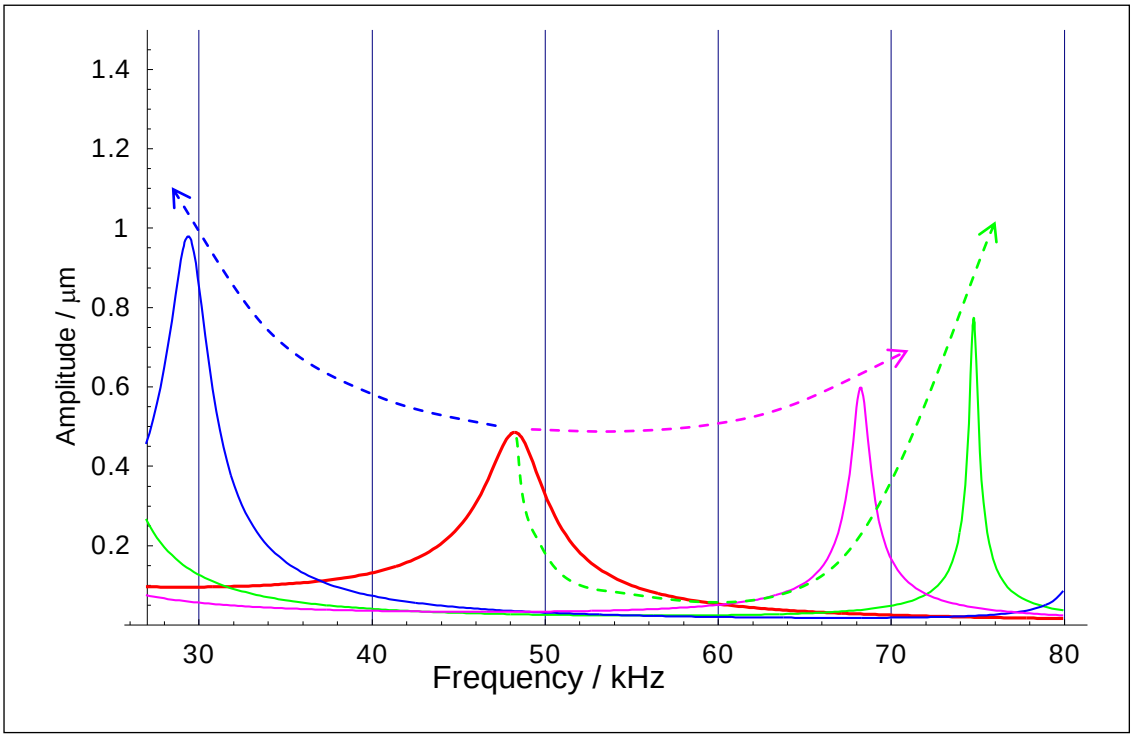

Figure 18: *Frequency response for large changes of the impedance* Z_c.

(red):	$Z_c = 0$
(green):	$Z_c = 10^6\ Ns/m$
(blue):	$Z_C \approx i1500 Ns/m$
(pink):	$Z_C \approx -i1500 Ns/m$

For significantly higher impedance values (10 to 1000 times) the system shows for all three terms a peak movement towards a limit – the boundary condition becomes an ideal fixed support[71].

[71] See also above the limit calculation for amplitude coefficients.

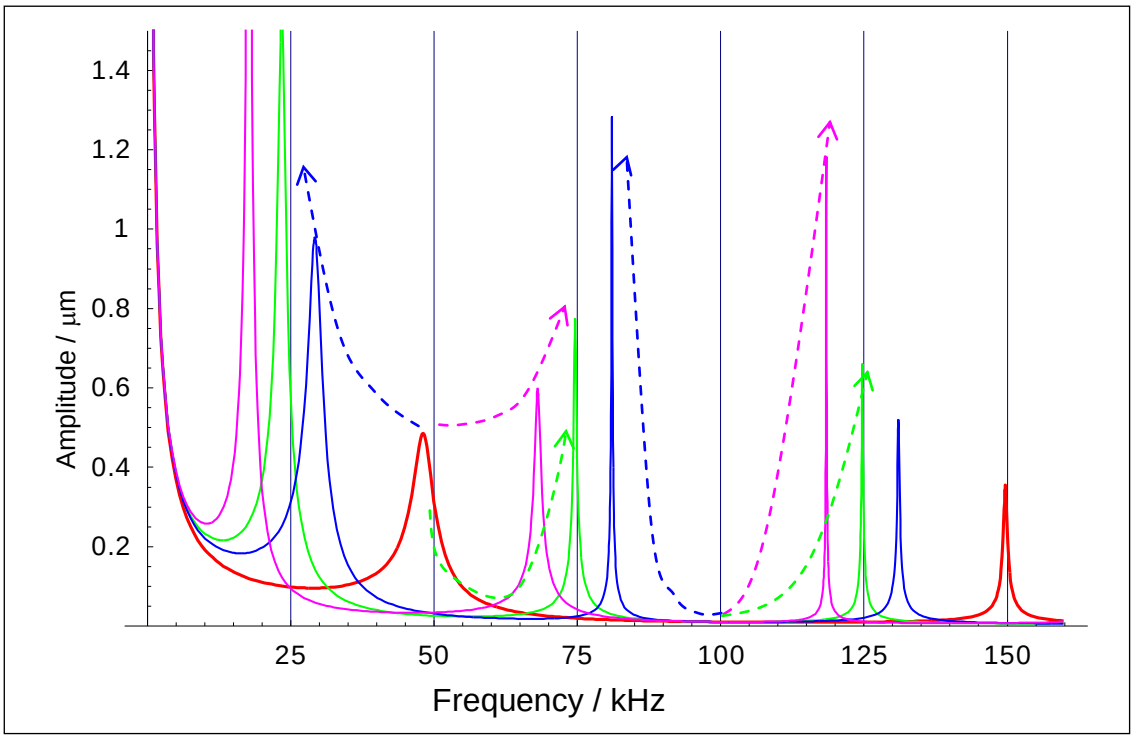

Figure 19: *Frequency response to the same conditions like in figure 18, with a wider frequency span.*

Figures 18 and 19 show the same curves, figure 19 with a higher frequency span. Now not only the peaks from first mode of oscillation are visible but also from second and third mode. While the behavior for the third mode basically equals the one for the first mode, a significant difference is visible for the second mode. With an increasing impedance these peaks appear “out of nothing”, due to an effect, which is not explainable with the analogy of a simple spring-mass-damper system. The absence of resonant peaks is explained above in chapter 4.1.2 (in this case it is even an anti-resonant-phenomenon). The red curve shows nearly a zero amplitude for 100 kHz.

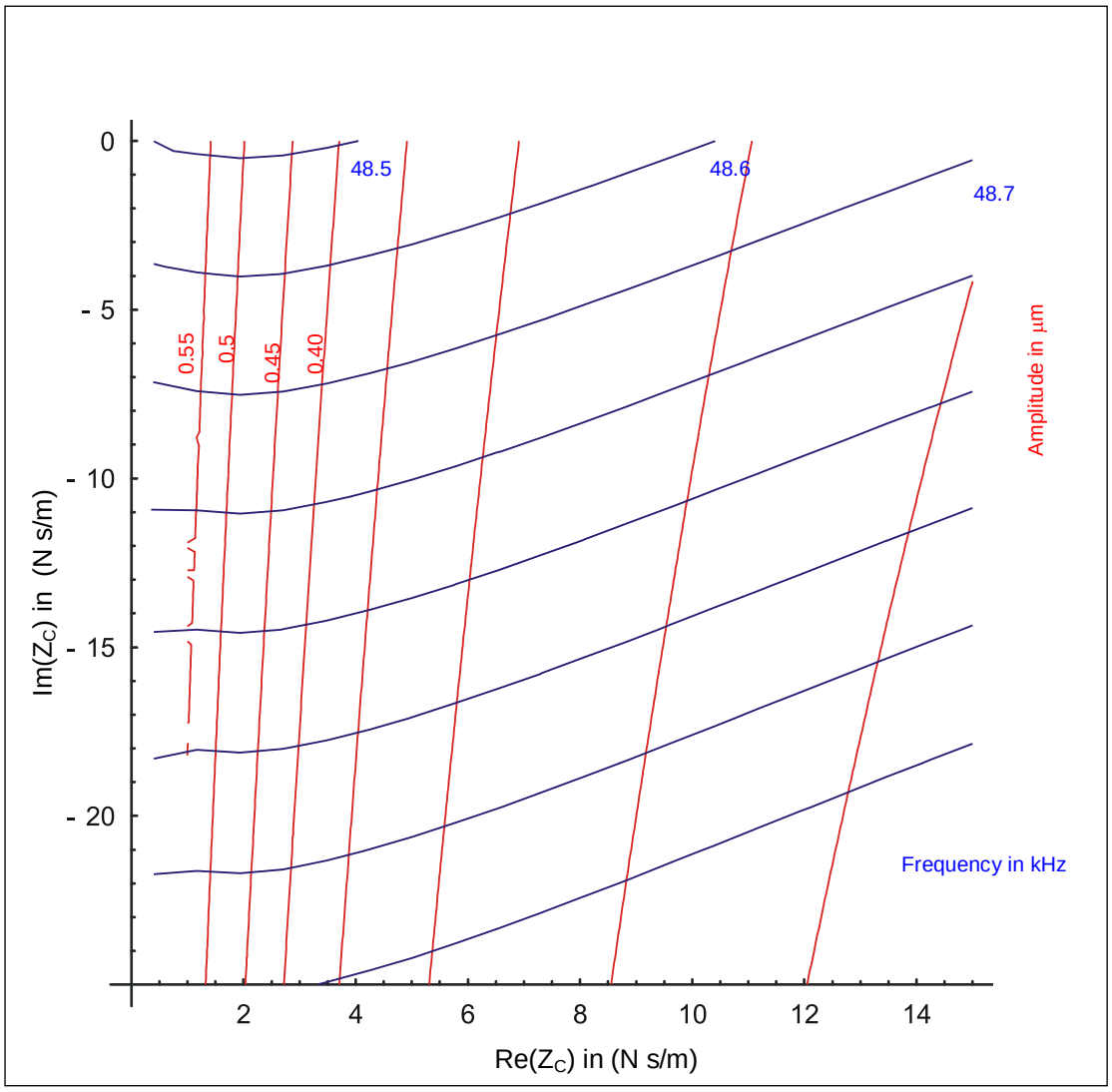

Figure 20: *Frequency and peak of first mode of oscillation, depending on real and imaginary part of the mechanical contact Impedance Z_C.*

Figure 20 shows level curves for the local maximum[72] of the peak at about 50kHz. This has two purposes:

First, it shows the movement of the peak due to specific values of the mechanical impedance. Most polymers will have an impedance in this range.

Second, the numerical values of such curves can be saved in a table, which is further used to find approximated functions. Having simple functions to determine the peaks allows inverting the problem – mechanical impedance can then be calculated from a frequency and amplitude as input values. This is

[72] The maxima were found by numerical differentiation.

important because the LabVIEW measurement software measures the frequency response and determines the peak properties.

4.2 A Preliminary Model for Relating Mechanical Properties of a Polymer with a Contact Impedance

Two mechanical properties of a polymer are of great interest during curing – the viscosity η until the polymer reaches the gelation point and afterwards the Young's-modulus or the shear-modulus of the material.

Viscosity and the degree of cure

Theoretically it is possible to calculate a degree of cure with a given viscosity[73,77]. An example is the Mark-Houwink equation, valid for monodisperse systems:

$$\eta = K \cdot M^{\alpha} \qquad (36)$$

With:

K, α *Constants, dependent on the type of polymer*

M *Molecular weight*

Equation 36 shows two very important relations. First, because of the material constants, it is not possible to calculate the degree of cure without knowing about the chemistry of the polymer. Second, it explains the behavior of a curing polymer at the gelation point. When the polymer reaches the gelation point, the molecular weight (theoretically) increases towards infinity because an infinite molecular network is built. The equation shows that also the viscosity becomes infinite at that point.

[73] See Willoughby: Understanding Cure with the Vibrating Needle Curemeter, p.4.

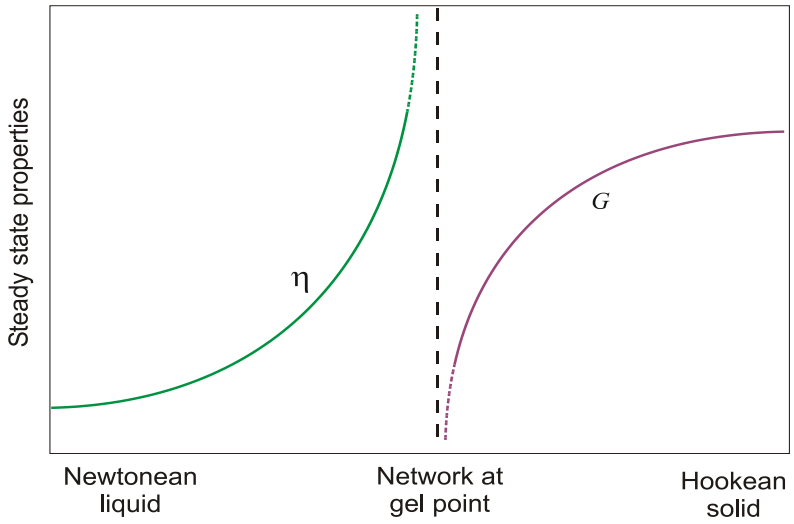

Figure 21: *Viscosity and shear-modulus during curing*[74].

However, it seems to be very difficult to obtain the viscosity of a fluid from the mechanical impedance of a flat circular indenter that performs longitudinal vibrations. The acoustic impedance in the liquid[75]

$$Z = \rho c \qquad (37)$$

is dependent on the density of the liquid and on the velocity c of the spreading of the ultrasonic longitudinal waves in liquid. The relationship of this impedance to viscosity is very complicated and anomalous[76,77,78]. Therefore it was not possible to create a simple model for the liquid state of the polymer.

Shear-modulus and the degree of cure

When the polymer is already in a solid state, a relation between the shear-modulus and the degree of cure can be calculated with the "Gaussian condition"[79], which is valid for several polymers (ideal case):

$$G = N k T \qquad (38)$$

---

74 See Winter: A […] Model for Viscoelastic Liquids and Solids, p. 127.

75 Here for plane waves, what is not exactly the case for the MCM sensor. Actually the indenter has to be treated as a disc piston. It causes a combination of spherical and plane waves.

76 See Taraba: Some thoughts on viscosity measurement with ultrasonic transducers.

77 See White: Principles of Polymer Engineering Rheology, p. 155 et sqq.

78 See Abramov: High-Intensity Ultrasonics, p.20 et sqq.

79 See Willoughby: Understanding Cure with the Vibrating Needle Curemeter, p. 4 et sqq.

With:

N	*Number of chains per volume*
k	*Boltzmann's constant*
T	*absolute temperature*

Equation 38 describes an ideal case, but this is still suitable even for many industrial or commercial polymers. This shows the significance of the shear-modulus during the curing process.

Combining viscosity and shear-modulus

Stress and strain in an ideal elastic material are always in phase if a sinusoidal force is applied. A purely viscous material instead reacts with a 90º phase-lag (stress is in phase with the *rate* of strain). A material, which is neither purely elastic nor purely viscous (hence visco-elastic), will have a phase-lag between 0º and 90º. It is possible to express this with a shear-modulus in terms of a storage- and a loss-modulus:

$$G = G' + i\,G'' \qquad (39)$$

With:

G'	*Storage-modulus or in-phase-modulus*
G''	*Loss-modulus or out-of-phase-modulus*

The in-phase component relates to the elasticity in the material and the out-of-phase component relates to the viscosity.

The process of curing can be divided into the following steps[80]:

1. The viscosity increases due to chain extension.
2. Elasticity develops due to entanglements. The end of work life is reached.
3. Gelation point is reached. (No flow beyond this point.)
4. The crosslink density increases, hence *G'* increases. *G'* is proportional to the degree of cure (see below).
5. The network content increases, *G''* reaches maximum.
6. Network flaws decrease, *G''* decreases and levels out.
7. The crosslinking reaction ceases and *G'* reaches a maximum.

[80] See Willoughby: Understanding Cure with the Vibrating Needle Curemeter, p.14.

G’ is strongly related to the frequency-shift of the MCM resonator during curing, while G’’ is related to the inverse amplitude. However, it could be shown above that these parameters are not independent from each other and that an exact determination is quite complicated.

In the following model the shear-modulus of the curing polymer is calculated because it is proportional to the degree of cure in the later stages of curing.

Both equations 36 and 38 are only valid for steady state conditions. In general the viscosity as well as the Young’s- and shear-modulus have to be considered as frequency-dependant[81]. The mechanical behavior of the resin is determined by the mobility of molecular segments, which can be characterized by a relaxation time. However, in the following model these effects are neglected.

[81] See Djordjevic: Non-contact ultrasonic techniques […].

4.2.1 Mathematical Derivation of the Model for Solids

The second model described in this thesis calculates the shear-modulus from given complex impedance and vice versa.

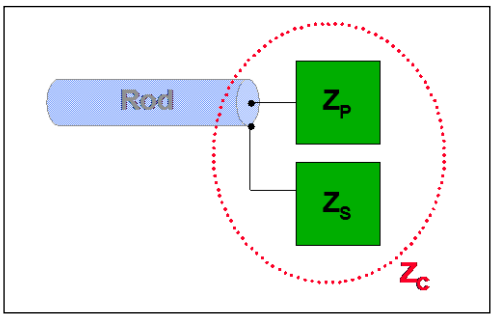

Figure 22: *The contact impedance Z_c.*

First it is assumed that the contact impedance Z_c consists of an impedance Z_P for the attached polymer and constant impedance Z_S for the silicon sealant:

$$Z_c = Z_P + Z_S \qquad (40)$$

The impedance of the sealant is unknown and has to be determined by calibration.

This following model is created to evaluate the mechanical impedance of polymers at the end of a curing process, when the test-piece is already in a purely solid state. It is based on equations for the measurement of the shear-modulus with a "contact impedance meter", developed by G. M. L. Gladwell[82]. The impedance may be written as:

$$Z_P = r_P + i\,\omega\, m_P - \frac{i}{\omega\, q_P} \qquad (41)$$

With:

r_P *resistive term (radiation) ("r_s" referring to Gladwell)*
m_P *inertia ("m_s" referring to Gladwell)*
q_P *compliance ("q_s" referring to Gladwell)*

Gladwell assumes that a rod causes propagating surface waves on a test-piece. This is an important difference to the situation when the polymer is in a liquid

[82] See Gladwell: The contact-impedance meter.

state – when the impedance is mainly defined by wave propagation into the bulk material.

The following assumptions have to be made:

- The test-piece is semi-infinite.
- The wavelength λ_P in the polymer is larger than the circumference of the contact area.

One very important assumption of Gladwell is that the influence of wave propagation inside the bulk of the test piece is negligible. This is possible because the shear-modulus is mainly calculated from the frequency shift of the resonator, and the wave propagation causes mainly losses, which mostly contribute to the decrement of the amplitude but not to the frequency shift[83].

This may be true for a solid, semi-infinite test piece but as mentioned by Gladwell, in case of a piece with finite thickness standing waves can occur. If one imagines the huge and continuous change of sound velocity during the curing process, it is easily possible that this involves one point when resonant conditions are present – the wavelength equals a multiple of $\lambda_P / 2$. Experiments with thin test pieces (3mm to 5mm) showed an additional peak in the frequency plot, what seems to strengthen this theory[84]. To deal with this effect in the right way, additional boundary conditions would have had to be included in an extended model but this is not done here – in this model the part is semi-infinite.

From the second assumption follows the extreme limitation of the model to the end of the curing process. The reason is the indenter that is calculated as a point-source of vibrations (see below).

Resistive term

The resistive part can be calculated as a radiation resistance excited normally by means of a small rigid indenter of circular cross section:

$$r_P = \sqrt{\rho_P E_P}\, A_c (A_1 + B_1 \beta^2) \qquad (42)$$

With:

ρ_P *Density of Polymer.*
E_P *Young's-modulus of polymer.*
A_c *Contact area between magnetostrictive rod and polymer.*

[83] See chapter 4.1.3.
[84] See appendix VII.

A_1, B_1 *Functions of the Poisson's-ratio of the polymer.*

β *Wave number:*

$$\beta = \frac{r_c \omega}{c_{P,s}} \qquad (43)$$

With:

$c_{P,s}$ *Sound velocity of shear waves in polymer:*

$$c_{P,s} = \sqrt{\frac{G_P}{\rho_P}} \qquad (44)$$

r_c *Radius of the circular contact area:*

$$r_c = \sqrt{\frac{A_c}{\pi}} \qquad (45)$$

The coefficients for r_P:

$$A_1 = a_{21} \frac{2\sqrt{2}}{\pi(1-\nu P)\sqrt{1+\nu P}} \qquad (46)$$

$$B_1 = a_{22} \frac{2\sqrt{2}}{\pi(1-\nu P)\sqrt{1+\nu P}} \qquad (47)$$

With:

ν_P *Poisson's-ratio of the polymer*

a_{ij} *Functions of the Poisson's-ratio*[85]

Note: The value of A_1 is about 1, and $B_1 \cdot \beta^2$ is between 0.01 (for low frequencies of about 60kHz and a Young's-modulus of about 3GPa) and 0.30 (for frequencies up to 150 kHz and a Young's-modulus of about 0.5GPa).

The relation between Young's-modulus and shear-modulus is:

$$G_P = \frac{E_P}{2(1+\nu_P)} \qquad (48)$$

[85] The values for these functions can either be taken from a table (see Gladwell: The contact-impedance meter) or they can be calculated from a polynomial approximation, see Mathematica file "contact impedance of curing polymers" on the CD-Rom.

Stiffness term

The surface compliance can be calculated as:

$$q_P = \frac{\sqrt{\pi}}{2} \frac{1-{\nu_P}^2}{E_P \sqrt{A_c}} \quad (49)$$

Inertia term

The inertia term is not included into this model due to Gladwell's conclusion that this term of the mechanical impedance is two magnitudes lower than the stiffness term.

$$m_P = 0 \quad (50)$$

Minimum Young's-modulus for model

Equation 42 is actually an arithmetic series, truncated after the second order term of β. This is only possible for values of $\beta < 1$. Gladwell suggests a value of $\beta < 0.7$ to keep the error in an acceptable range[86]. The following calculation shows the minimal value of the Young's-modulus, for which this is valid:

$$\beta = \frac{r_c \omega}{c_{P_s}} < 0.7 \quad (51)$$

From this follows:

$$\frac{2\sqrt{2\pi}\sqrt{A_c}\, f}{\sqrt{\frac{E_P}{(1+\nu_P)\nu_P}}} < 0.7 \quad (52)$$

This can now be solved for the Young's-modulus:

$$E_P > \frac{8\pi^2 f^2 {r_c}^2 (1+\nu_P)\rho_P}{0.7^2} \quad (53)$$

Typical values for the MCM sensor and for an epoxy-resin are:

$$f \to 65kHz,\ r_c \to 1mm,\ \rho_P \to 1100kg/m^3,\ \nu_P \to 0.35 \quad (54)$$

Herewith the Young's-modulus can be calculated as:

$$E_P > 1.011 \cdot 10^9 \quad (55)$$

---

[86] See Gladwell: The calculation of mechanical impedances [...].

In that case the minimal shear-modulus would have to exceed $1GPa$, a value that will be reached by an epoxy, but for softer materials like some polyurethanes this is probably not the case. The conclusion is that for further reduction of errors either the model has to be adapted to larger indenters, or the contact area of the indenter itself has to be reduced.

Determining the Young's-modulus

By applying all the given formulas to equation 40 the contact impedance becomes a function of E_P, ν_P, f, A_c, and ρ_p. A_c is definitely a constant value and for a first approximation ν_P and ρ_P can be set constant for the end of the curing process. Then it is possible to solve for E_P, and with the further assumption that all variables except Z_c are real, this can be done by just considering the imaginary part:

$$\mathrm{Im}(Z_c) = -\frac{1}{2\pi f q_P} = -\frac{\sqrt{A_c}\, E_P}{\pi^{3/2} f(1-\nu_P{}^2)} \qquad (56)$$

Now solving for E_P:

$$E_P = -\frac{\pi^{3/2} f(1-\nu_P{}^2)}{\sqrt{A_c}} \cdot \mathrm{Im}(Z_c) \qquad (57)$$

4.2.2 Studies of System Behavior

Figure 23 shows the frequency response of the sensor due to contact impedance calculated with Gladwell's model.

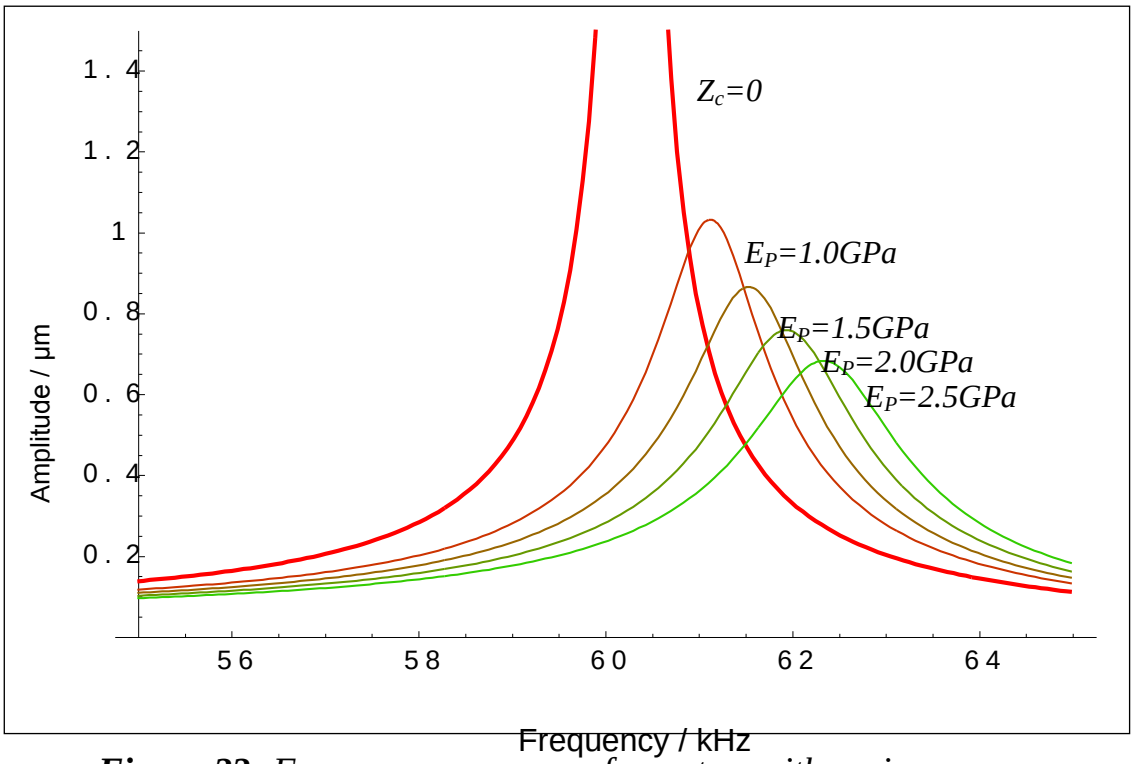

Figure 23: *Frequency response of a system with curing epoxy.*

The following values were used:

- $\rho_P = 1200\,kg/m^3$
- $\nu_P = 0.35$

As shown above, the equations for the contact impedance depend on several functions of the Poisson's-ratio. For the curves in figure 23 these values were kept constant, but in general it has to be assumed that the Poisson's-ratio changes during a curing process. While the final value for an epoxy resin may be about 0.35, short after gelation it could have a rubber-like value of about 0.5. If the development of this parameter is known, it can easily be included into the model[87].

[87] See Mathematica file "contact impedance of curing polymers" on the CD-Rom.

4.3 Inversion of the Models

The purpose of the inversion of the models is to determine mechanical properties by analyzing a sensor output. These measured values can be an input for the following model, and the output will be the shear- or Young's-modulus[88] of the test sample.

The calculation consists of the following steps:

- All constant values and formulas are applied to equation 32 to calculate the effective output power P_2 of the receiving coil as a function of f and of the real- and imaginary part of the contact impedance[89].
- For discrete values of the real- and imaginary part of the contact impedance the resonant frequency and amplitude is found with a numerical solving for a local maximum. This is done for about 100 values of $\mathrm{Re}(Z_c) \in [0.5,15]$ and $\mathrm{Im}(Z_c) \in [-25,0]$ in Ns/m. A table is generated with the values.
- A least-square fitting is performed with a linear combination of hypothetical functions of Z_c, for both resonant amplitude and frequency.
- The formulas of the fittings are exported as strings, and imported to a numerical function solver in LabVIEW. Up to this step everything has to be done manually. And after every change in the system setup (if mathematical parameters change) this has to be repeated.
- The LabVIEW program is now able to solve for the matching values of the contact impedance, after it has measured the frequency response of the sensor and determined the resonant peak. This is done for each measurement point.
- The determined impedance is used for a further calculation to determine the Young's-modulus of the material with equation 57.

---

88 Actually Gladwell's model determines the shear-modulus. However, a Poisson's-ratio is needed therefore, hence the output can be given either as shear- or young's modulus.

89 See Mathematica file "Reverse determination of Zc" on the CD-Rom.

5 SENSOR DESIGN

In this chapter the design considerations for the sensor are described. First, the boundary conditions for the development are discussed. Then some parameters are discussed by performing some case studies using the theoretical model. This leads to several conclusions to improve the design. In the last part the final sensor design for the prototype is described[90].

5.1 Boundary Conditions for Sensor Design

The following boundary conditions were given during the design of the sensor:

- Magnetostrictive rod diameter shall not exceed 2mm.
  Otherwise an important assumption for the model is invalid – the circumference of the contact area has to be less than the wavelength in the polymer. See chapter 4 for details.
- Magnetostrictive rod length : diameter shall not exceed 20 : 1.
  Otherwise transversal vibrations can occur in the rod[91].
- Magnetostrictive rod diameter shall not fall below 2mm.
  Otherwise manufacturing of the sensor core becomes too difficult.
- Sealant thickness (between rod and sensor core shell) shall not fall below 1mm.
  No experiments were performed with thinner sealants; these could cause a stiffer support of the rod at the end where it is in contact with the polymer and therefore decrease the sensitivity.
- Sensor housing diameter shall not exceed 20mm.
  Otherwise the sensor becomes too big to be mounted into a mold for industrial applications.
- Sensor core shall be independent of the shape of the mold.
  This assures that the sensor can be adapted to different geometrical needs, without changing the active parts.
- Excitation voltage amplitude shall not be more than 10V.
  This allows using standard function generators for excitation.

---

90 As shown in appendix VI.

91 See Vadel: Magnetostrictive Sensor with variable boundary condition […].

- Internal resistance of power supply shall be 50Ω. (Together with the voltage condition this limits the peak power output to 0.5W.) 50Ω is a standard value. It is necessary to define an internal resistance to limit the power output for the theoretical model, otherwise resonant conditions would lead to infinite amplitudes.
- Studies with the theoretical model as well as preliminary experiments showed good results with nickel or nickel based alloys as magnetostrictive materials. Using so-called "giant magnetostrictive materials" like Terfenol-D or other rare-earth-based materials was under theoretical consideration but no experiments were carried out. For the current sensor configuration nickel was chosen because of its durability (even at high temperatures) and reliability, and because of its low price. The following material properties are assumed for the magnetostrictive rod:

Relative permeability:	μ_r	*60*
Magnetostrictive constant:	Θ	$-15 \cdot 10^6 Pa/T$
E-modulus nickel:	E_R	*210GPa*
Density nickel:	ρ_R	*8900kg/m³*

The following system variables were leftover for case studies (and probably real optimization in future research):

- Position and length of the excitation coil.
- Position and length of the receiving coil.
- Number of windings for both coils.
- Length and diameter of the magnetostrictive rod.
- The operating mode of resonance.

Theoretical case studies and experiments were performed to optimize the sensor in the following way:

- The quality of the resonant peak should be maximized.
- The amplitude drop during the beginning of the curing process should be significant[92].

[92] Initial experiments showed amplitude drops to less than 10% of the initial value. This seems to be too much to maintain linear relations in the signal-conditioning. Therefore

- The frequency shift (especially during the end of the curing process) should be maximized.

One coil vs. two coils

A fundamental question about acquiring any information from the magnetostrictive rod is whether one or two coils (combined or separated excitation and reception) should be used. In general it is possible to measure a change in the impedance of the excitation coil and therefore it is not essential to have a separated receiving coil[93]. However, in this case the desired information has to be electrically separated from the excitation circuit. The theoretical model cannot be of help for this decision because from a theoretical point of view (with no losses) both methods are equal.

Initial experiments showed a better S/N ratio for a setup with two coils. Hence this configuration was chosen for the MCM sensor prototype.

5.2 Case Studies

For a real optimization of the sensor it would be necessary to evaluate the model with all variables at once, what would lead to the mathematical difficulty of finding a maximum in a multidimensional problem. However, it is possible to achieve the following conclusions from the theoretical sensor model by dealing with the variables separately or just in relation with one or two other variables[94]:

1. Operation at first resonant mode is best

- Power output is higher than at 2nd mode.
- Frequency shift during end of curing process is higher.

All initial experiments showed approximately a 10 times higher output for 1st mode compared to 3rd mode operation, what strongly supports the theory. However, initial experiments with an open magnetic flux return part showed similar results for 2nd mode operation compared to 1st mode operation. As mentioned above, this cannot be explained with the theoretical model, which shows *zero* output for 2nd mode. However, further experiments with a better magnetic flux return path showed a *weaker* output for 2nd mode.

---

the value should not be maximized but kept at a significant value to maintain a good S/N ratio.

93 See Ackermann: [...] Characterization of Magnetostrictive Actuators.

94 Detailed information about these case studies (including graphs) can be found on the CD-Rom, Mathematica file “optimization”.

2. Longer rod is better than shorter rod

The resonant frequencies of the rod are anti-proportional to the rod length. But the frequency shift during the end of the curing process is *not* anti-proportional to the rod length. The shift decreases only slightly by increasing the rod length (in the range of *50kHz* to *200kHz*). Assuming the frequency resolution is anti-proportional to the frequency the S/N ratio becomes better for longer rods.

Additional to the data from the model the following information support this conclusion:

- Longer rods lead to longer sensor cores, which can be manufactured easier.
- Longer rods (with the same diameter) have a higher volume, which can be pervaded by magnetic flux. Hence more magnetic energy can be transferred to the mechanical system and back.

3. Receiving coil should be at the free end

The increment of the power output at the 1^{st} resonant frequency is slightly higher if the receiving coil is placed at the free end.

However, the difference for both cases is nearly negligible and could not be measured in initial experiments. On the other hand it causes no constructional difficulties to realize this.

4. Rod diameter

Reasonable conclusions about the optimal rod diameter are difficult to obtain because this parameter cannot be studied independently. Changing the rod diameter causes also a change in the coil diameter and therefore the number of turns has to be adapted to maintain certain impedance (see below). However, the output power was calculated for two discrete values of the diameter: 2mm and 4mm. The 4mm-rod showed a higher output power, what could again be explained with the higher volume (see above). Further, the imaginary part of the contact impedance (Gladwell's model) is proportional to the square root of the contact area ($\sqrt{A}$), what indicates a higher frequency shift for a bigger diameter.

On the other hand, a problem of diameters was discussed in chapter 4 (minimum Young's-modulus), what led to the conclusion that it is better to have smaller diameters. Therefore, the final diameter was chosen to be 2mm.

5. Number of turns at the coils

It is assumed that the best results can be achieved if the coil impedances match the impedances of the function generator and the input amplifier, respectively. The function generator has an output impedance of 50Ω and (as shown in chapter 8) the first stage of the input amplifier "*A1*" *has* an input impedance of about 25Ω.

With this boundary condition the optimized number of turns is a function of coil radius, coil length, and the frequency. It is not necessary to calculate this with the sensor model; instead more simple formulas can be used[95].

[95] See Collins: Analog Elecronics Handbook, pp. 33-38.

5.3 Final Design

Magnetostrictive rod

As mentioned in chapter 5.1 nickel was chosen as magnetostrictive material. It must not necessarily be pure nickel but can also be a nickel alloy. Nickel 200 for example (99% Ni) has nearly the same magnetostrictive properties as pure nickel (99,9% Ni or more). To archive optimum magnetostrictive properties it can be annealed after machining (an oxide layer will emerge at the surface).

The magnetostrictive rod has a diameter of 2mm and a length of 40mm. It is supported by a silicon sealant at the top of the rod and a rubber o-ring as a slide rest at the middle of the rod. The sensor housing is sealed at the tip of the rod but the circular abutting face of it is in direct contact with the polymer.

Solenoids

The magnetostrictive rod is surrounded by two solenoids. The “upper” solenoid (near the polymer) is the excitation coil.

The coils have to be made of (insulated) magnet wire. This wire has to be connected either in the sensor housing itself or outside the housing to standard hook-up wire. The first solution has the advantage that the usually thin and vulnerable insulation is protected but the connections have to be made in a very small space.

Core shell:

Two identical tubes are used to close the magnetic circuit. Each tube has some kind of tapering at one end, to create a transit area for the magnetic flux.

The material has to match the following conditions:

- It has to be a material with a high permeability (at least more than 100) and low magnetic losses at frequencies up to 100kHz.
- It has to be machinable.
- It has to be corrosion resistant because it is in direct contact with curing polymers and probably with aggressive cleaning fluids. (A coating could also be possible, but it would be difficult to apply a reliable protection at the edges.)

Housing:

To mount the sensor into a mold a drill hole with a diameter of 18mm±0.3mm is needed. The mold needs to have a thickness of 33mm to 38mm.

The sensor is fixed to the mold with three Philips screws, therefore three holes with M3 threads are needed in the mold. Rubber o-rings can act as springs and help to attach the sensor in the right position. Once the hex screws are fixed, the Allen-key setscrews can be fastened to secure the housing in its position.

Further it is required that the mold surface is flat in the region where the sensor is mounted.

If the mold does not meet the requirements mentioned above it is possible to change the housing without changing the design of the sensor core.

Electric connection:

Two wires from each of the two coils are bundled in a heat shrink tubing and led out of the sensor housing.

The current design does not describe further electric connectivity to the signal-conditioning unit but the interface connector is a 9-pin Sub-d connector. Either a direct connection is possible, or a multiplexing unit (4 wires per sensor) can switch to a sensor array.

5.4 Discrepancies between the Theoretical Model and the Practical Realization

The following items describe discrepancies between the theoretical model (including the assumptions) and the practical realization of the sensor, e.g., how the sensor is built:

1. Support of the rod:
   The model does not include a support other than the sealant at one end. However, the o-ring in the middle of the rod creates an additional support. Because the o-ring is located at a node of displacement (for first mode operation), its influence is neglected.
2. Closed magnetic circuit:
   An ideal magnetic flux return-path was assumed in the model. A sensor core shell made of Permalloy 80 shall assure this. However, a gap between the rod and the shell exists, and the field lines have to cross a

small volume of air and sealant, respectively. This increases the magnetic resistance significantly, but was neglected in the model.

3. Magnetic field lines leave rod not at its faces.

6 MANUFACTURING THE SENSOR

Magnetostrictive rod

Raw material:

The magnetostrictive material used for the sensor prototype comes as a hard tempered nickel wire[96], with the wanted diameter of 2mm. The wire is straightened by hand and then cut to the desired length of 40mm[97].

Surface preparation:

The rod surface, which is in contact with the polymer, is grinded and polished with a machine that is normally used for microscope sample preparation. The side of the rod is polished to remove metal oxides but not grinded. The surface, which is in contact with the sealant, is prepared with a Primer[98].

Support:

Two high-temperature o-rings are used to support the rod.

Sealant:

The rod is sealed with a 100% silicon sealant[99]. The sealant is applied into the gap between the rod and the core shell with a syringe.

Solenoids

The coils are made of 0.01mm^2 (36AWG) magnet wire[100]. Figure 24 shows the manufacturing of the coils. Some adhesive tape is attached around a thin rod. After winding the coils onto this tape a few drops of glue with very low viscosity are applied to it. This helps to keep the wire together. Then the coils are removed from the rod, and fixed into the core shell with silicon sealant before the rod is mounted into it. Now it is possible to pull out the tape inside the coil but this is not necessary when it sticks to the wire strongly.

---

96 99.9% pure nickel, temper: hard. Contains less than 0.008% silicon. Manufacturer: *GoodFellow*. See appendix III for detailed information about magnetostrictive materials. As mentioned above, cold drawn or hard tempered wire may not have appropriate magnetostrictive properties. Hence it should be annealed after all mechanical preparation but this was not done during manufacturing of the prototypes.

97 The final length has to be measured with high accuracy; this value has to be entered into the theoretical model.

98 RTV 1200 Primer. Manufacturer: Dow Corning, USA. Several experiments showed that the primer improves the bonding to the sealing significantly.

99 RTV 732 High temperature silicon sealant. Manufacturer: Dow Corning, USA.

100 Manufacturer: Belden electronic division, USA. Insulation stands 130˚C.

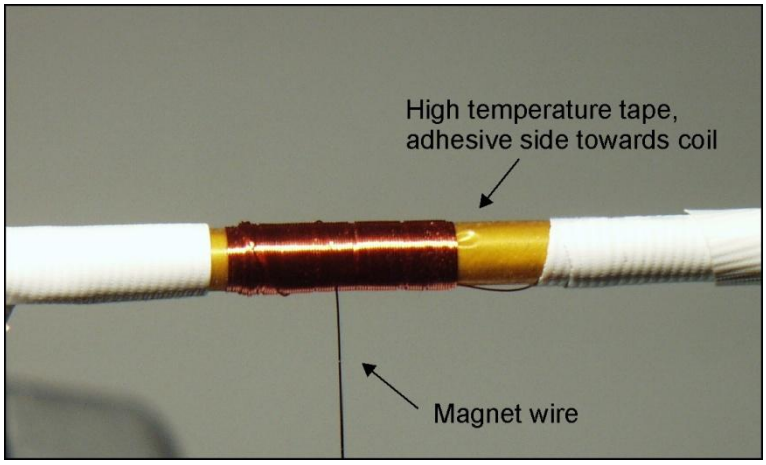

Figure 24: *Manufacturing of the coils.*

Core shell

Two identical *Permalloy 80* tubes are used to close the magnetic circuit[101]. Both tubes got several windings of Teflon tape around them, to create an electrical insulation and to reduce the gap between the core and the housing.

The wires from the coils are guided through a small channel (made by hand with a file) to the outside of the shell. There they are guided in between the Teflon tape for protection.

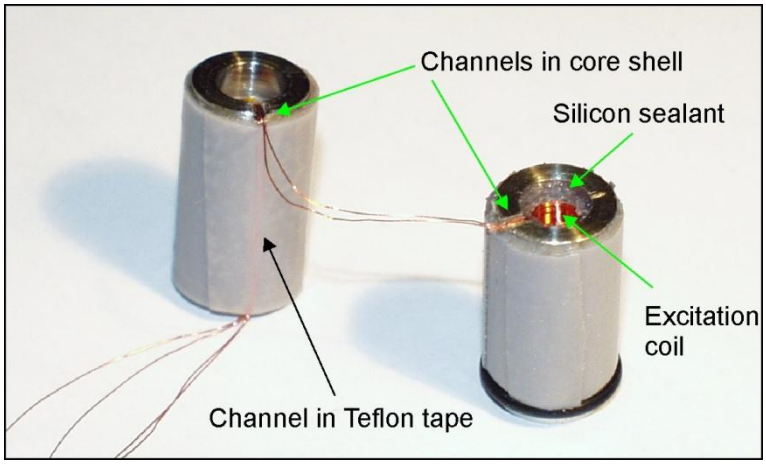

Figure 25: *Core shells with coils.*

[101] These parts were manufactured by an external machine shop.

Housing

The sensor housing is made of aluminum. It consists of a housing tube and a cover plate[101]. The cover plate is fixed with three metric M2 Philips screws (8mm length). The outer, disc shaped part of the housing contains thee threads M3 for setscrews, to maintain an exact distance to the mold where the sensor is mounted. Three holes allow fixing the whole sensor with M3 screws to a mold.

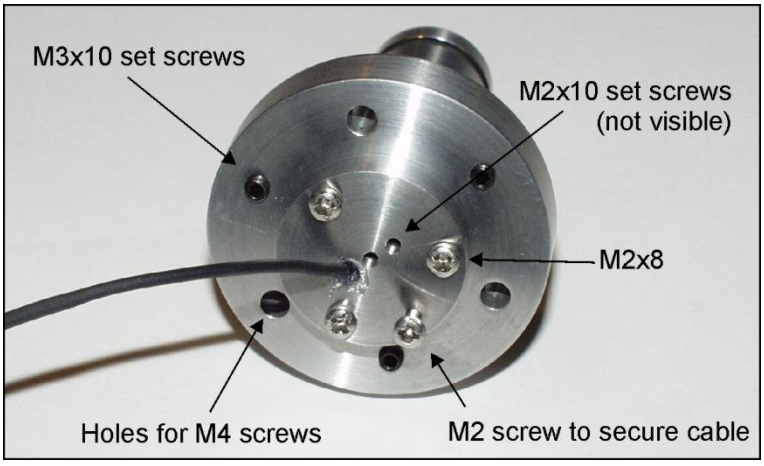

Figure 26: *Bottom view of assembled sensor.*

Electric connection

Two wires from each of the two coils are bundled in a heat shrink tubing and led out of the sensor housing. Each sensor has a male 9-pin sub-d connector.

Assembling the sensor components

The sensor is assembled in the following order:

1. Filing small channels into the face sides of the core shells. Putting a small o-ring into the upper shell part.
2. Winding Teflon tape around the core shells, then cutting a small channel into this tape. Putting one o-ring around the upper shell part.
3. Winding the coils and attaching them into the shells. Protecting the wires with silicon from being harmed at the sharp edges of the channel in the metal. Then guiding the wires from the excitation coil through the channel at the other part and closing it with one more layer of tape. (See figure 24.)

4. Attaching the o-rings for the center support at the shells. Then closing the core shell (with an additional layer of tape) and inserting the rod through one end.
5. Inserting the core unit into the housing.
6. Protecting the wires with a shrink tube and guiding them through the cover plate.
7. Inserting a thin plastic washer (not shown in drawings) into the housing, between the cover plate and the sensor core. Then closing the housing.
8. Adjusting the height of the core and the rod using two setscrews M2.
9. Sealing the rod and the core with silicon sealant (applied with syringe).

7 THE MEASUREMENT CHAIN

In this chapter the complete measurement chain is described, from the sensor itself up to the software, which controls the measurement hardware and evaluates the acquired data. Further, errors are analyzed and some characteristics of the measurement system are given.

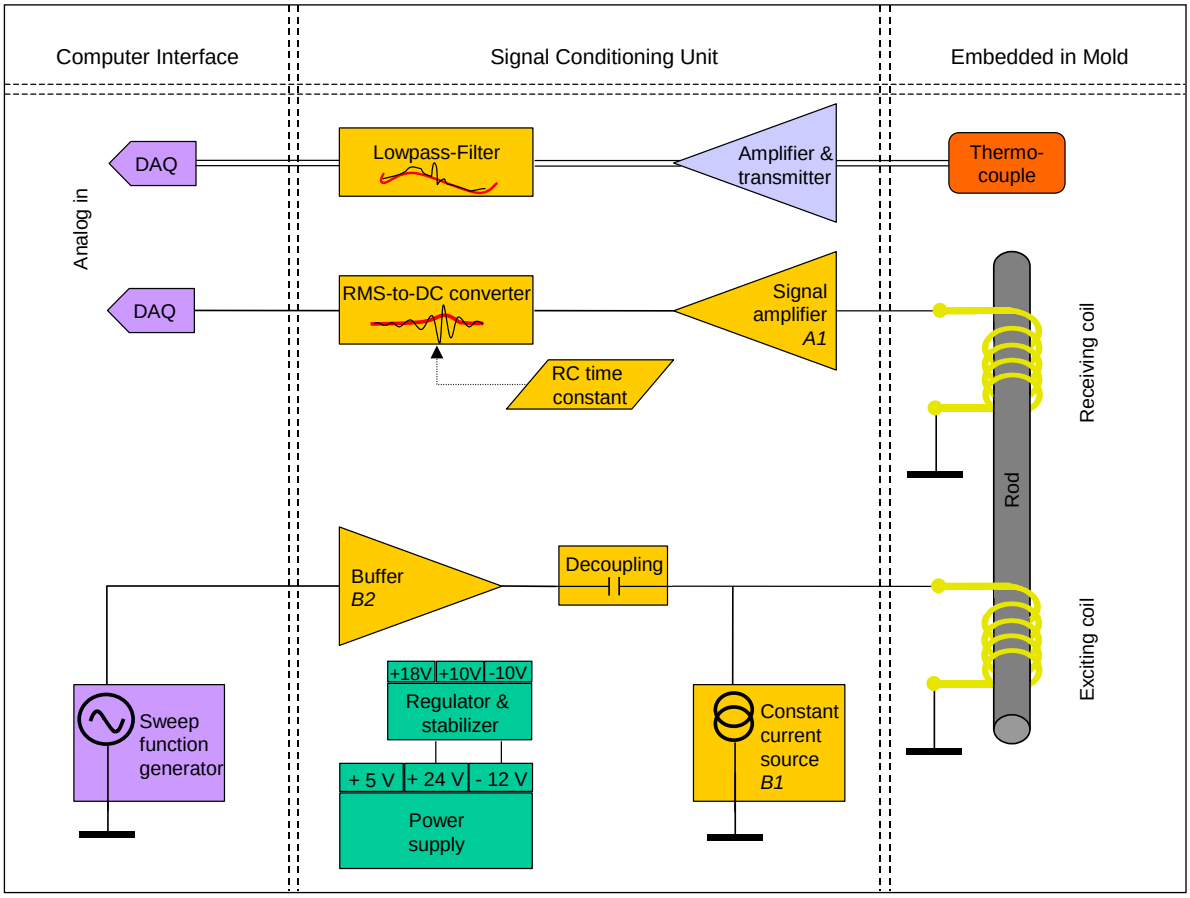

Figure 27: *Signal-conditioning and interface*[102] *(simplified).*

7.1 Sensors

MCM sensor

The first element in the measurement chain is the sensor itself. All experiments were performed with a sensor that conforms to the drawings in appendix VI, unless otherwise noticed.

[102] See appendix V for schematics.

Temperature probe

The temperature sensor is not directly included in the MCM sensor and is therefore placed separately. During the experiments the thermocouple was mounted in an additional drill hole, 12mm away from the sensor tip, but also in contact with the polymer. The sensor is a K-type thermocouple and connected via a mini-thermocouple connector with the signal-conditioning unit.

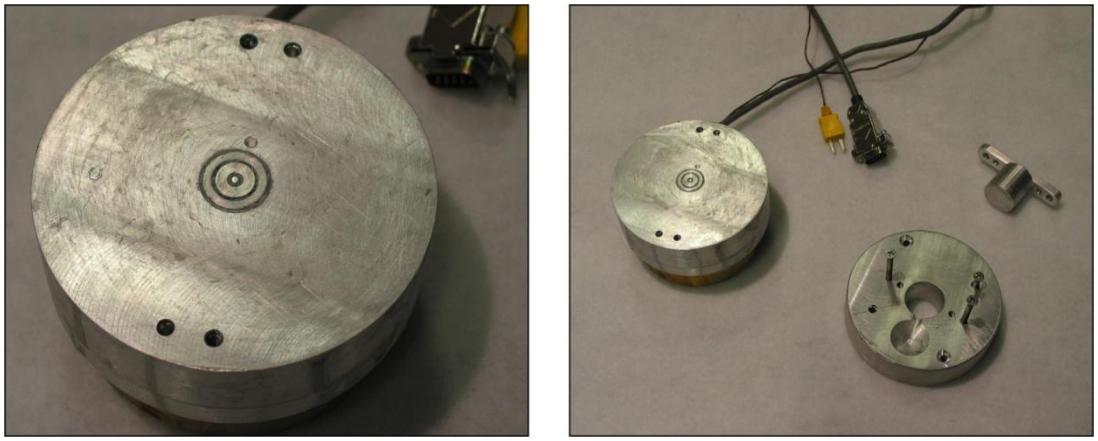

Figure 28: *MCM Sensor and a thermocouple mounted in a small experimental mold.*

Both sensors are mounted into a small experimental mold[103] (made from solid aluminum). It consists of three parts:

1. Base plate with mounted sensor.
2. Plate with a cylindrical hole (height: 27mm, diameter: 25mm) for the test piece.
3. Piston to close the mold.

7.2 Signal-Conditioning and Interface Unit

The MCM signal-conditioning unit consists of a power supply, an industrial thermocouple transmitter (4-20mA), several different electronic circuits, which are directly connected to the sensor solenoids, and some electronic components for TTL signal generation and switching on and off the amplifier circuits[104].

[103] Made by A. Dominauskas.
[104] For schematics of the constant current source see appendix V.

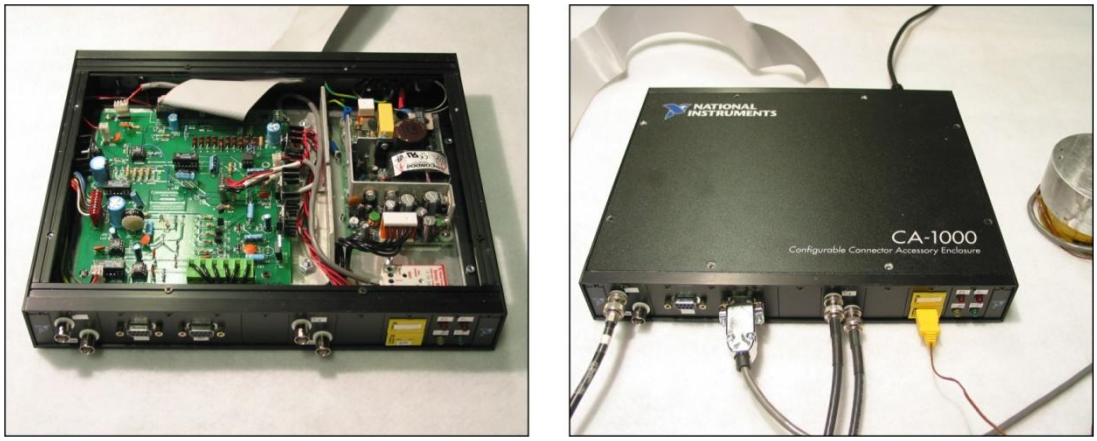

Figure 29: *Signal-conditioning and interface unit.*

Figure 29 shows a picture of the signal-conditioning unit. The housing is a *CA-1000* by *National Instruments*. On the left hand side the self-designed PCB is mounted and on the right hand side the power supply[105].

Power supply

The used power supply serves +5.1, +24 and –12 Volt. The efficiency is about 70%.

Table 2: *Power consumption and heat dissipation*

	Power supply max. Permanent current	Average current with all subsystems enabled	Power supply heat dissipation
+ 5 V	4 A	0.5 A	1.1 W
+ 24 V	1 A	0.4 A	4.1 W
- 12 V	0.4 A	0.2 A	1.0 W

The available power of the power supply is more than sufficient. Even a smaller power supply could be used in the future.

[105] A small aluminum plate exists to cover the power supply when the housing is open, for safety reasons when the system is running.

Table 3: *Heat dissipation in the signal-conditioning unit.*

PCB power dissipation	11.6 W
Power dissipation in sensor during measurement	3.0 W
Overall circuit power consumption (sensor + PCB)	14.6 W
Overall power supply heat dissipation	6.2 W
Overall heat dissipation in signal-conditioning unit	17.8 W

Thermocouple transmitter

The transmitter by *Weed Instruments* is calibrated for K-Type thermocouples. The output is between 4mA for 0ºF (-17.8ºC) and 20mA for 250ºF (121.1ºC). This current is led through a 1%-tolerance shunt resistor of 220Ω. The voltage drop is RC-filtered and led to the multifunction-interface-board (see below).

"*B1*" Constant current source for excitation coil

The constant current source is necessary for the actual sensor design because no permanent magnets are used to generate a biasing magnetic field. The circuit consists of a *78R033* voltage regulator together with a constant resistor (actually several resistors in parallel for better heat dissipation). A diode protects the circuit from reverse current. The voltage source can be activated or deactivated via pin 4, therefore the operational amplifier (OP) *U32* is used as a voltage level shifter.

"B2" Amplifier for excitation signal

The amplifier is a common collector amplifier (emitter follower) with one npn-transistor. The input impedance is some $k\Omega$. There is no voltage amplification. The output is decoupled from the coil with capacitor. The amplifier can be activated with a TTL signal at the optocoupler *U1*. The signal is routed through this amplifier stage with the relays *K2* and *K3* enabled. Hence all digital outputs *B0*, *B2*, and *B3* have to be high to use the amplifier.

However, all experiments with the current sensor configuration showed that the amplifier is not necessary to maintain a clear signal. It was necessary in preliminary experiments without a magnetic flux return path (and therefore high power losses) and could become necessary again for new sensor configurations.

"A1" Low impedance receiving signal amplifier

The circuit is a low input impedance common base amplifier. The output impedance is high. The transfer function was measured[106] with a connected receiving coil and showed a good linear behavior for input voltage and current, respectively. Therefore the output voltage is proportional to the square root of the input power:

$$U_{out} = \sqrt{x \cdot P_{in}} \qquad (58)$$

x could be determined to: $21730V/A = 21.7k\Omega$.

It is assumed that the input power P_{in} equals the output power of the receiving coil P_2, which contains a correction factor K_2.

RMS-to-DC Converter

The next stage of the receiving signal conditioning is a so-called true root-mean-square to DC converter[107]. The converter gives an output signal of $1V_{DC}$ per $1V_{rms}$ of the AC input signal. The maximum value is $1.0V_{rms}$.

By using this converter it is not necessary to sample the high frequency signal itself and calculate the RMS-value of the oscillations via software. The output signal of the converter changes only slightly with the steps of the frequency sweep and therefore allows significantly lower sampling rates.

For example a NI-5411 function generator uses about 500 steps during a frequency sweep. The programmed time for this sweep is 1000ms, which means a sampling rate of only 5kSamples per second is sufficient for achieving 10 samples per step.

The converter is configured with a capacitor, which forms an RC time constant together with an internal resistance (see the manufacturer's datasheet for a detailed transfer function). In the working range of the MCM sensor the converter can be assumed to work with the transfer function:

$$U_{Out} = U_{RMS} = \sqrt{\frac{1}{T}\int_T (U_{in}(t))^2\, dt} \qquad (59)$$

---

[106] See appendix VII.3.

[107] A one-chip solution *AD737* from *Analog Devices, inc* is used.

The error is (according to the datasheet):

$$\frac{\Delta U_{out}}{U_{out}} = 2\% \qquad (60)$$

Voltage amplifier

The last stage of the receiving signal conditioning is a proportional voltage amplifier with high input impedance and low output impedance:

$$U_{out} = 5 \cdot U_{in} \qquad (61)$$

The error could be determined with a separate measurement:

$$\frac{\Delta U_{out}}{U_{out}} \leq 2\% \qquad (62)$$

The purpose of this amplifier is to increase the voltage to a level between *0V* to *5V*, what can easily be acquired with the multifunction-interface-card. This span is the same for the temperature reading – this allows the same gain settings for both channels and reduces the noise level.

7.3 Data Acquisition (DAQ) and Sine-Wave Generation

The data to be acquired consists of a temperature measurement (every couple of seconds) and of the resonance peak, which is between *0V* and *5V* and a sampling rate of at least 1kSamples per second.

A necessary input signal for the interface circuit is a sine wave with a frequency sweep. The function generator for this sweep must be software programmable and hardware triggered. The voltage should be up to $10V_{pp}$ at 50Ω load. The frequencies are between *50kHz* and *300kHz*.

7.4 MCM LabVIEW Measurement Software

The MCM Software is created in *LabVIEW*, which is a graphical programming language. LabVIEW uses symbols instead of text. Internally the software is controlled by the flow of data from one symbol to the next.

Figure 30 shows the front panel of the main VI (*virtual instrument*), which is the user interface. The big graph in the center shows the development of four parameters over time: Resonant frequency and amplitude, predicted Young's-modulus of the test sample, and temperature. The upper graph shows the frequency response of the sensor during a sweep. The buttons in the upper right are for activation of the *B1* constant current source and for restarting an

experiment. Restarting means that the time counter is set to zero, what affects the output files.

Two output files are generated: One file saves the acquired data as shown in the big graph, together with exact timing information in minutes. The other file is only generated after pressing the "save" button. This saves one frequency response as shown in the upper graph. Both files can easily be opened with Microsoft Excel.

On the left hand side the status of the DAQ system is visible. In the lower left corner the predicted complex and real part of the contact impedance of the test piece is shown, as well as the Young's-modulus.

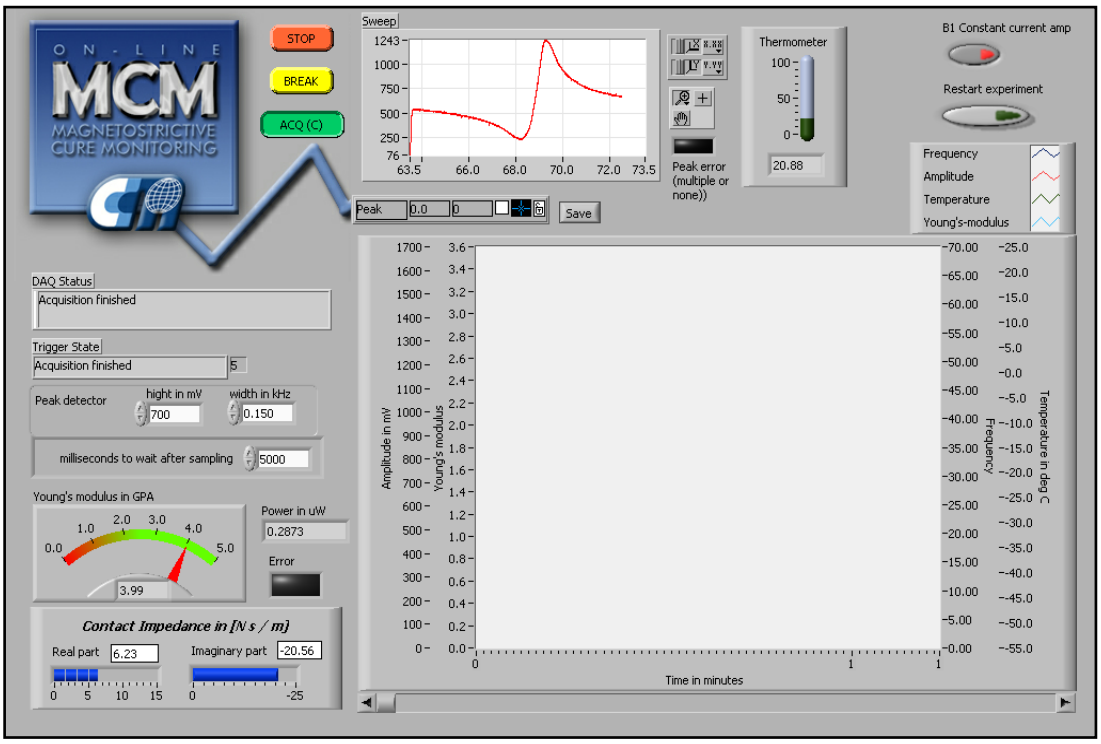

Figure 30: *MCM LabVIEW measurement software main VI frontpanel.*

Internally the program consists of the following parts:

- Filter for the frequency response: A 4th-order Butterworth filter (available as a preprogrammed standard function in LabVIEW) with a cutoff frequency of *120Hz* is used to smooth the data before they get processed in the peak detector. As a result also the peak maximum shifts to higher frequencies because of the time lag created by the filter. However, this effect is only in the range of 0.05kHz and it can

be assumed that it is always constant because the shape of the peak does not change significantly and is therefore neglected.

- Peak detector: It detects frequency and amplitude of the maximum of the frequency response. The parameters *width* (in kHz) and *height* (in mV) have to be adjusted carefully to assure that the right peak is detected and not a local maximum generated by noise. The peak detector is available as a preprogrammed standard function in LabVIEW.
- Arm and Trigger: A loop with the sequence of the following steps is generated:
  - Arming the DAQ hardware.
  - Resetting and arming the sweep generator.
  - Generating a TTL impulse at the multifunction board, which is connected to both the function generator and the DAQ board via the signal-conditioning unit.
  - Waiting until the sweep is finished and the DAQ data is transferred to the computer memory.
  - Handing the data to the filter, peak detector, impedance converter, etc.
- Impedance converter[108]: Input is peak voltage and peak frequency; output is real and imaginary part of the contact impedance, and the Young's-modulus.
  Additionally the approximated formulas from the inversion of the theoretical model (chapter 0) have to be entered separately into this sub-VI. It contains a numerical function solver (start values have to be defined as well), which solves for the impedance values. These values are processed in a formula node, which contains the inverted expression from Gladwell's model.
- Several components to set up and communicate with the measurement hardware: These components do not affect the principle of the measurement and are not further described in this thesis.

[108] See appendix IV.

7.5 Sensor Characteristics and Error Analysis

Determining sensor characteristics of a novel sensor system in an accurate way is very time-consuming and could only be done in a small attempt. Hence the following list is not complete – missing characteristics are accuracy of the system, the resolution, hysteresis effects, and a calibration error.

Transfer function

The following equation describes the output voltage of the signal conditioning circuit as a function of the power at the receiving coil:

$$U_{out} = 5 \cdot \sqrt{\zeta \cdot P_{in,RMS}} \qquad (63)$$

A transfer function for the complete system could not be defined because the mechanical properties of the attached polymer are related to the frequency response of the sensor in an essential nonlinear way. However, it could be possible to linearize the relations for a certain range of the contact impedance but this was not tried yet.

Span (Input Full Scale)

The span of the contact impedance is approximately:

$\mathrm{Re}(Z_c) \in [0.5,15]$ and $\mathrm{Im}(Z_c) \in [-25,0]$ in Ns/m. (See chapter 0.)

Output Full Scale

The output of the signal-conditioning circuit is between *0V* and *5V*.

Signal-to-Noise ratio

The S/N ratio of the output amplitude can be calculated as:

$$S/N\big|_{dB} = 20 \cdot \log_{10}\left(\frac{U_{Signal}}{U_{Noise}}\right) dB \qquad (64)$$

It could be determined to about *40dB* when U_{Signal} was calculated as the difference of the maximum and minimum detectable peak height. In general it is also possible to determine a S/N ratio for the frequency of the resonant peak but this was not done yet.

Repeatability

In appendix VII a graph with three cure measurements under the same conditions is given. The curves show a maximum derivation of 0.35kHz ($\cong 13\%$ of the overall frequency shift) and 200mV ($\cong 10\%$ of the overall

amplitude drop). However, this is only based on three measurements of one epoxy resin. To determine repeatability in a more accurate way it is necessary to repeat these experiments with different polymers.

Saturation

With correct software setting the sensor cannot be saturated (actually the saturation level depends on the excitation voltage). The frequency span can be adapted, and also the power output is even for highly viscous fluids significantly above a saturation level.

Dynamic errors

- Warm-up time:
  The IMTEC DAQ card needs about 1h to warm up. It is assumed that this is also sufficient for all other components involved, including the sensor itself.
- Measurement intervals:
  Measurements cannot be made continuously; the minimum interval is about 2s between each measurement (1s for the sweep and 1s for data evaluation and rearming of the system). However, this is far enough for cure measurements of conventional polymers. For very fast polymers, or for an array of multiple sensors, the software has to be adapted to perform faster measurements. A measurement interval of approximately 0.7s could be achieved with the current hardware configuration and optimized software.
- Another dynamic error could result from insufficient settling time for the oscillations of the magnetostrictive rod to reach a steady state. Preliminary experiments showed that a sweep time of *1s* for $\Delta f = 63kHz - 73kHz$ is sufficient.

Accuracy of the temperature measurement

The accuracy of the thermocouple itself is ±1.1K, and tolerances of the transmitter unit (±0.2% of the calibrated span of 250ºF ≅ ±0.5K), the shunt resistor (±1% of the calibrated span of 250ºF ≅ ±0.5K), and the DAQ (1 of 12 bit resolution ≅ ±0.1ºK) contribute to the error. This causes overall maximum error of ±2.3K. A comparison with an accurate mercury thermometer showed an error of about –1K (that means the DAQ reading is about 1K to low).

Conclusion

The given characteristics are not complete, but they indicate that the current MCM sensor configuration is already very sensitive but not accurate. Especially the repeatability is not sufficient yet. The S/N ratio is good; this justifies the efforts for the signal-conditioning unit.

8 FIRST RESULTS & VALIDATION OF THE SENSOR MODEL

This chapter contains several different measurements in comparison with theoretical calculations from the sensor model and with measurements found in literature[109].

The chapter is divided into three main sections:

1. Validation of the sensor model.
   Several parts of the model are under consideration. The theoretical results are compared to own measurements or to measurements found in literature.
   a. Resonant frequencies of the MCM sensor are compared to resonant frequencies of a free, oscillating rod.
   b. The power P_2 at the receiving coil, calculated with the theoretical model for a cured epoxy, is plotted over the frequency. This is compared to actual measurements with the MCM sensor (frequency response).
   c. The calculated impedance of the excitation coil is compared to the impedance of an ideal solenoid in air.
   d. The calculated impedance of the excitation coil is compared to the impedance of a magnetostrictive transducer developed by A. Ackermann.
2. Actual cure measurements.
   a. Discussion of a cure measurement of an epoxy resin.
   b. Comparison of curing curves of samples with different thickness.
   c. A measured curing curve for epoxy is compared to a curing curve recorded by A. Dominauskas with a miniature MCM sensor.
   d. Measured curing curves for Epoxy and rigid polyurethane foam are compared to curing curves of polyurethane foam, measured with a "Vibrating Needle Curemeter".
   e. Measured curing curves are compared to TDR and DSC data, for the same SC15 Epoxy resin.

[109] In appendix VII additional measurements can be found.

3. Conclusions about the validation.

8.1 Validation of the Sensor Model

In this chapter the frequency response of the sensor is under consideration. The model output is compared to measurements, to simple calculations with formulas for ideal resonators and ideal transformers, and to literature data.

8.1.1 Frequency Response Compared to Natural Resonant Frequencies

Figure 31 shows the calculated frequency response of the sensor, here actually the absolute value of the amplitude of the oscillations of the magnetostrictive rod, if the sensor is connected to an ideal voltage source. The ideal resonant frequencies of a nickel rod can be calculated as shown in table 4.

Table 4: *Ideal resonant frequencies of nickel rod.*
Length l_r: 40mm, sound velocity c_r: 4700 m/s

	free – free	free – fixed
Formula	$f_n = \frac{c_r}{2 \cdot l_r} \cdot n$	$f_n = \frac{c_r}{4 \cdot l_r} \cdot (n \cdot 2 - 1)$
First resonant frequency	*58.75kHz*	*29.375kHz*
Second resonant frequency	*117.5kHz*	*88.125kHz*

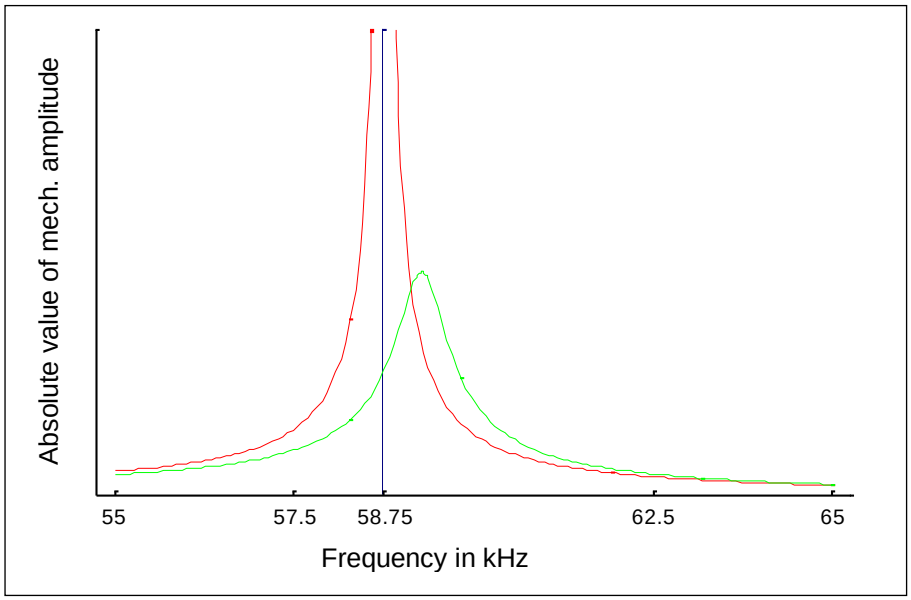

Figure 31: *Absolute values of amplitude plotted over frequency. The red curve shows the response of the free sensor rod; for the green curve the mechanical impedance of a cured epoxy resin is set as a boundary condition.*

One conclusion out of this comparison is that the rod behaves nearly as free, even if a polymer is attached to one end. If one compares the E-modulus of both materials (nickel: about 210GPA, Epoxy: about 3GPa) this seems to be very reasonable. To create a significant frequency shift towards the fixed support conditions, a material with a higher strength than nickel would be necessary.

8.1.2 Power of Receiving Coil Plotted over Frequency

Figure 32 shows an actual measurement of the frequency response of the MCM sensor, obtained with the LabVIEW software described in appendix IV. The same figure shows also the frequency response calculated with the theoretical model.

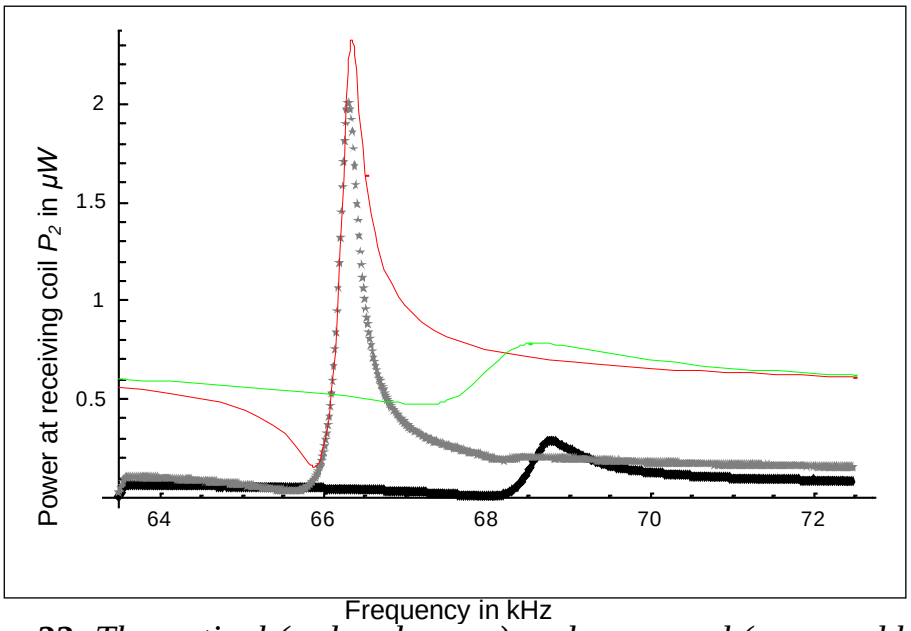

Figure 32: *Theoretical (red and green) and measured (gray and black) sensor frequency response for a free sensor and for cured epoxy.*

Table 5 shows the parameters that were used to calculate the frequency response of the sensor with the theoretical model.

Table 5: *Values used as input parameters for the theoretical model to generate the curves in figure 32.*

Parameter	***Value***	***Annotations***
E_R: Young's-modulus rod	$280 \cdot 10^9$ *(Pa)*	literature value[110]: $200 \cdot 10^9 Pa$
c_R: sound velocity in rod	*5361 (m / s)*	literature value: 4.7 km/s
Θ: magnetostr. constant	$-5 \cdot 10^6$ *(Pa / T)*	literature value: up to $-20 \cdot 10^6 Pa/T$, but depends on biasing magnetic field.
$\mu_{r,R}$: rel. permeability rod	*110*	literature value: 60..110
U0d: voltage amplitude at function generator	*4 (V)*	actual value
l_R: length of rod	*40.8/1000 (m)*	actual value
r: radius of rod	*1/1000 (m)*	actual value
$l_{Coil_1} = l_{Coil_2}$: length of coils	*12/1000 (m)*	actual value
x_1, x_2: position of coils	*0.0041, 0.0226 (m)*	actual values
K_1: correcting factor for excitation coil	*1*	determined by calibration (best curve fit)
K_2: linear correcting factor for output power	*0.000238*	determined by calibration (best curve fit)
Z_c: mech. impedance	*0.8-i 2.0 (N s / m)* for the red curve	realistic value for the mechanical impedance of the silicon sealant
	5.5-i 16.0 (N s / m) for green curve	realistic value for the silicon sealant plus the impedance of cured epoxy, respectively.

[110] The Literature value is for annealed nickel, but the rod is actually hard tempered.

All values seem to be reasonable, but the correcting factor K_2 requests further explanation. Without this factor, the calculated output power would be in the range of *0.05W* to *0.5W*, but the measured power is actually in the range of several μW. This implies that there is either a big error in the model or a wrong assumption. A critical assumption is the perfect magnetic circuit with no flux leakage: a separate measurement was performed[111] to determine the correcting factor in a different way, without the sensor model.

Besides the resonant frequencies, the sensor works like an electromagnetic transformer with two coils. The output Voltage of an *ideal transformer* can be calculated as:

$$U_2 = 1 \cdot \frac{N2}{N1} U_1 \qquad (65)$$

The *measurement* with the free sensor at about *75kHz* showed about:

$$U_2 = 0.00237 \cdot \frac{N2}{N1} U_1$$

This calculation is not an explanation for the derivation between model and experiments, but it proves that it is related to the assumption of the ideal magnetic circuit. Still a factor of *10* remains for the correcting factor, but this is now in a reasonable range and could be related to mechanical losses, internal resistance of the coils, etc.

From a further comparison of the curves it can be concluded that the theoretical model describes the behaviour of the sensor in the right way, but still a nearly constant derivation of the output power remains. This cannot be adjusted with a linear correction factor.

8.1.3 Comparison of Coil Impedance

The impedance of an ideal solenoid can be calculated as:

$$Z_{coilideal} = i\omega L = 2\pi i f L \qquad (66)$$

With:

L *Coil inductance for an ideal solenoid in air (assuming that the magnetic resistance, the "reluctance", is dominated by air:*

$$L = N^2 \mu_{Air} \frac{A}{l_{Coil}} \qquad (67)$$

[111] See appendix VII.

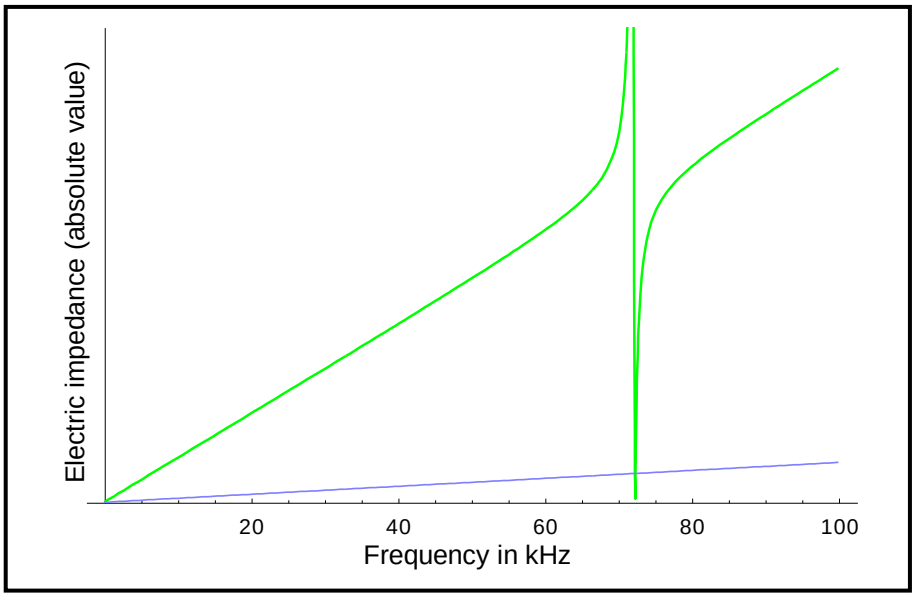

Figure 33: *Impedance plots. The green curve shows the impedance of the MCM sensor while the blue curve shows the impedance of an ideal solenoid in air*

Figure 33 shows a plot for the impedance calculated with the formulas above and another plot for the impedance of the MCM sensor (from the theoretical model), both with the same number of turns, length, and area of the coils. Naturally, the first curve shows no resonant phenomena – it is a simple linear relationship.

At the Center for Intelligent Material Systems and Structures, Virginia, a model for characterization of magnetostrictive actuators (figure 34) was developed[112]. Although several differences between this approach and the MCM sensor model prohibit a comparison of quantities, the qualitative behavior of both systems can be compared.

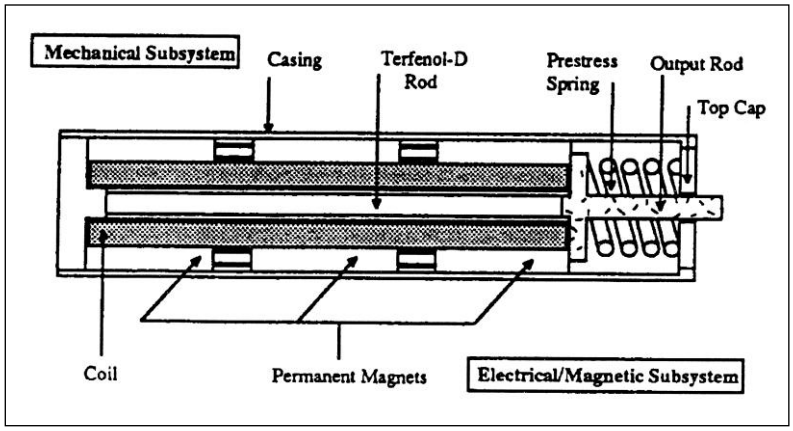

Figure 34: *Magnetostrictive transducer from the Center for Intelligent Material Systems[112]. The most significant differences compared to the MCM sensor are: 1. Prestress mechanism and fixed support at the left end. 2. Only one coil over the whole length of the rod. 3. (Not visible in this figure.) Transducer is several times larger than the tool-mounted MCM sensor.*

The magnetostrictive actuator has a resonant frequency of about 3100 Hz, and therefore much lower than in the case of the MCM sensor. The coils are much bigger and have less windings; hence the impedance is in the range of several hundred ohms compared to several thousand in case of the MCM sensor. However, by changing some system constants the MCM sensor model can be partially adapted to the conditions discussed by Ackermann. This was done to create the curves in figure 36, the electric impedance of the magnetostrictive transducer, divided into real and imaginary part. Figure 35 shows both experimental and theoretical results from Ackermann himself.

[112] See Ackermann: […] Characterization of magnetostrictive actuators.

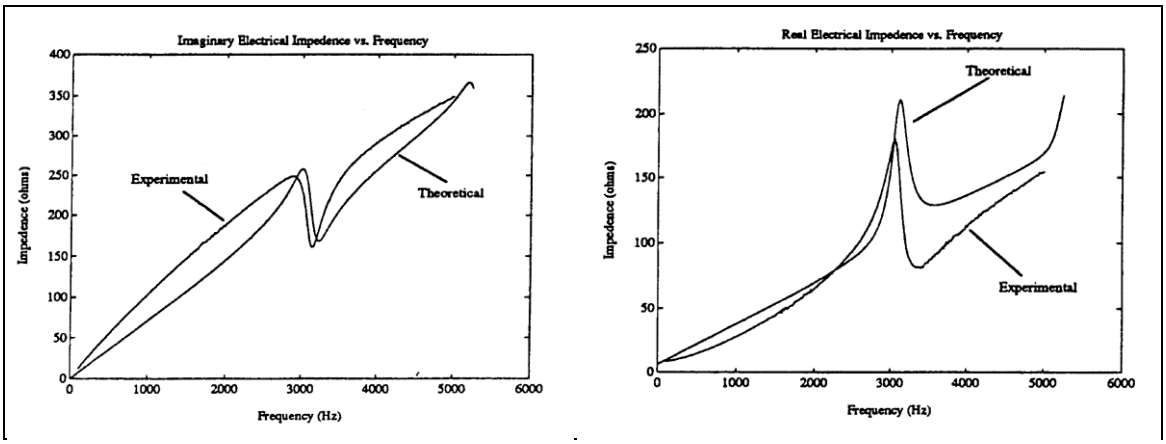

Figure 35: *Real and imaginary part of coil impedance of the magnetostrictive actuator*[112].

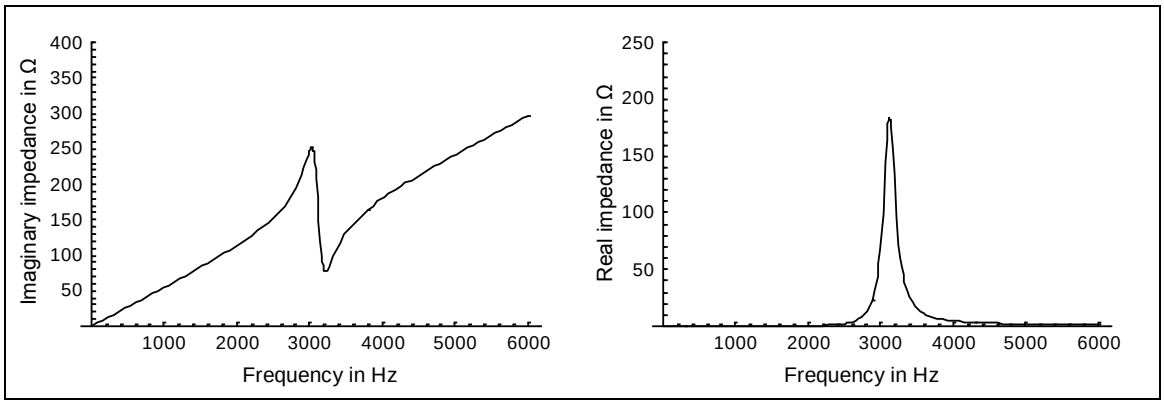

Figure 36: *Real and imaginary part of coil impedance of the adapted MCM sensor model.*

The following values were assumed for calculating the curves in Figure 36:

- E-modulus of rod: 30GPa (typical value for Terfenol-D).
- Sound velocity of rod: 1750 m/s (typical value for Terfenol-D).
- Length of rod: 140 mm (hence the first resonant frequency with one fixed and one free support would be 3125Hz).
- Rod / coil radius: 25mm, 75 windings.
- Magnetostrictive constant Θ: $5 \cdot 10^6$ (see below).

Since the MCM model is made for one free end of the rod, the boundary conditions cannot match exactly and the contact impedance Z_c was just adapted for a good curve fit[113].

Two issues are interesting in the behavior of the MCM sensor model. First, the model does not show a linear increasing component of the real part of the impedance. It shows the peak at the resonant frequency, but at higher frequencies the real part decreases again to zero, a logical consequence of the pure imaginary impedance of an ideal solenoid (see equation 66). The reason for this behavior in the model of Ackermann is unknown. Second, the assumed value for the magnetostrictive constant Θ is only about 10% of the value found in literature[114]. If the literature value is set into the equations, the impedance decreases significantly and does not show narrow resonant peaks any more.

Because of these two differences, which cannot be explained at this time, a conclusion out of this comparison can hardly be drawn. Further research would be necessary to understand these differences.

[113] As shown in chapter 4, high values of this impedance can be an approximation for a fixed support.

[114] See Bright: Better Sonar Driven with new […] Materials.

8.2 Cure Measurements

In this subchapter several cure measurements are discussed.

8.2.1 Discussion of the System Behavior During Curing of an Epoxy Resin

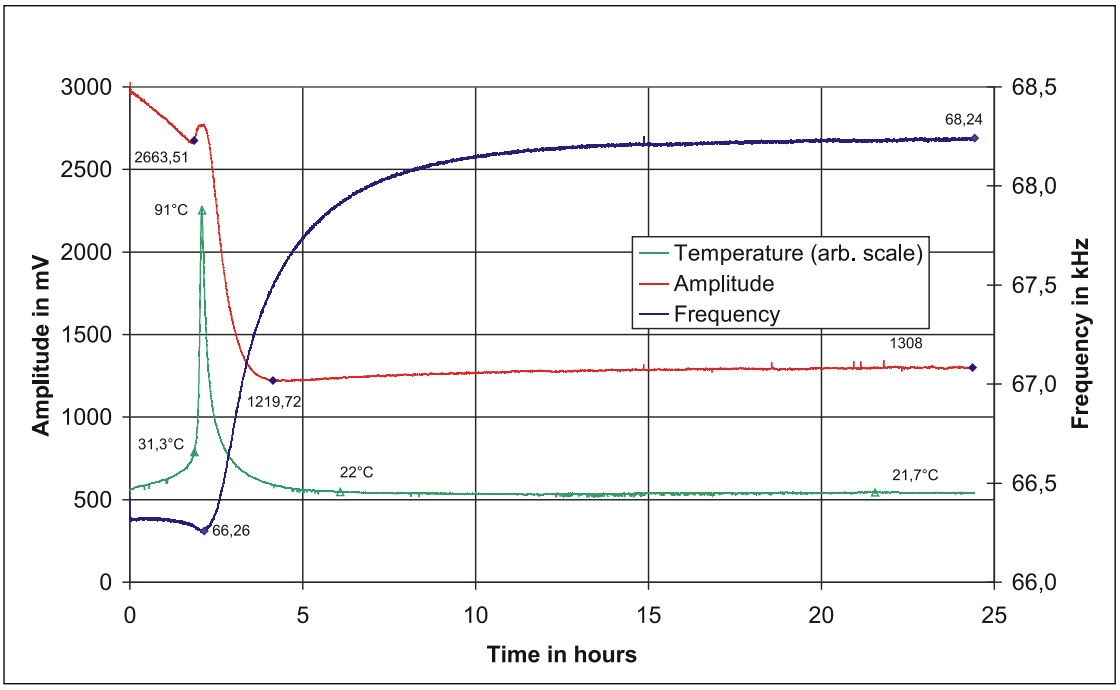

Figure 37: *Curing of Loctite Hysol 120HS Epoxy.*

Figure 37 contains curves for the resonant amplitude, the resonant frequency, and the temperature during curing of a high-strength epoxy adhesive:

1. The curves start with a hard amplitude and frequency drop as a result of resin coming in contact with the sensor tip (at 0 minutes, nearly not visible).
2. Onset of cure[115]: With this epoxy the curing reaction starts by mixing the components (at room temperature), therefore the amplitude starts to decrease immediately. This can be explained with increasing viscosity due to chain extension.

[115] See appendix II "Glossary" for an explanation of this term.

3. The exothermic reaction causes high temperature in the sample[116], in this case about 90ºC. Increasing temperature causes an increasing resonant amplitude and decreasing resonant frequency. This effect is superposing upon the curing effects.
4. The resonant frequency starts to increase due to the development of elasticity. Experimental correlation shows that the gelation point matches with the maximum of the first derivative of the amplitude (the deflection point in the dropping amplitude). This happens approximately after a 5% frequency increment (see chapter 8.2.4). (The manufacturer of this epoxy specifies the *work life* time with 120 minutes).
5. The amplitude reaches a minimum and then levels out. The frequency is still increasing, even after 20 hours of curing. The specified curing time is 24 hours. A comparison with the development of the shear-modulus during the curing process shows the significance of the frequency shift during the end of the curing process (see chapter 4.2).

8.2.2 Influence of Sample Thickness

Initial experiments showed that the assumption of a semi-infinite test piece is actually very critical. Boundaries of the samples can have a strong impact on the resonant system. Figures 38 and 39 show the curing of three different samples of the same Epoxy *(Loctite Hysol 120HS)*. Sample *F1* had a thickness of 22mm and a volume of 50ml, *F2* had a thickness of 44mm and a volume of 100ml. *F3* had also a thickness of 22mm but it was covered with another (cured) epoxy part[117], to test if this cover is able to absorb some ultrasonic waves and minimizes the effect of boundaries.

[116] The sample volume was about *200ml*. The increasing temperature is typical for this kind of adhesive. E.g. industrial epoxies for manufacturing of composites do not show significant exothermic reactions for this volume / amount of resin.

[117] The surface was grinded with sandpaper to provide the best possible contact.

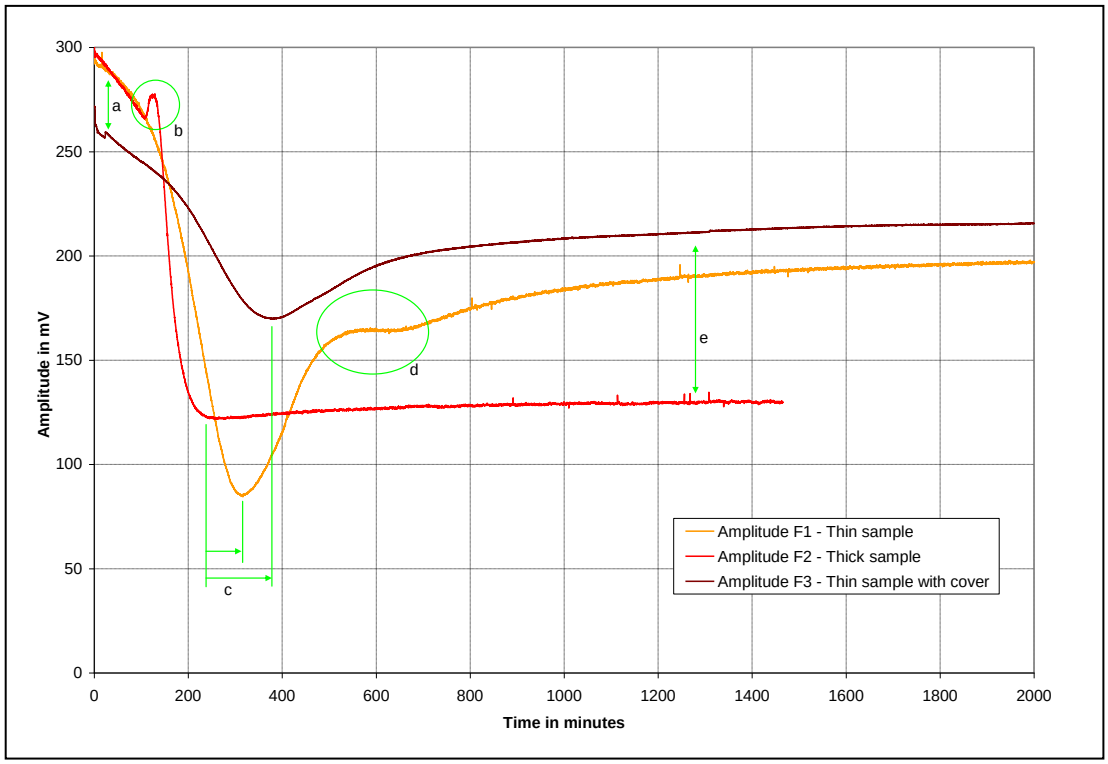

Figure 38: *Amplitude during curing of three samples: (F1) thin sample without cover, (F2) thick sample, (F3) thin sample with cured epoxy as a "cover" for the curing resin.*

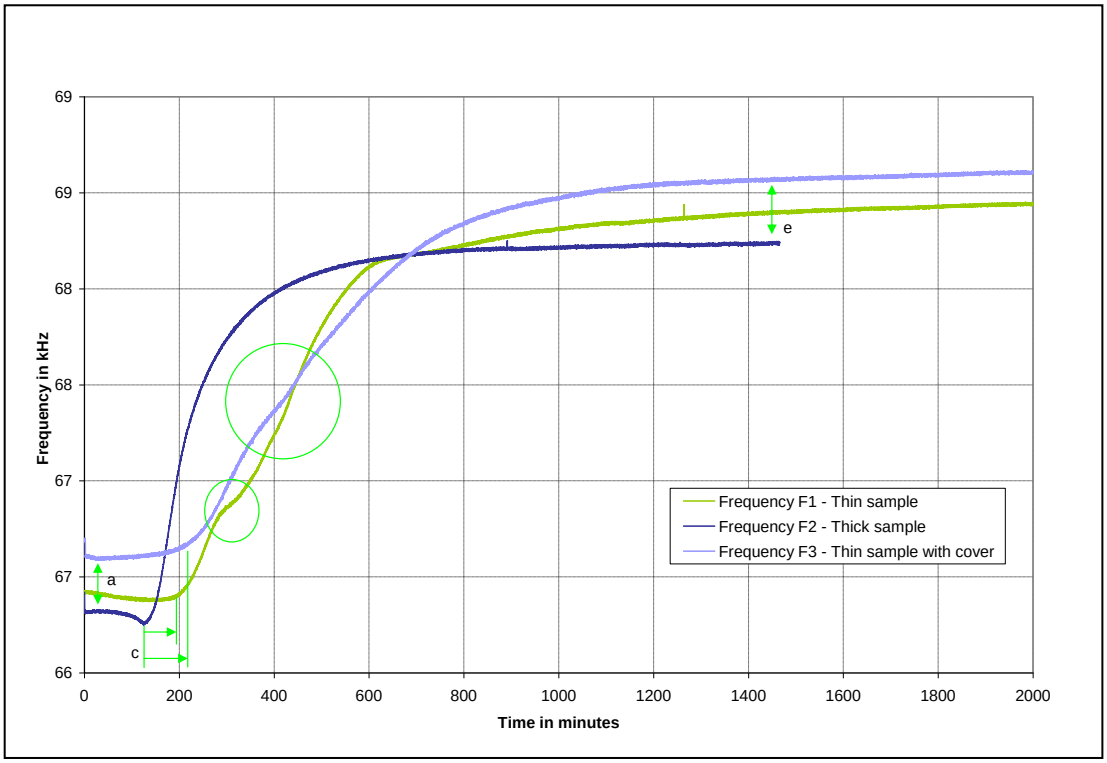

Figure 39: *Frequency during curing of three samples.*

Discussion of the curing curves:

a. The offset of frequency and amplitude at the beginning of the curing process differs with every sample (see also chapter 7.5 "repeatability"). It is assumed that this is *not* related to the boundaries of the samples, because absorption of ultrasonic waves is very high for highly viscous fluids.

b. The peak in the curve of sample three is related to high temperatures (the part temperature increased to 95ºC while the environment temperature was constant at 22ºC. This happens especially with high amounts of resin because of the exothermic reaction.

c. As a result of higher temperatures (discussed in *b*) the curing process is faster and hence the minimum of amplitude is reached earlier.

d. The "deformation" in the curing curve is typical for thin samples. The curve for sample *F3* also shows these effects, which proves that the cover does not work in a perfect way. It is assumed that the boundaries of the test piece cause reflections of longitudinal ultrasonic waves, generated by the MCM resonator. When the mechanical properties of the polymer change during curing (e.g. the sound velocity) it can happen that standing waves are formed and resonant conditions can occur[118]. This has an influence on the resonant frequency and on the amplitude of the MCM sensor.

e. The boundaries of the samples have an influence also at the end of the curing process, by virtually increasing the stiffness. This is the most significant indicator for samples that are too thin, in nearly all experimental results thin test pieces showed increasing amplitude at the end of the curing process.

From this experiment it can be concluded that it is possible to reduce the influence of boundaries of the test piece, but not to eliminate it. It is practically not possible to create the assumed conditions of a semi-infinite sample, because of exothermic reactions in large quantities of resin. Covering the pieces to absorb waves can cause effects that are hardly to predict with a model and that could change for different polymers. One way to deal with this problem would be to reduce the mechanical power, which causes the

[118] See Gladwell: The contact impedance meter.

ultrasonic waves, or to reduce the contact area, with the result of more spherical wave components, which are probably not as problematic as longitudinal components.

8.2.3 Comparison with Isothermal Curing of an Epoxy Thermoset

Figure 40 shows the isothermal curing of an epoxy thermoset ("Thermoset 285"), recorded by A. Dominauskas with an embedded miniature MCM sensor. The graph shows the resonant frequency and a "resonant power spectrum", measured directly at the magnetostrictive resonator.

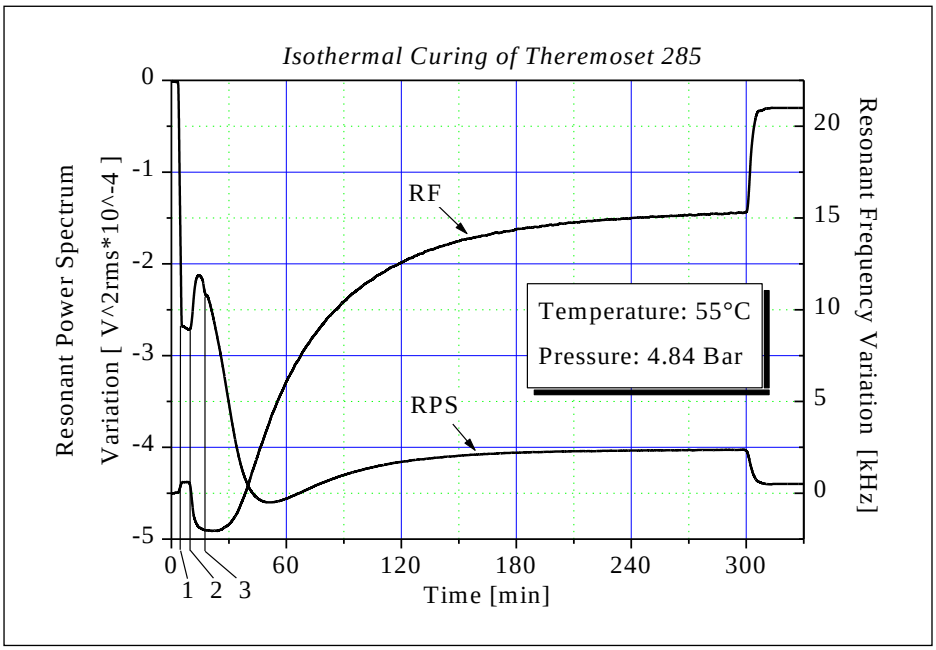

Figure 40: *Isothermal curing of an epoxy thermoset[119]. The measurement curve is smoothened. (0) Sensor is in air; (1) contact with thermoset; (2) mold is closed; (3) maximum pressure reached in mold.*

Several conclusions can be drawn from a comparison between both MCM sensors. First, the tool-mounted sensor behaves qualitatively in the same way as the miniature sensor. Second, although the resonant frequencies of the miniature sensor are more than one magnitude higher (1-2MHz compared to 50-100kHz), the relative frequency shift of both systems is about 1-3%. And third, the miniature MCM sensor is highly influenced by pressure. This also

[119] See Dominauskas: Magnetostrictive Sensor for On-Line Cure Monitoring of Thermosets.

has to be expected for the tool-mounted sensor, and therefore further research is required if the system shall once be used in pressurized molds.

8.2.4 Curing of a Rigid Polyurethane Foam

Figure 41 shows the curing of a rigid polyurethane foam, measured with a "vibrating needle curemeter". The sensor principle is quite similar to the MCM sensor, and the curve shows many similarities to the ones in figure 42.

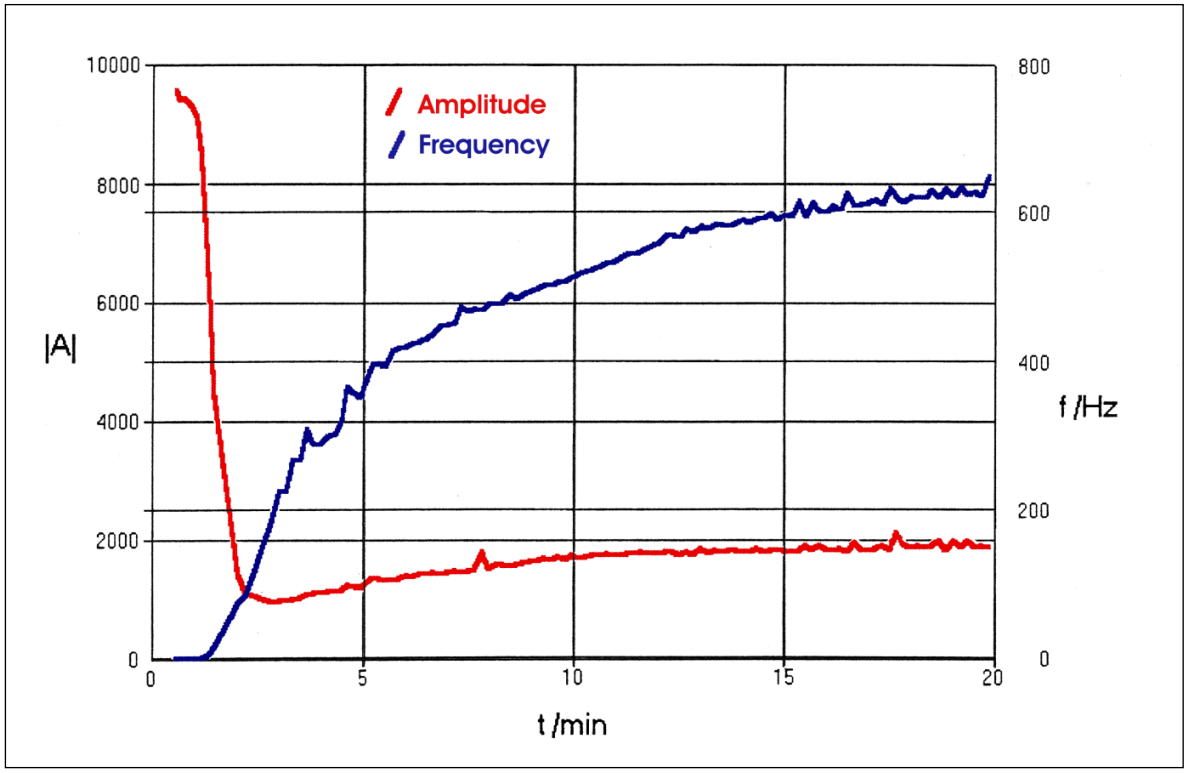

Figure 41: *Curing of a polyurethane foam, recorded with a "vibrating needle curemeter"*[120].

[120] See Willoughby: Understanding Cure with the Vibrating Needle Curemeter [...].

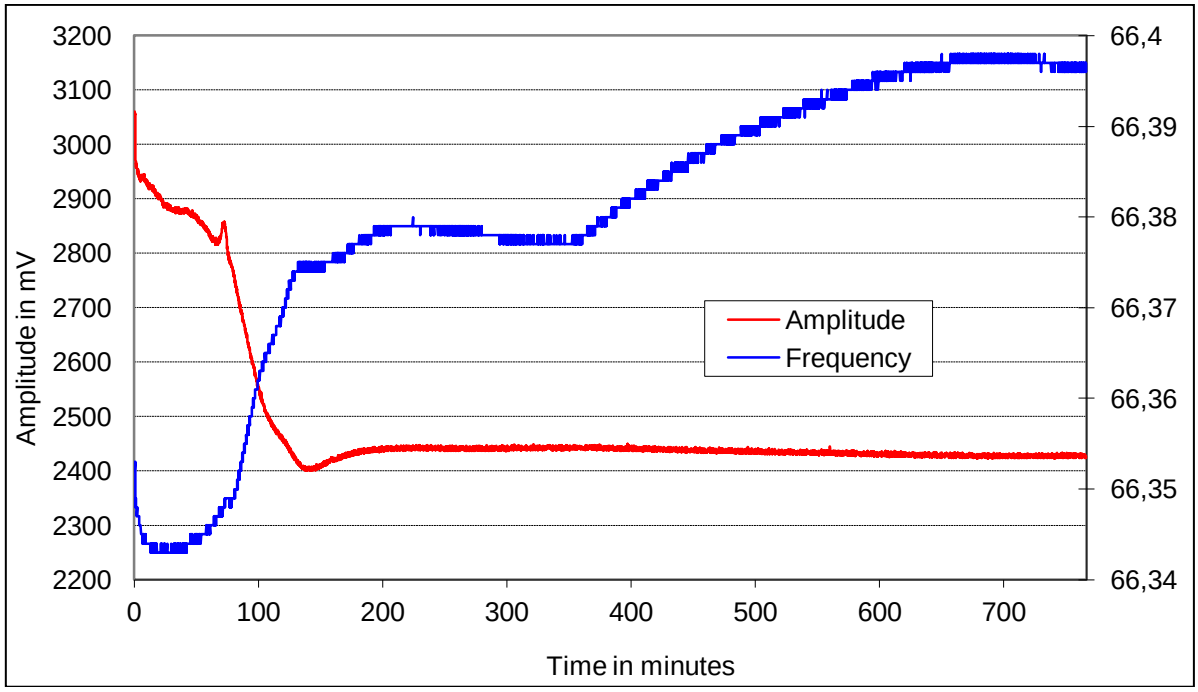

Figure 42: *Curing of a polyurethane foam*[121]*, recorded with the MCM sensor. Environment temperature: 21°C.*

Comparison between the two measurements:

- Both measurements show in general the same behavior of the sensors.
- The much longer curing time in the MCM measurement is related with the used polyurethane, which cures much slower. Additionally the MCM sensor measures at the surface of the polymer at the mold, where the humidity of the air cannot reach the polymer as fast as at the outer side. (The curing reaction of this PU foam is initiated by humidity).
- The frequency shift begins earlier at the MCM sensor, compared to the amplitude drop.
- The frequency shift in case of the MCM sensor is very low and in the range of the resolution. Hence temperature effects can cause high errors.

It is obvious that the curing of a PU foam is far from the optimized application of the MCM sensor, which works much better with solid

[121] "*touch 'n foam*" rigid polyurethane foam (MDI Monomer, PU, Propane / Isobutane). Manufacturer specifies the track-free time as 30 minutes.

polymers. Nevertheless the similarities of the curves show that the MCM sensor responds in the expected way.

Willoughby defines the gelation point of the polymer by a 5% Frequency increment. The similarities in the curves compared to the MCM sensor imply the question if this definition is also valid here (e.g. 5% of the overall frequency shift).

8.2.5 Curing of SC15 Resin Compared to DSC data

The following measurement was performed with SC15 Epoxy resin (100:30) in a temperature-controlled oven to maintain constant temperature. Isothermal conditions were assumed.

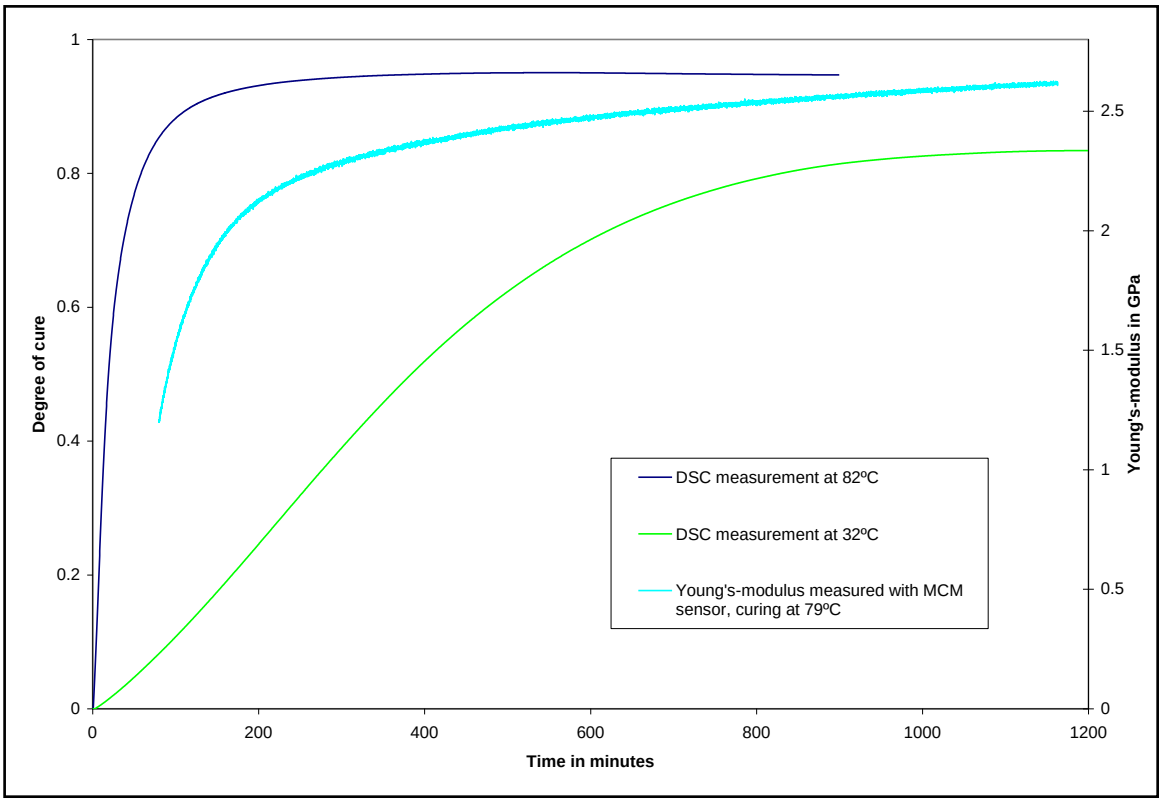

Figure 43: *Corrected Young's-modulus during curing of SC15 resin at 78ºC, compared to DSC data*[122] *for curing at 82ºC and 32ºC.*

The experiment was carried out at 79ºC. From separated measurements the Young's-modulus of the cured SC15 epoxy could be determined to *2.6GPa*. The MCM system showed about 1.2GPa too less, what can easily be explained with the high temperatures of the sensor itself (the sensor was

[122] The DSC data was provided by Amit Chatterjee, Research Associate at the Center for Composite Materials.

calibrated for room temperature – higher temperatures cause lower resonant frequencies and therefore show virtually a lower Young's-modulus). Therefore this influence had to be corrected, by adding a constant value of *1.2GPa* to the measured Young's-modulus.

Because of the relations described in chapter 4, the development of the Young's-modulus should be proportional to the degree of cure. From what can be seen in figures 43 and 44 this is not exactly the case.

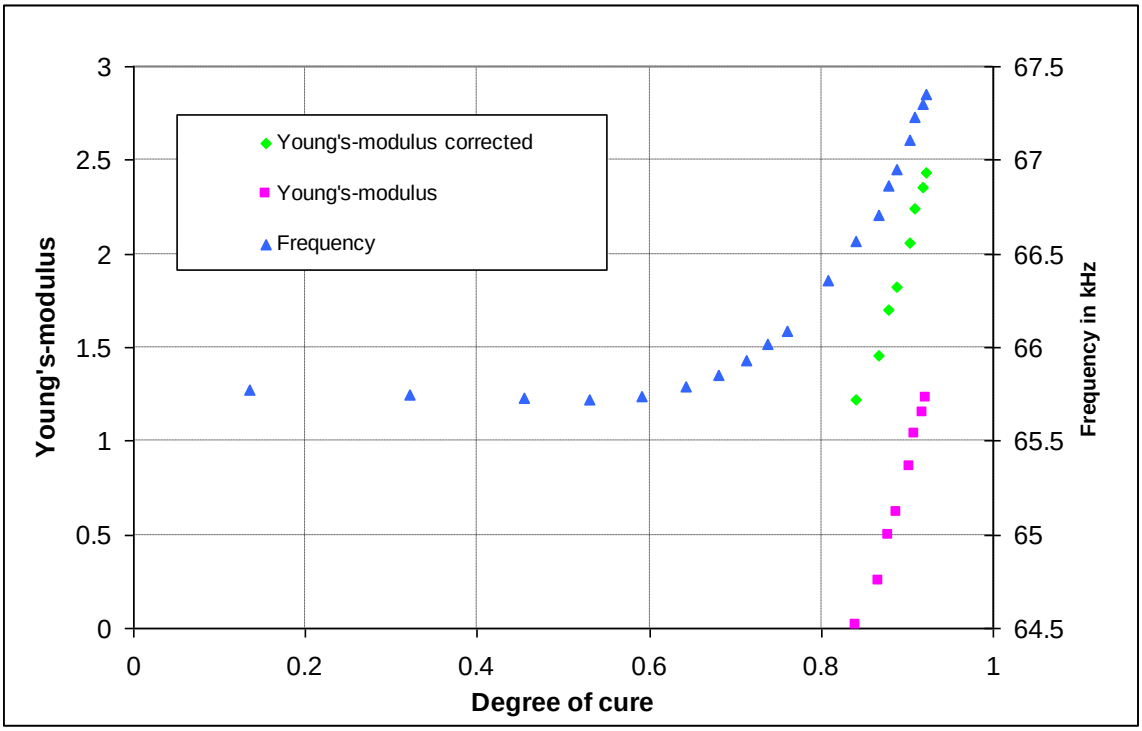

Figure 44: *Young's-modulus and resonant frequency plotted over the degree of cure (determined with DSC[122]).*

Plotting the Young's-modulus over the degree of cure (also sometimes called "α" in literature) should show a straight line through the origin for an ideal case. Figure 44 shows that this is not the case for this particular measurement. However, the Young's-modulus seems to be at least a straight line in this plot.

8.3 Conclusion about the Validation

It could be shown that the sensor behaves in a way, which is predicted by the theoretical model, at least from a qualitative point of view. However, the validation is not complete, and as a result some sensor characteristics cannot be given yet. The approach to describe the sensor output in a quantitative way

was only partially successful, although the errors of the first results are already acceptable for initial experiments

.

9 CONCLUDING REMARKS

The following chapter describes some problems with the current sensor configuration and possible improvements for the future. Finally it contains some conclusions about the tool-mounted MCM sensor.

9.1 Possible Improvements / Future Sensor System

- Gain / phase measurements:

  With an appropriate amplifier it could be possible to measure gain and phase of the response to the excitation signal besides the resonant frequencies of the MCM sensor. This would give more information about mechanical properties of the polymer like a frequency dependant storage- and loss-modulus.

- Switching unit to connect several sensors:

  Because of the signal strength of the MCM sensors it is not necessary to have a signal-conditioning unit installed directly near the sensor. Therefore several meters of wire for each sensor could lead to a central switching unit and only one signal-conditioning / DAQ system.

- Industrial connector at the sensor:

  The current sensor design contains no details for an electrical connector outside the sensor. For industrial use a connector should be mounted somewhere on the sensor housing for easy installation and maintenance and as a strain relief for the leads that go inside the sensor.

- Constant current source for higher frequencies:

  J. Fraden[123] gives suggestions to build a current source out of discrete components and operational amplifiers which could be suitable for frequencies up to several MHz.

9.2 Problems with Current Sensor Configuration

- Constant current source with 78(R)00 Voltage regulator:

[123] J. Fraden: Handbook of Modern Sensors, p. 162 et sqq.

A 7800 has a bandwidth of approximately 100kHz. Therefore the actual configuration should not be used to measure at higher frequencies. Nevertheless we did this during experiments with the second or third mode of oscillation.

- Bad heat conduction in between the sensor:

  The sensor prototype has a gap of 0.75mm between the sensor core unit and the aluminum housing. This gap should be filled with several layers of tape, for electric insulation and to center the core properly. These layers form a barrier for heat transportation and can therefore cause high temperature gradients in both directions. The same problem can occur between the solenoid and the outer core assembly. Especially when a high biasing current is used, the heat dissipation of the coil can locally cause high temperatures. During preliminary experiments this was not a problem, which led to the destruction of the sensor, but if the sensor is used in a high temperature environment[124], the system has first to be validated. Especially the thin insulation layer of the magnet wire of the solenoids could became a limitation.

- Erroneous assumption for sensor model:

  In chapter 4.1.1 equation 21 describes an integration to determine an average magnetic field strength. It is integrated over the length of the coil. Probably this is not correct and it should be integrated over the whole magnetic circuit. In this case also the part of the rod asides from the coil and the air gap influences the magnetic field. This should be reviewed during further research.

9.3 Outlook and Future Work

I can make three strong suggestions about further work on the MCM project. The first and most important suggestion is to further validate the theoretical models, with a more sophisticated calibration. Also a determination of sensor properties by different means could be helpful, e.g. measuring properties of the resonator precisely, so that it is not necessary to rely on literature values. Then it could be valuable to validate if the sensor also works in different applications like in big molds, with composite materials, and under pressure.

[124] Temperatures up to 82ºC were tested.

As described above, one of the biggest problems of the current sensor configuration is the occurring ultrasonic wave propagation. Further research could focus on sensor modifications to decrease this effect, e.g. by decreasing the intensity of the vibrations and increasing the sensitivity of the sensor. However, this should first be considered theoretically by using the sensor model.

My last suggestion would be regarding the software for the MCM sensor. It is definitely a key factor in the measurement chain, and also the most visible part for the user. I think it should be completely revised because it was developed on the basis of a specific data acquisition system, which is not in complete use anymore. But this revision should be made only after the measurement setup is complete (especially the DAQ hardware). Then additional features could be included, for example a determination of the end of work life or the gelation point.

9.4 Valuing the MCM-Sensor and Overall Comparison

I would like to look at the tool-mounted MCM sensor from two different points of view.

On one hand it must be said that the interpretation of the obtained data is more difficult as originally expected. The goal to determine mechanical properties like exact viscosity and shear-modulus of a polymer was not reached. A preliminary model is only able to determine the shear-modulus with a relative big error. The theoretical model of the sensor is complicated and anyway important factors like losses in the magnetic circuit are not included. As a result of the complicated formulas the model can only be analyzed numerically (except for some keen simplifications). Further research is necessary to increase the value of the obtained data, or the sensor concept has to be changed, e.g. to another mode of excitation.

On the other hand it could be shown that the sensor works as a highly sensitive cure monitor during the whole curing process of many different polymers. Only a very few systems are known to me, which are capable of following all the different stages of curing with such a high S/N ratio and such a clear output, considering the amplitude and frequency shift. By calibrating the sensor for a specific resin, it has an enormous potential for QA / QC applications, and maybe beyond that to study different polymers in a pragmatically way. For sure it can be said that the output is related to purely mechanical properties of the polymer, and a big source of errors is avoided

compared to other sensor principles. MCM data show good accordance with data from other measurement techniques, for example DSC, FTIR, or DSC. And the existing model shows a still acceptable accordance with experimental results at the very end of the curing process.

Finally, I would like to take an overall view of the system, including the complete measurement chain. One may question the quality and reliability of every single piece, which still has to be validated and proved in many ways, but anyway the collectivity is already functional. It was possible to present a complete working setup for on-line cure monitoring, that means an experimental mold, the sensor, an electric signal-conditioning unit, data acquisition hard- and software and evaluation of results.

APPENDICES

I VARIABLES

Indices

R	*Magnetostrictive rod*
r	*"relative", like in* $\mu = \mu_0 \mu_r$
c	*"contact" means the boundary condition between the rod and the polymer and sealant*
P	*Polymer*
S	*Sealant*
1	*Excitation coil*
2	*Receiving coil*
d	*Index used for amplitude values, like in* $U(t) = Ud \cdot e^{i\omega t}$

Annotations

- If a variable related with a solenoid does not contain an index like "1" or "2", the excitation coil ("1") is meant.
- If an impedance "Z" does not contain an index, an electric Impedance (in Ohm) is meant.
- In *MATHEMATICA* files indices are not written as subscripts.

Variables

i	*complex unit* $\sqrt{-1}$	
		<u>SI-unit</u>
β	*Wave number (in polymer)*	
ε	*Strain*	
λ	*Wavelength*	m
μ	*Magnetic permeability*	$V\,s\,/\,(A\,m)$
ν	*Poisson's-ratio*	
ω	*Angular frequency*	$1/s$
ρ	*Density*	kg/m^3
σ	*Stress*	N/m^2
Θ	*Magnetostrictive material constant*	$Pa\,/\,T$
ζ	*Factor for amplification of coil power (circuit "A1")*	Ω
a_1, a_2	*Amplitude coefficients*	m
a_{21}, a_{22}	*Functions of the Poisson's-ratio of a polymer in Gladwell's model*	
A_1, B_1	*Functions of the Poisson's-ratio of a polymer in Gladwell's model*	

A	*Area*	m^2
B	*Magnetic flux density*	T
c	*Sound velocity*	m/s
E	*Young's-modulus*	Pa
G	*Shear-modulus, with* *G' Storage-modulus* *G" Loss-modulus*	Pa
H	*Magnetic field strength*	A/m
I	*Current*	A
K	*Wave number (in rod)*	
K_1, K_2	*Combined geometry and field factors for the solenoids*	
l	*Length (of rod)*	m
L	*Inductance*	$V\,s/A$
m	*Mass*	kg
q	*Compliance*	m/N
r	*Radius* *But r_s and r_P are a mechanical resistance*	m $N\,s/m$
U	*Voltage*	V
Ud	*Voltage amplitude at the excitation coil*	V
U_0	*Voltage at the (ideal) voltage source*	V
t	*Time*	s
v	*Velocity*	m/s
x	*Length variable over rod*	m
Z	*Impedance. Without index: electric coil impedance* *With Index like Z_P, Z_c, Z_S: mechanical impedance*	Ω $N\,s/m$

Annotations

- In *MATHEMATICA* files the Latin letter "w" is used for circular frequencies ω.
- In *MATHEMATICA* files "i" instead of "I" is used for the current, because "I" is a reserved symbol.
- In literature about magnetostriction the Greek letters "λ" and "β" are sometimes used for the magnetostrictive constant Θ.

II GLOSSARY

Rheology:

"The study of the deformation and flow of matter, esp. the non-Newtonian flow of liquids and the plastic flow of solids."[125]

Polymer:

"A compound formed by the reaction of simple molecules having functional groups which permit their combination to proceed to high molecular weights under suitable conditions. Polymers may be formed by polymerization (addition polymer) or polycondensation (condensation polymer). When two or more monomers are involved, the product is called a copolymer."[126]

Polymerization:

Polymerization is the chemical process of chain extension, the combination of small molecules to form large chains.

Cure[127], cure time:

The term *cure* is used for the process of *polymerization*. The *cure time* is basically the complete time until this chemical reaction comes to an end. A more pragmatically definition is the time until the polymer has developed some desired physical properties which do not change anymore (except through beginning aging processes). Loctite for example gives some curves in datasheets for epoxy, which show the bonding to aluminum over the time[128].

Degree of cure (DOC):

The expression "degree of cure" or "DOC" is proportional to the amount of molecular connections. For many polymers the DOC will therefore be proportional to the amount of heat generated by the chemical reactions,

[125] See Oxford English Dictionary: "rheology".
[126] See Loctite: Worldwide Design Handbook.
[127] See Pethrick: Rheological Studies […], p. 161 et sqq.
[128] Datasheets Loctite Hysol, e.g. Hysol 120HS

assuming that each bonding releases the same amount of heat[129]. Note that a real resin will never reach DOC=1, because not every reactive group will "find" a counterpart during the process of cross-linking.

Onset of cure:

The onset of cure means the onset of chain extension. As a result the molecular weight grows, and the viscosity of the material increases[130].

Working life, working time:

The working life is the period of time in which the polymer can be molded and reworked. It may be somewhat shorter than the gel time.

Gelation, gel point, gel time:

At the point of gelation an infinite continuous matrix is formed. From this point on, the polymer is unable to flow. The time of the curing process up to this point is also referred as "gel time" and is an important characteristic of the polymerization.

Track-free time, track-free point, demold time:

After the track-free time the polymer has developed a robust state so that it can be touched and demolded without damage. Also dust and water does not cause any damage anymore. However the part has still not developed its final stiffness.

[129] See Theriault: The numerical determination of the TTT-Diagram, chapter 6.1: Modeling the degree of cure.

[130] See Willoughby: Understanding Cure with the VNC (RAPRA), p. 3

III MAGNETOSTRICTIVE MATERIALS

III.1 Finding Suppliers for Magnetostrictive Rods

The attempt to find suppliers for magnetostrictive materials that fit to the size and shape of the MCM-Sensor was divided into two parts – on one hand to find suppliers for nickel or nickel based alloys, and on the other hand to find suppliers of "giant magnetostrictive materials". Both searches were performed over the Internet by using the public search engines "AltaVista", "Google" and "Yahoo". On Yahoo no useful links were found.

Another approach was to search in Internet databases like "Thomas Regional[131]" for industrial suppliers.

AltaVista and Google returned some links using the following keywords in several combinations:

- *Nickel*, *alloy*, *200*, *nickel200* (because "Nickel 200" is a typical magnetostrictive alloy)
- *terfenol*
- *rod*, *wire*
- *magnetostrictive*, *magnetostriktiv* (the German spelling)
- *material*, *materials*, *supplier*, *suppliers*
- *filters* (because magnetostrictive rods are used in special filters)
- *piezomagnetic*, *piezomagnetisch*
- *magnetoelastic*, *magnetoelastisch*

Most of the results were links to educational institutions and links to descriptions of applications of magnetostrictive rods, e.g. from companies which produce ultrasonic equipment. After filtering these unwanted results, a manageable amount of links was left. A problem was now to identify companies that serve small quantities of the material in the wanted sizes[132].

[131] www.thomasregional.com

[132] For a list of contacted companies see appendix III.3.

III.2 Nickel Data

In the final sensor configuration nickel was chosen as magnetostrictive material. Data about nickel was found in various sources.

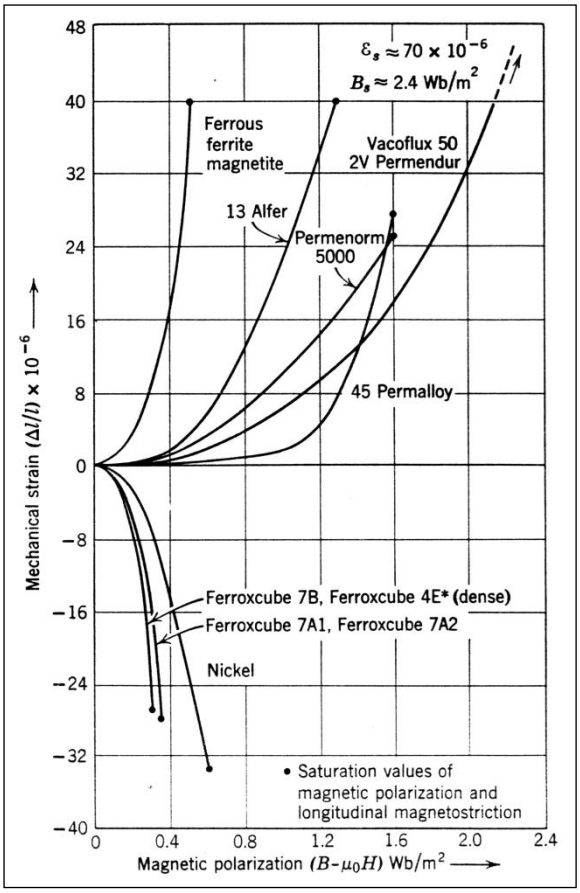

***Figure 45**: Strain produced in various magnetostrictive materials by an applied magnetic flux density*[133].

[133] See Frederick: Ultrasonic Engineering, p.76

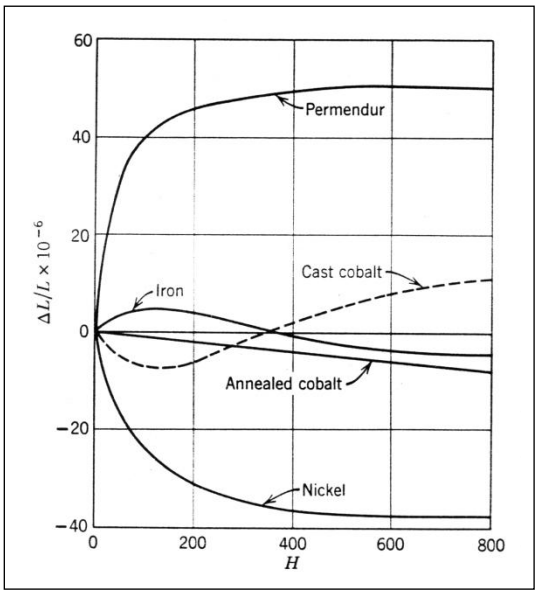

Figure 46: *Strain produced in various magnetostrictive materials by an applied magnetic field*[134]*. H is meant in the unit Oe.*

Figures 45 and 46 were found in a book about ultrasonic engineering. The same author gives some more data about 99.9% annealed nickel:

- $E = 2.0 * 10^{11} N/m^2$
- $\rho = 8900 kg/m^3$
- $c = 4700 m/s$ for longitudinal waves in bars[135]
- $\Lambda = \Theta = -20 * 10^{-6} Pa/T$
- Strain at saturation: $-33 \cdot 10^{-6}$

[134] See Frederick: Ultrasonic Engineering, p.75

[135] Calculation with the values given above: $c = \sqrt{E/\rho} = 4740.45 m/s$.

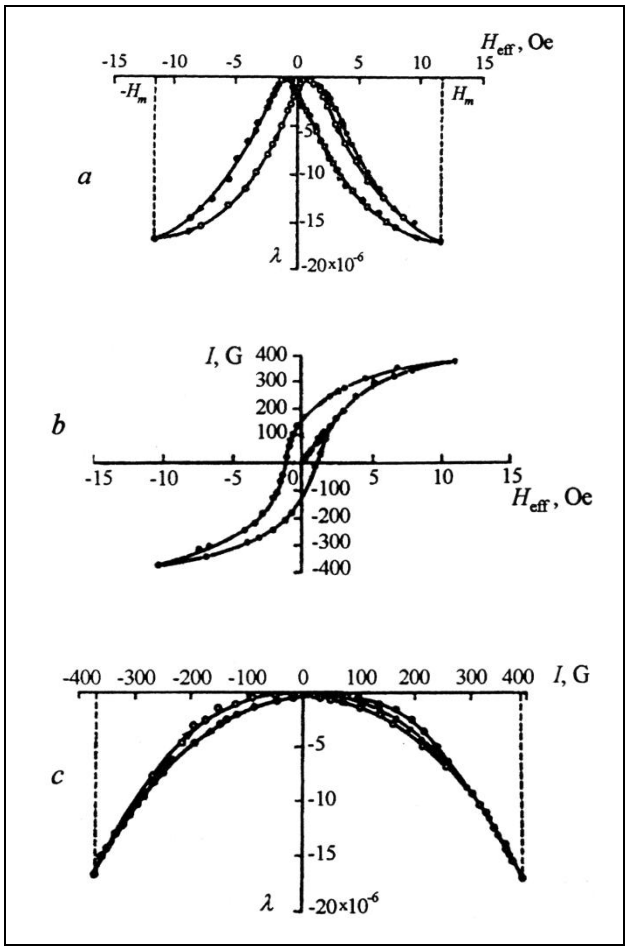

Figure 47: *Static magnetostriction hysteresis in nickel*[136]

[136] See Abramov: High Intensity Ultrasonics, p. 386

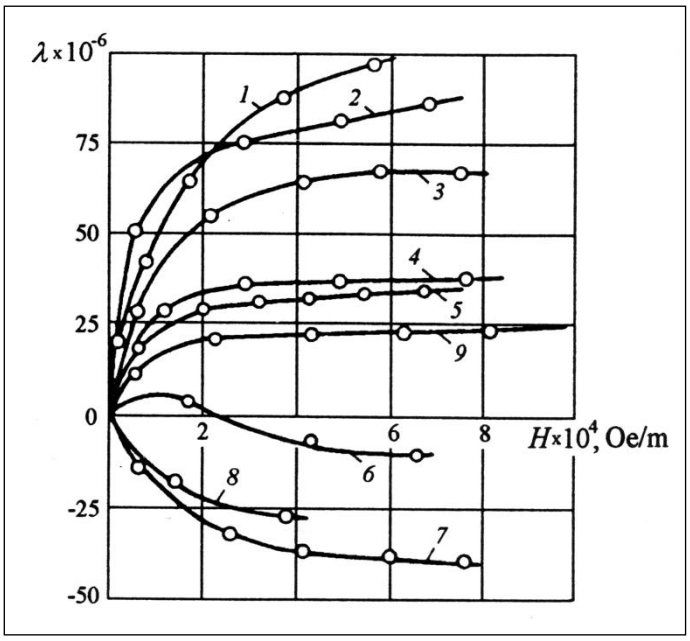

Figure 48: *Strain produced in various magnetostrictive materials by an applied magnetic field*[137]*: (1) 54%Pt+46%Fe, (2) 65%Co+35%Fe, (3) 49%Co+49%Fe+2%V, (4) 50%Ni+50%Fe, (5) 14%Al+86%Fe, (6) Fe,* ***(7) Ni****, (8) Ni-Zi-Ferrite, (9) 14%Cr+86%Fe*

Figures 47 and 48 show properties of nickel from another source. The differences between curve (7) from figure 48 and the curve for nickel in figure 46 are in between the accuracy of the drawings, about 5%.

[137] See Abramov: High Intensity Ultrasonics, p. 385

III.3 Suppliers for Magnetostrictive Rods

Table 6: *Contacted suppliers*

Company / Internet site	**Supplier of**	**Location**	**Result**
Complete Metal Works www.completemetalworks.com	Nickel Alloys	US	No answer
Special Metals www.specialmetals.com	Nickel Alloys	US, West Virginia	Samples would have cost about $1600 because of a minimum purchase
A-1 Wire www.a-1wire.com	Nickel Alloys	US	100 lbs minimum purchase amount
H Cross Company www.hcrosscompany.com	Nickel Alloys	US	Alloy temporary not available
McMaster Carr Supply www.mcmaster.com	Nickel 200, exact conditions not available	US	Cheap nickel rods and wire available, but only in standard sizes.
Good Fellow www.goodfellow.com	Nickel (pure)	US	Several good options, see website
Maritek Co, Ltd. www.materitek.com	"Giant Magnetostrictive Material"	China	The unit price for 4x40 sample rod is 32 US dollars
Gansu Tianxing Rare Earth Functional Materials, Ltd. www.txre.net	„Giant Magnetostrictive Material"	China	The unit price for 4x40 sample rod is 65 US dollars by taking ten pieces.
Etrema Products www.etrema.com	Terfenol-D	US	Quote was $ 180 per piece. High costs result out of labor.

IV LABVIEW MEASUREMENT SOFTWARE

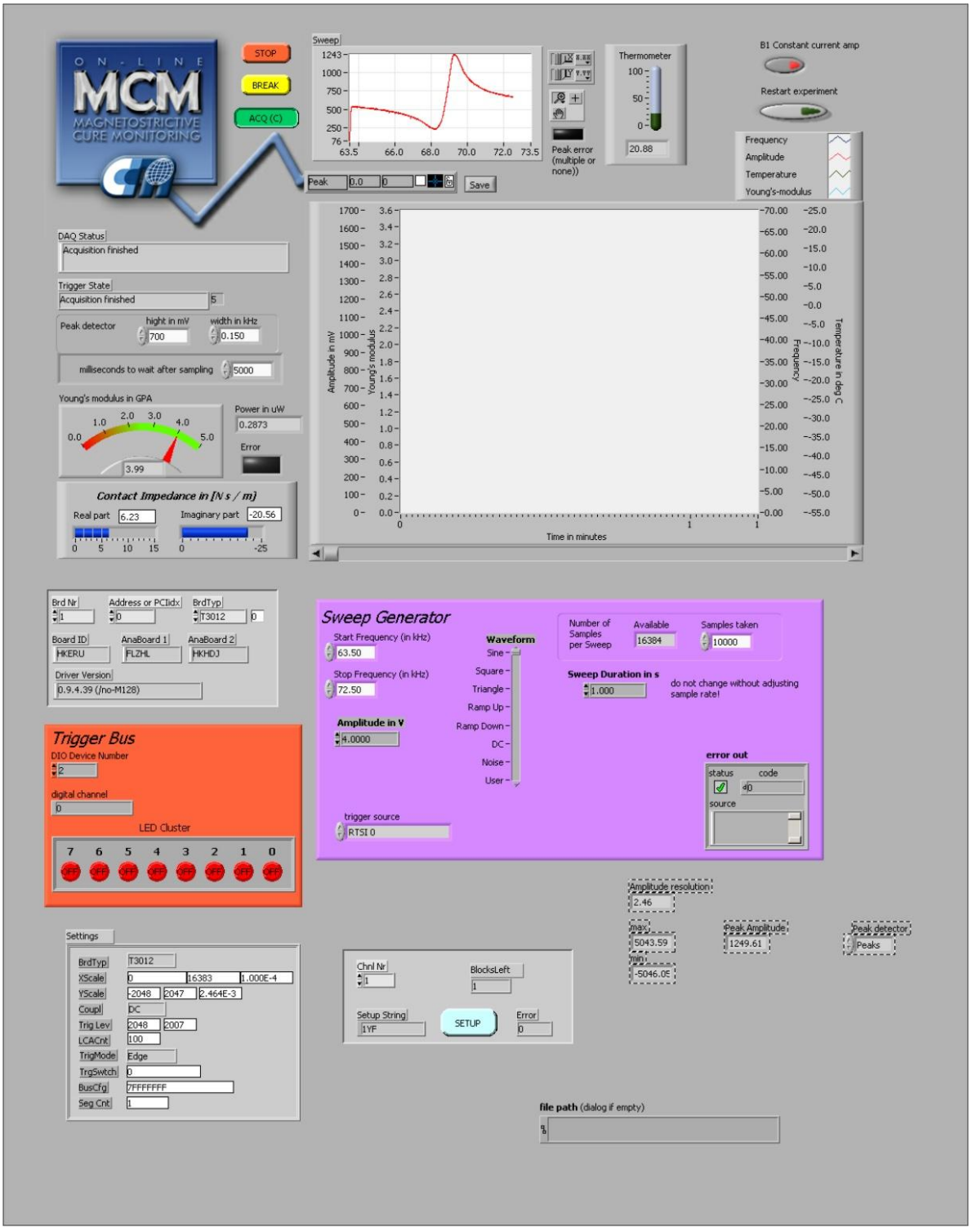

Figure 49: *The MCM main VI frontpanel.*

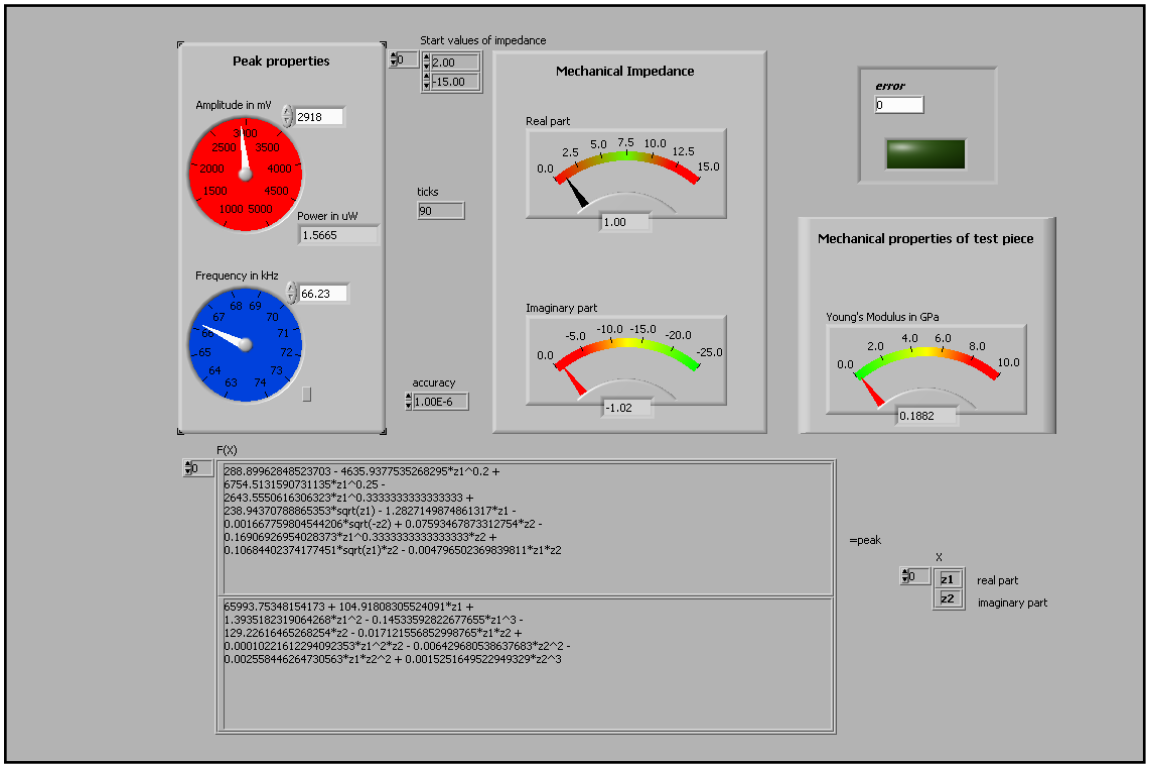

Figure 50: *The frontpanel of the "Mechanical Impedance" VI that determines the impedance and the Young's-modulus. The formulas have to be entered (or copied) directly into the VI .*

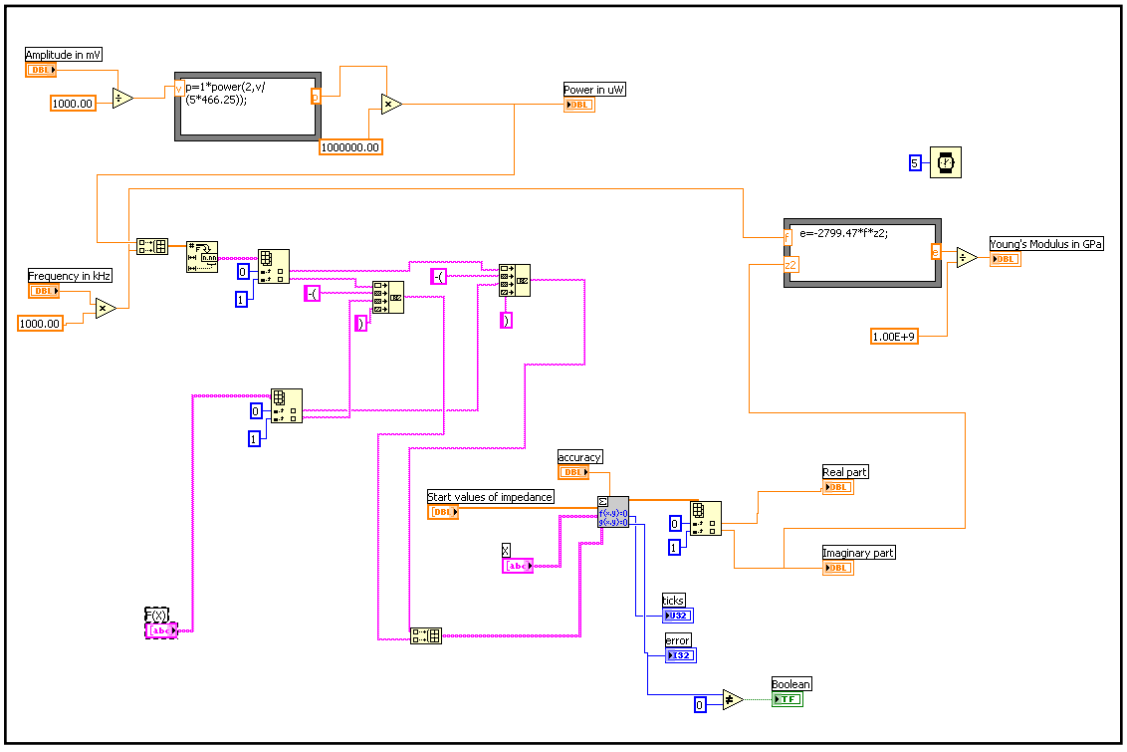

Figure 51: *The source code of the "Mechanical Impedance" VI.*

V SIGNAL-CONDITIONING AND INTERFACE CIRCUITS

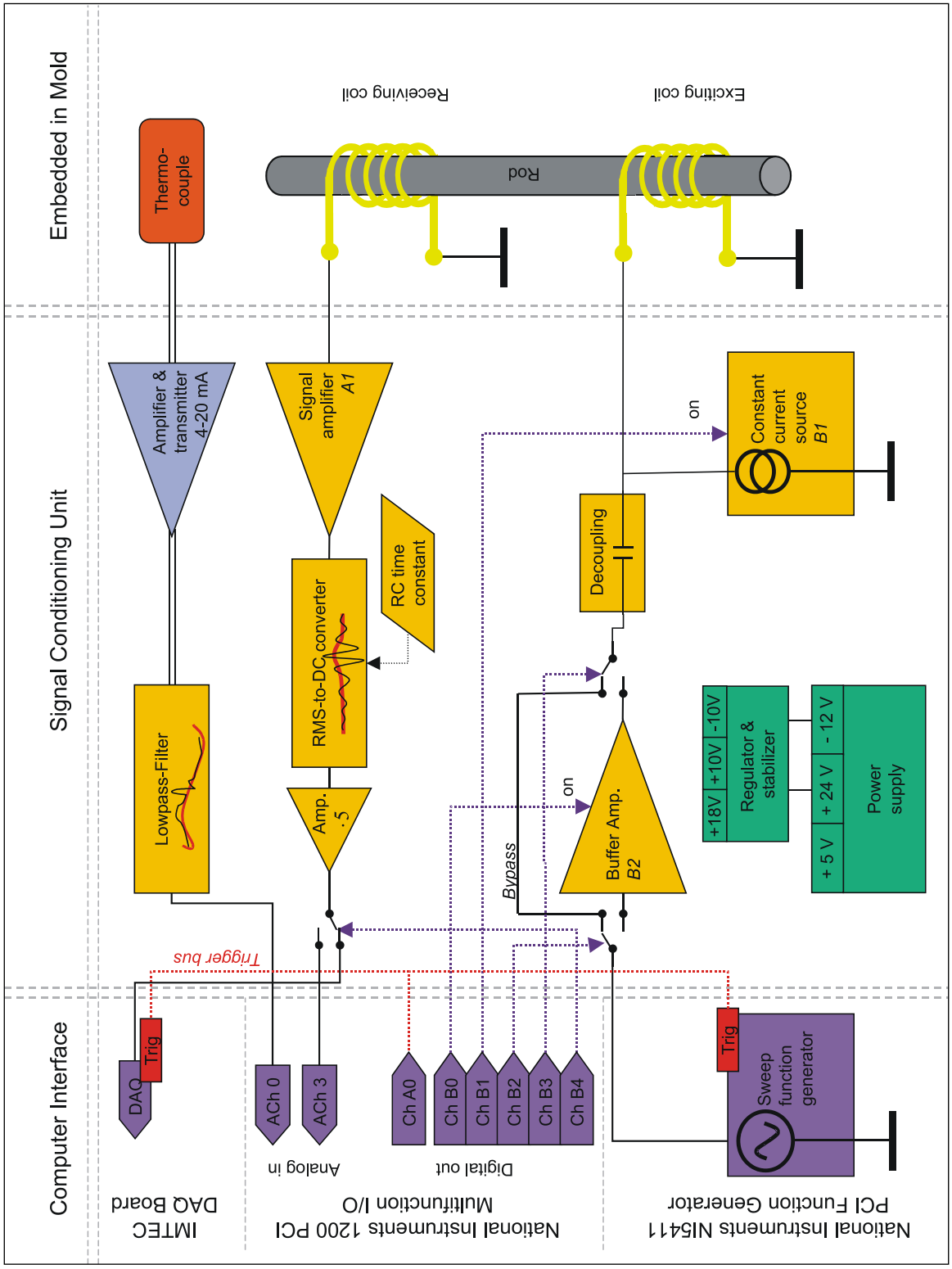

Figure 52: *Signal-conditioning and interface as described in chapter 8.*

V.1 Schematics

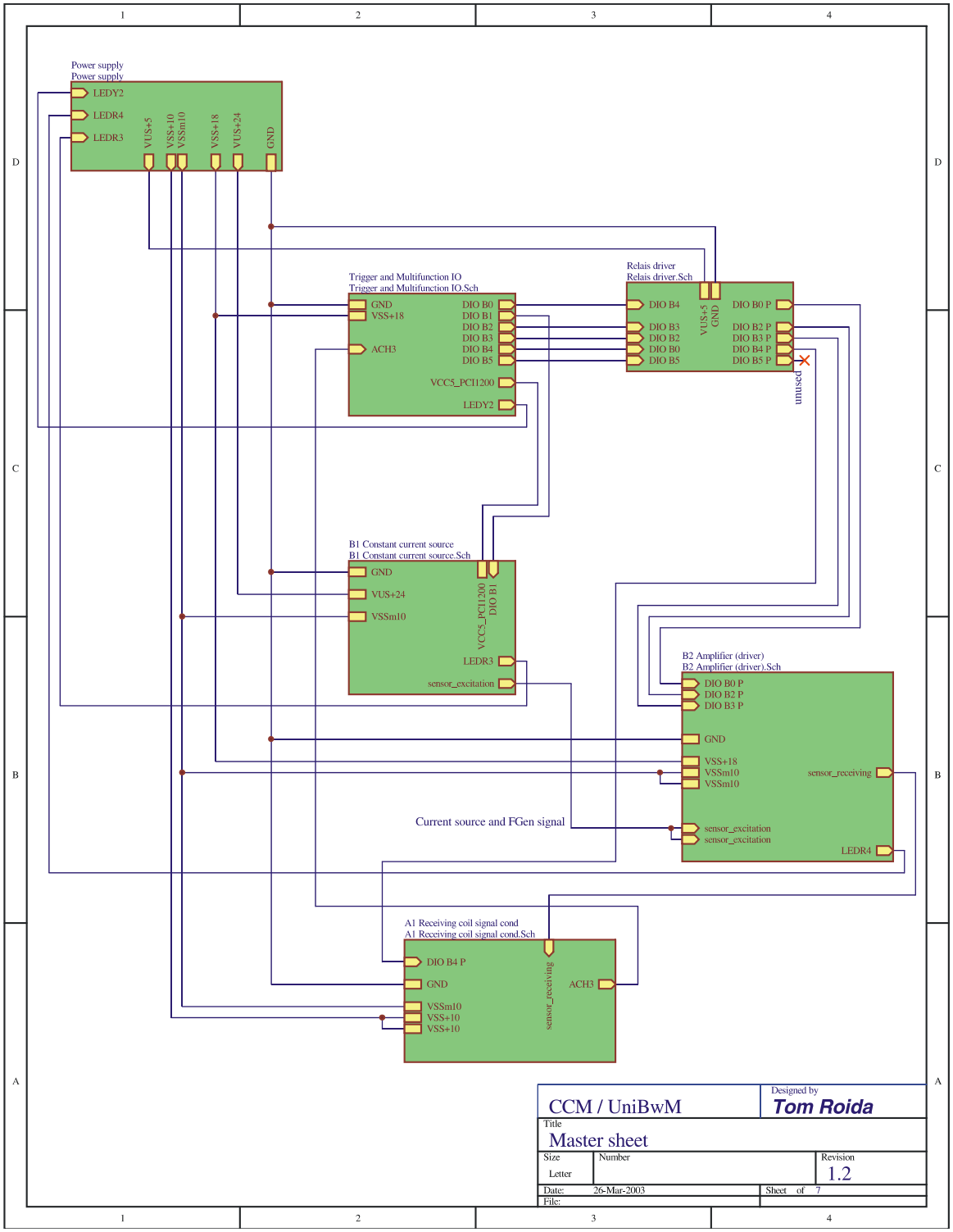

Figure 53: *Connections between the schematic sheets (see next 6 pages).*

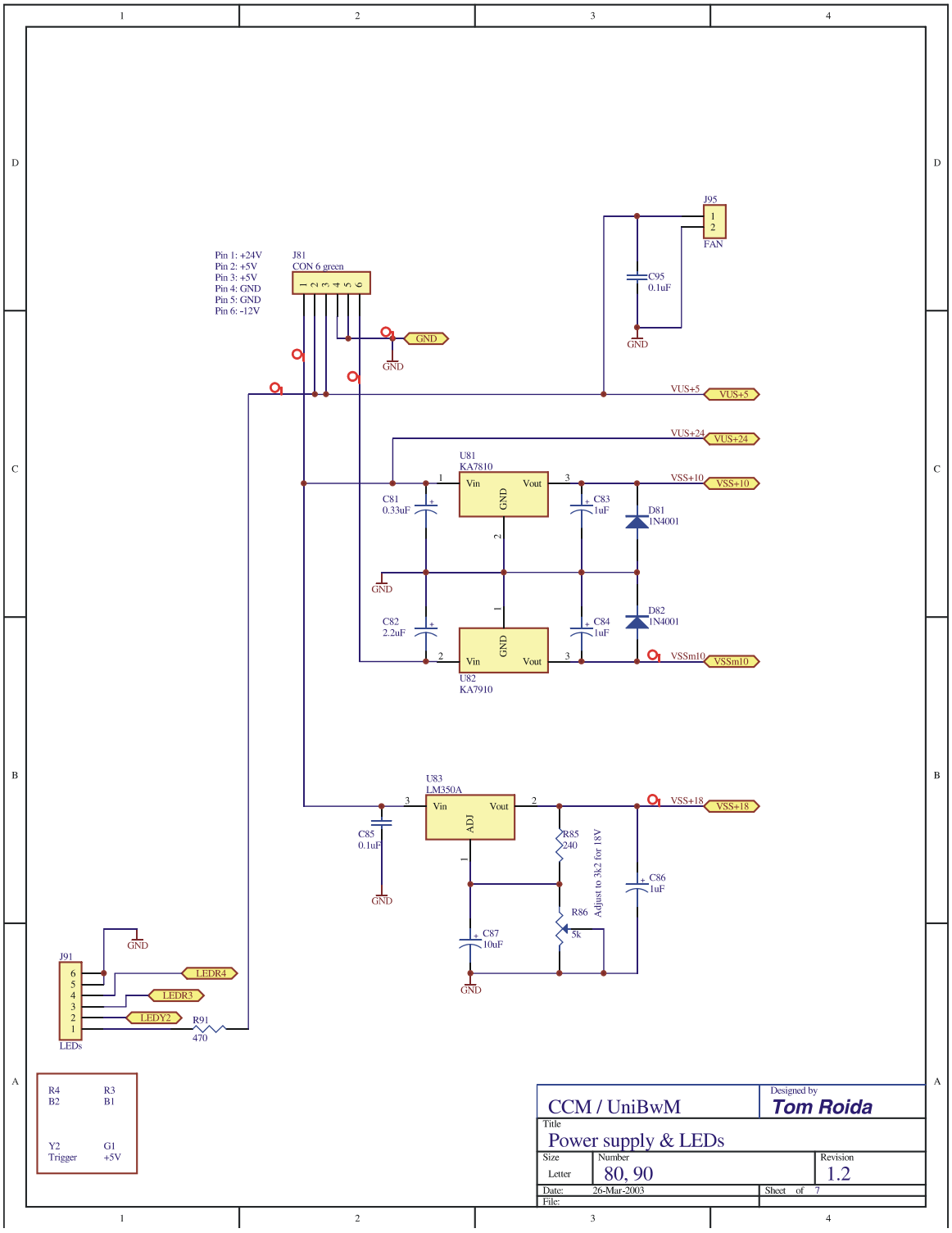

Figure 54: *Power supply, fan, and LEDs.*

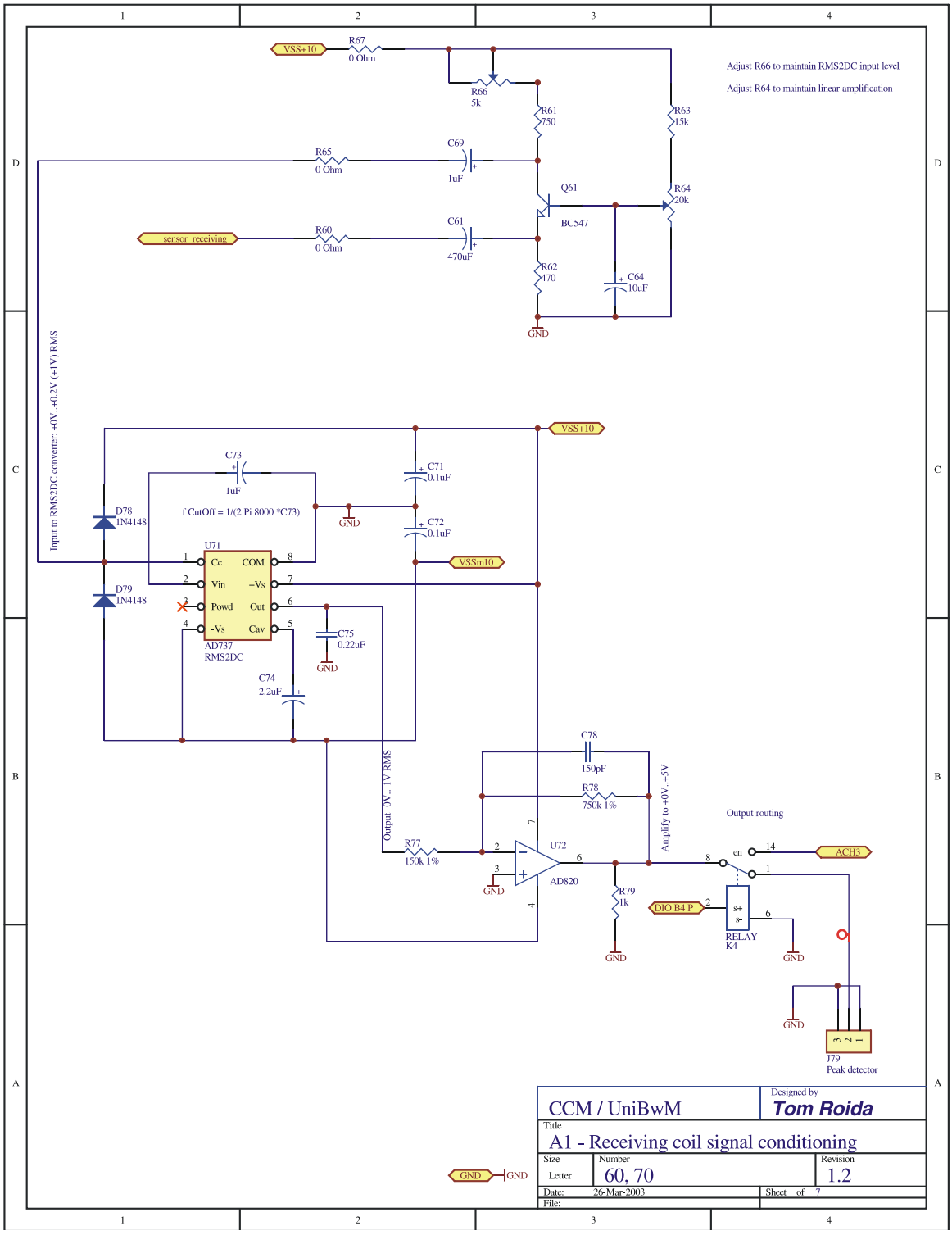

Figure 55: *"A1" signal amplifier for receiving coil.*

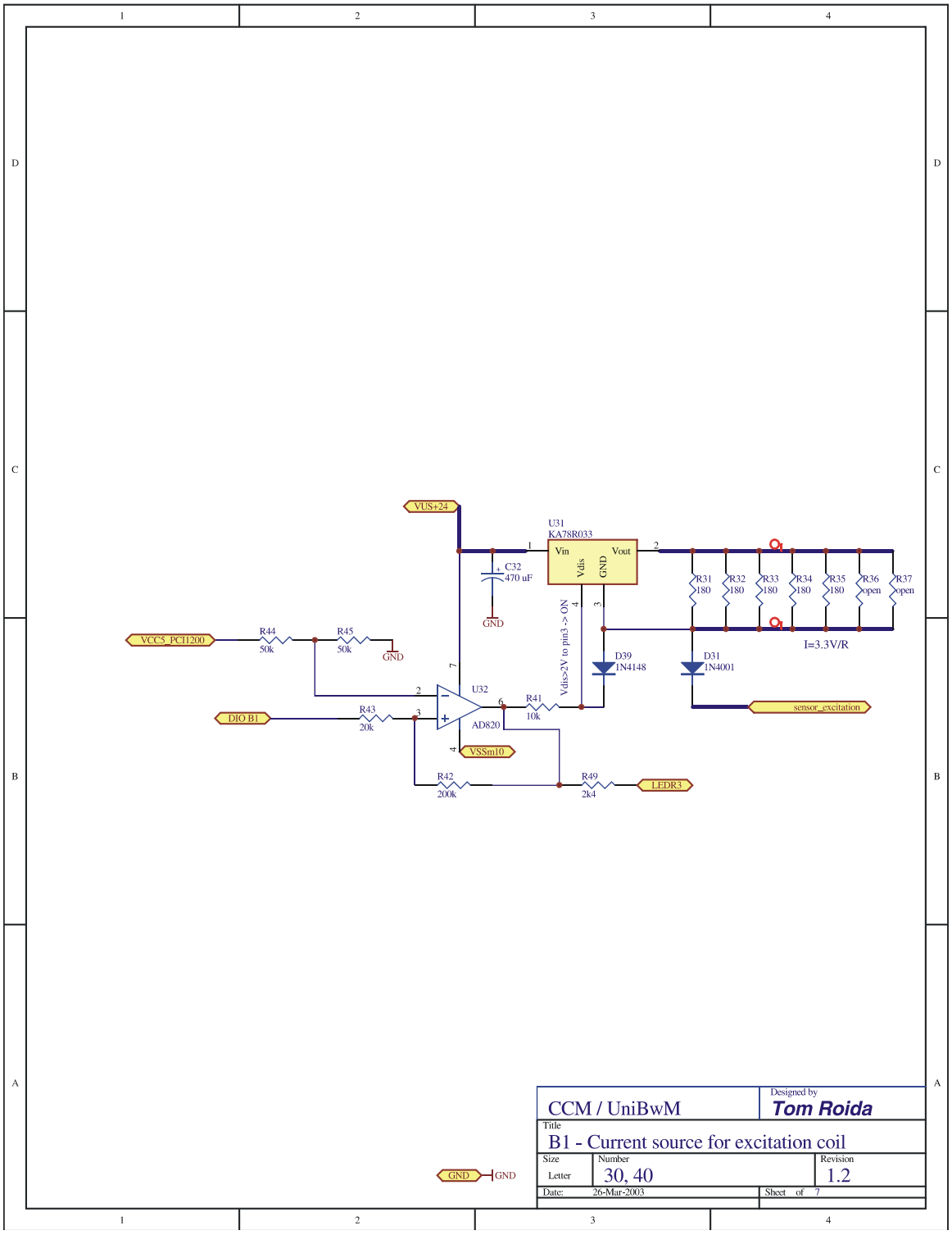

Figure 56: *"B1" constant current source, with control circuit to disable it.*

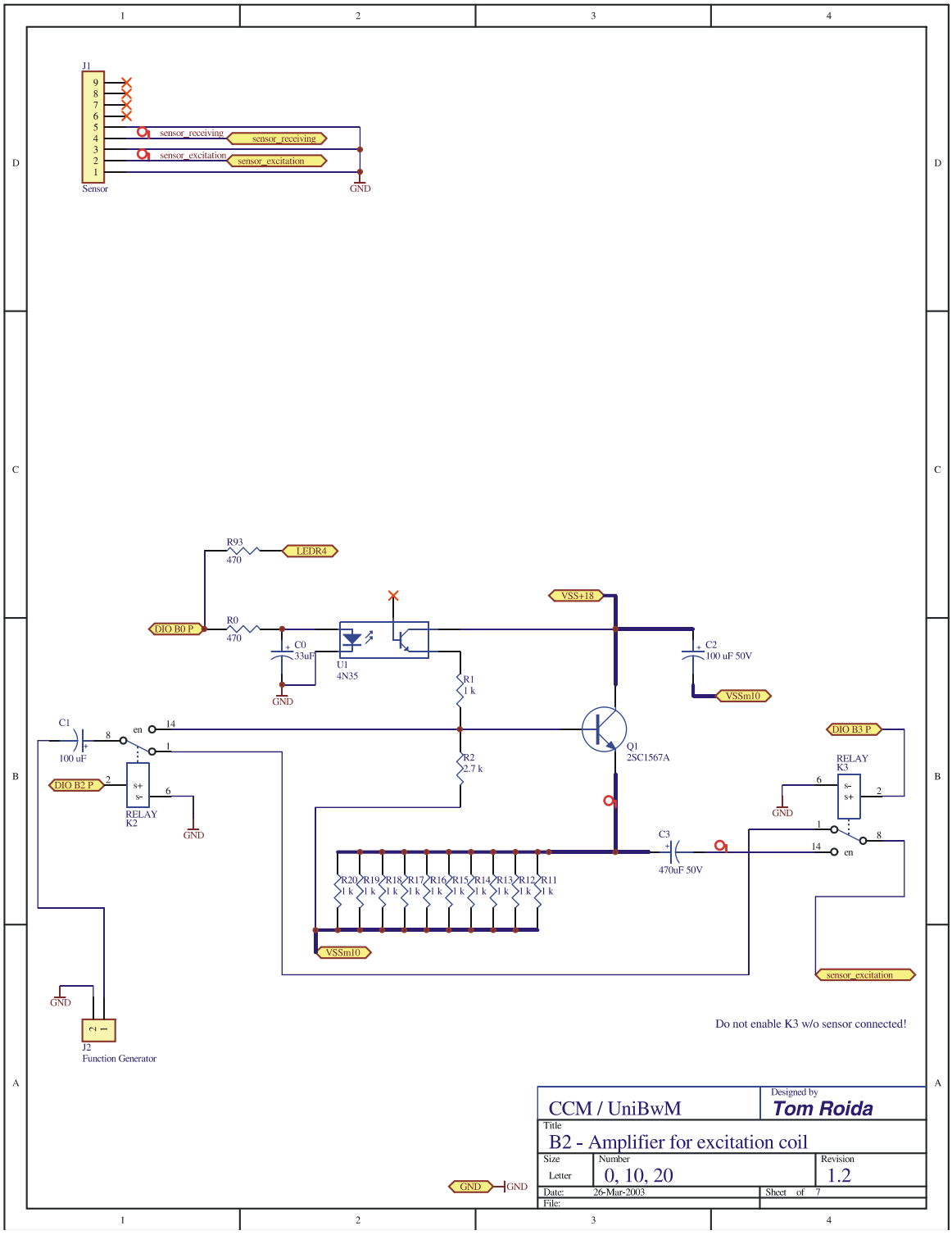

Figure 57: *"B2" amplifier for excitation coil, with relays to bypass it and an optocoupler to disable it.*

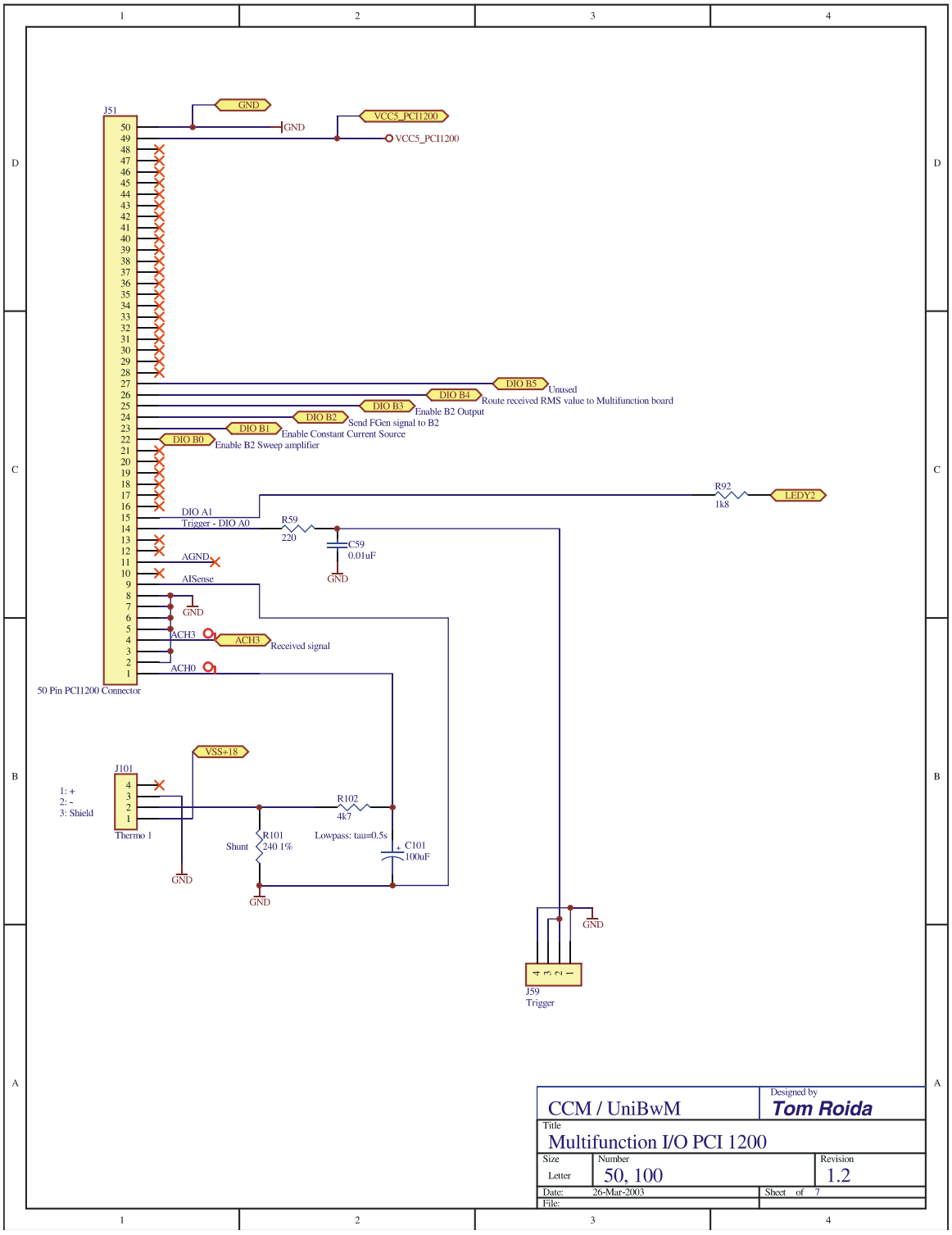

Figure 58: *Multifunction interface (trigger, digital outputs, analog inputs).*

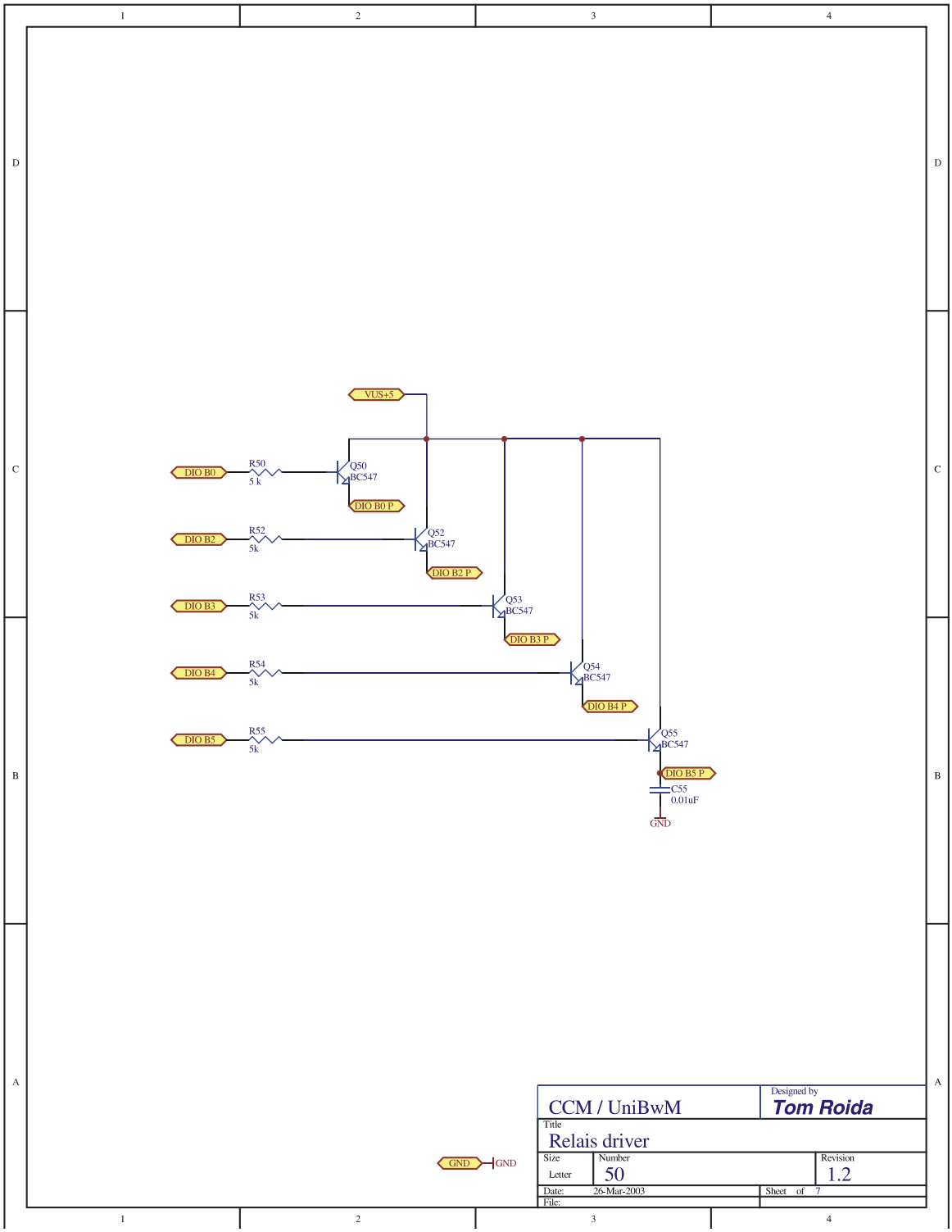

Figure 59: *Amplifier for digital outputs.*

V.2 PCB Layout

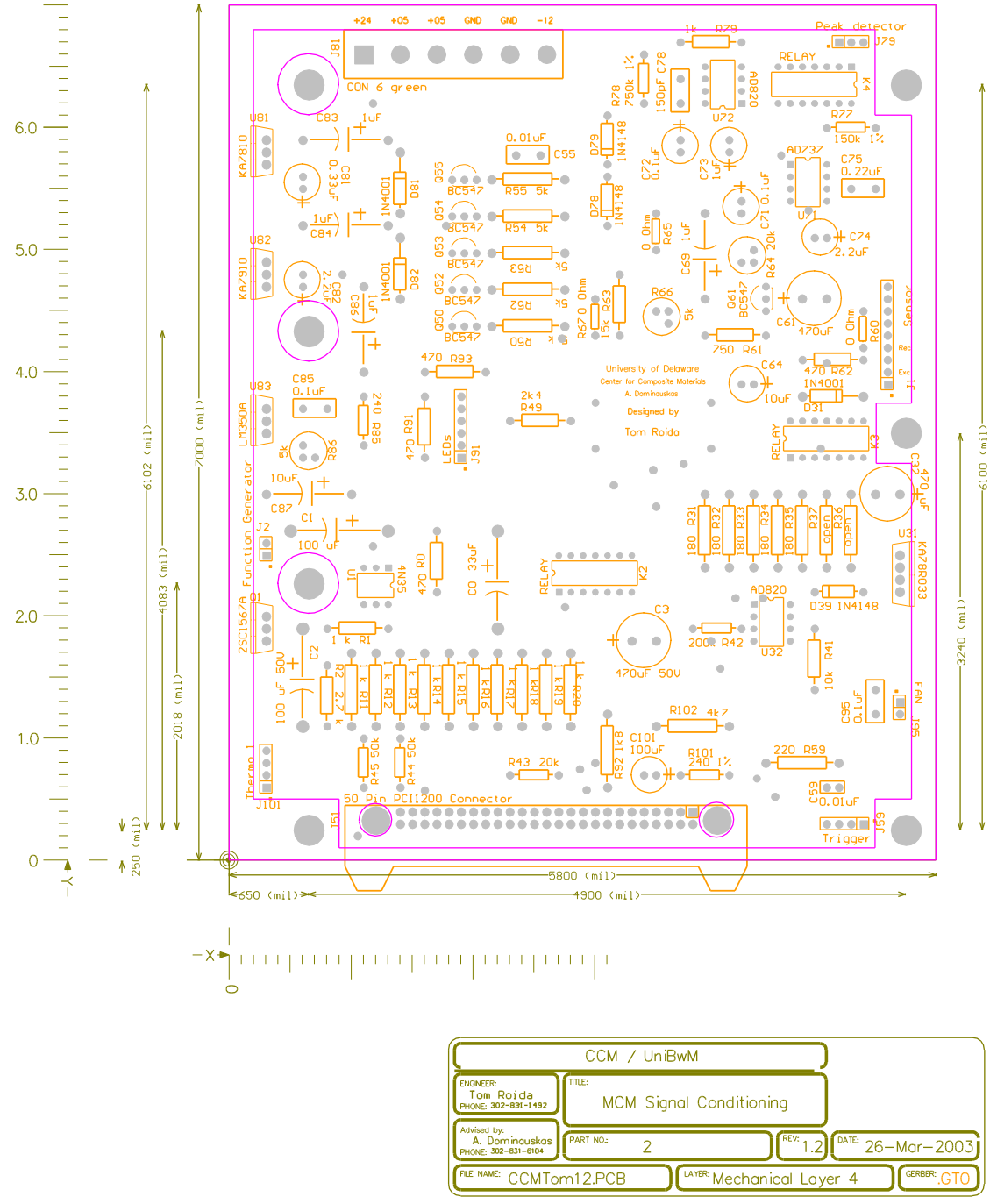

Figure 60: *Printed circuit board without copper layers.*

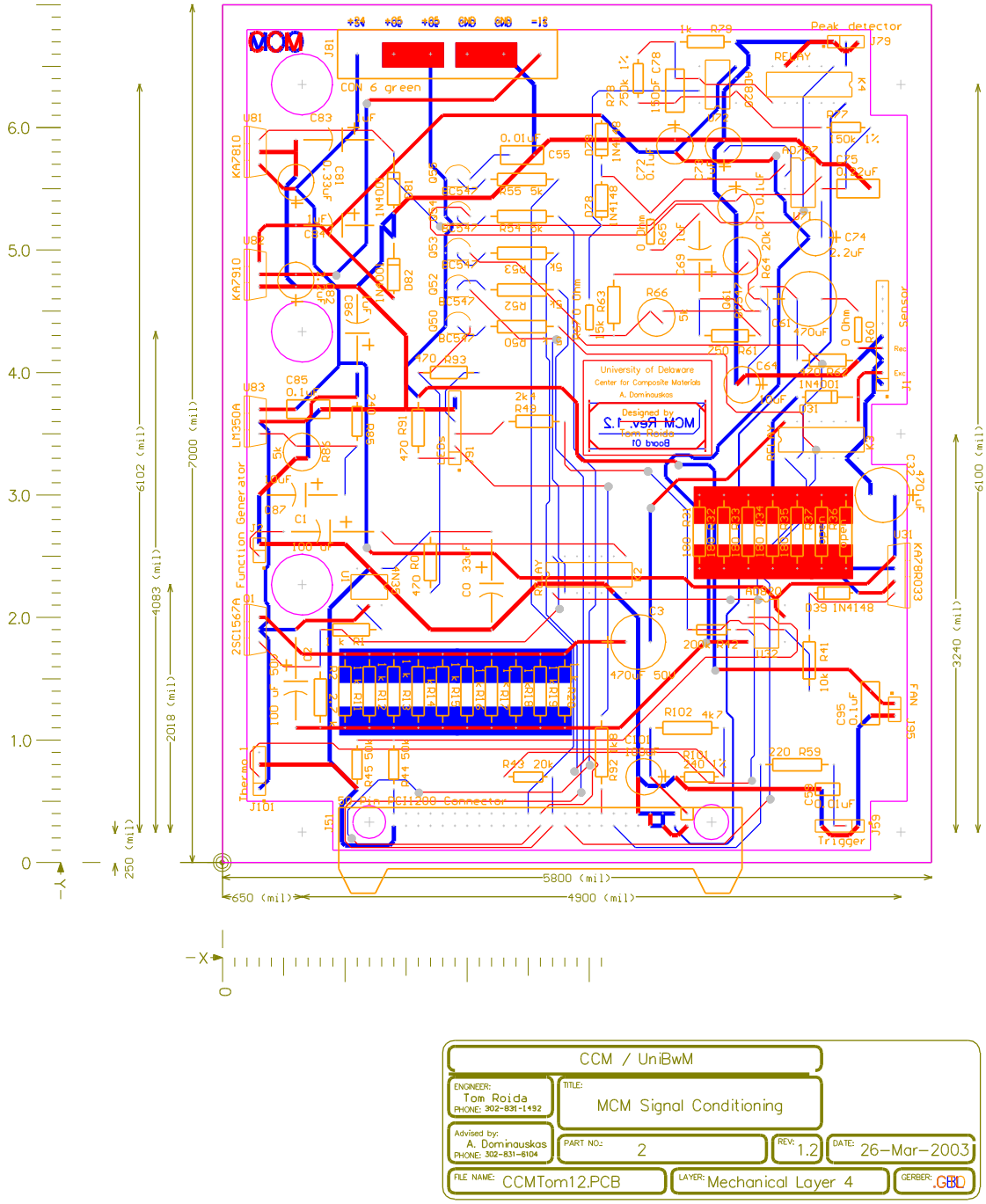

Figure 61: *Printed circuit board with copper layers.*

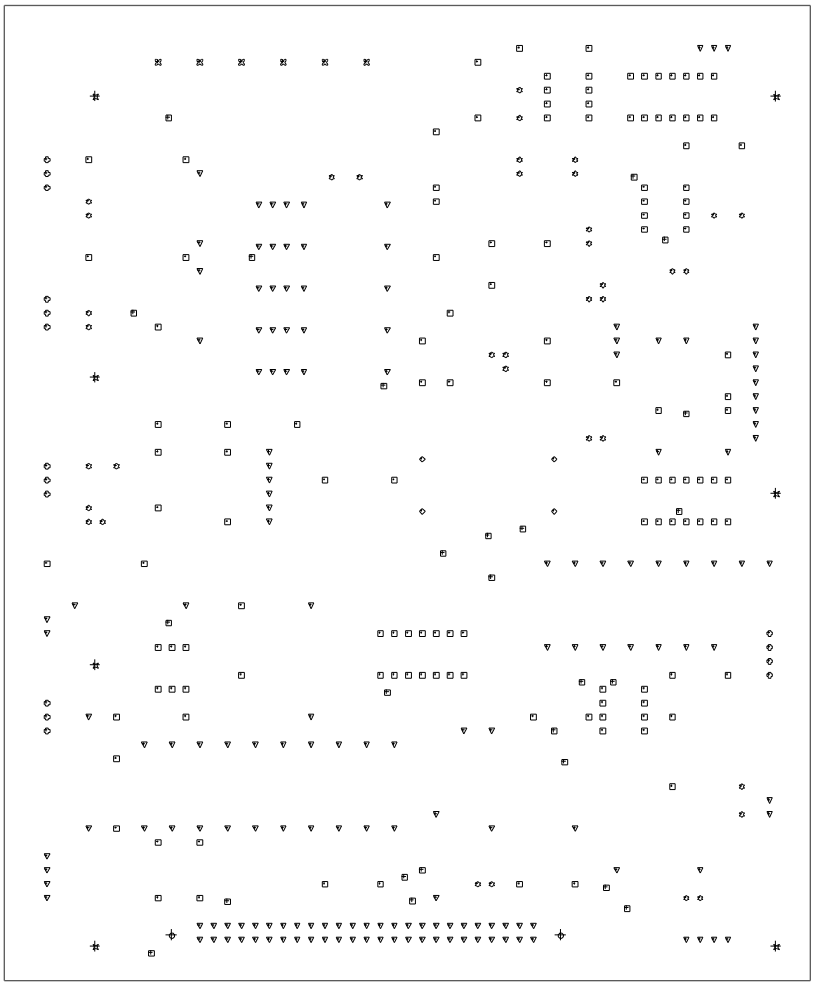

✡	37	28mil	0.7112mm	PTH
◇	4	30mil	0.762mm	PTH
□	157	32mil	0.8128mm	PTH
▽	166	40mil	1.016mm	PTH
○	16	45mil	1.143mm	PTH
⊠	6	56mil	1.4224mm	PTH
⌗	7	150mil	3.81mm	PTH
○	2	165mil	4.191mm	PTH
	395	Total		

Drill Drawing.

Figure 62: *Printed circuit board drill guide.*

V.3 Photos

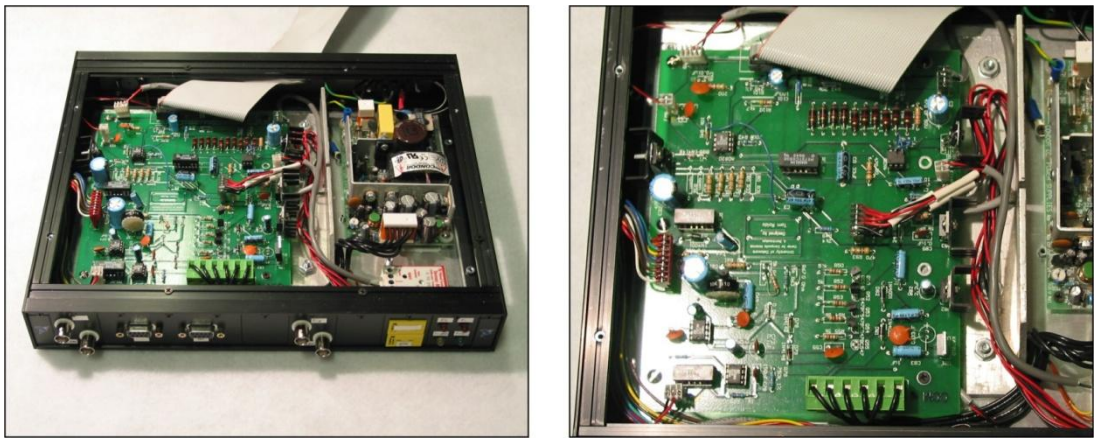

Figure 63: *Printed circuit board mounted in an enclosure with power supply and connectors.*

VI SENSOR CONSTRUCTION

Technical drawings

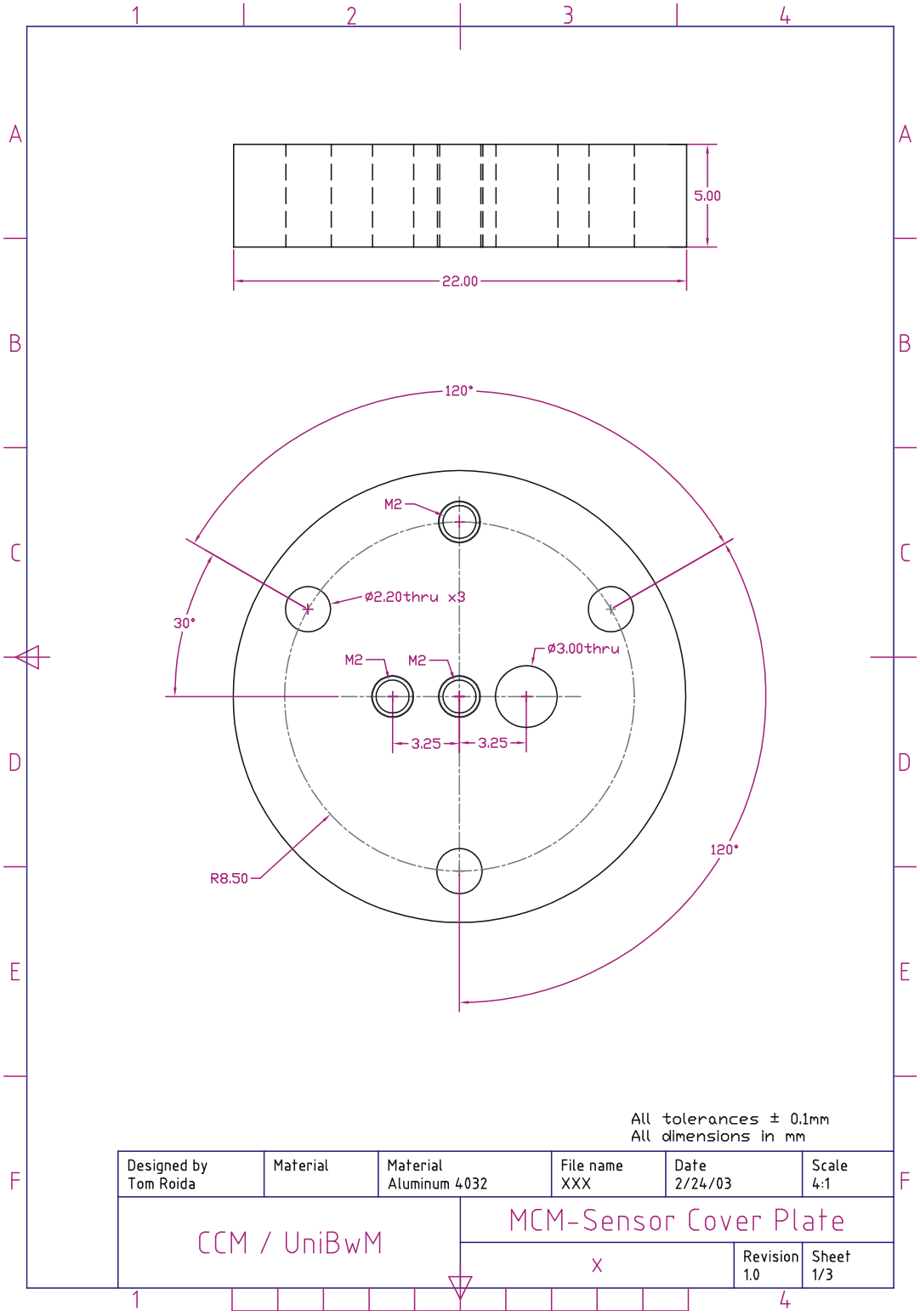

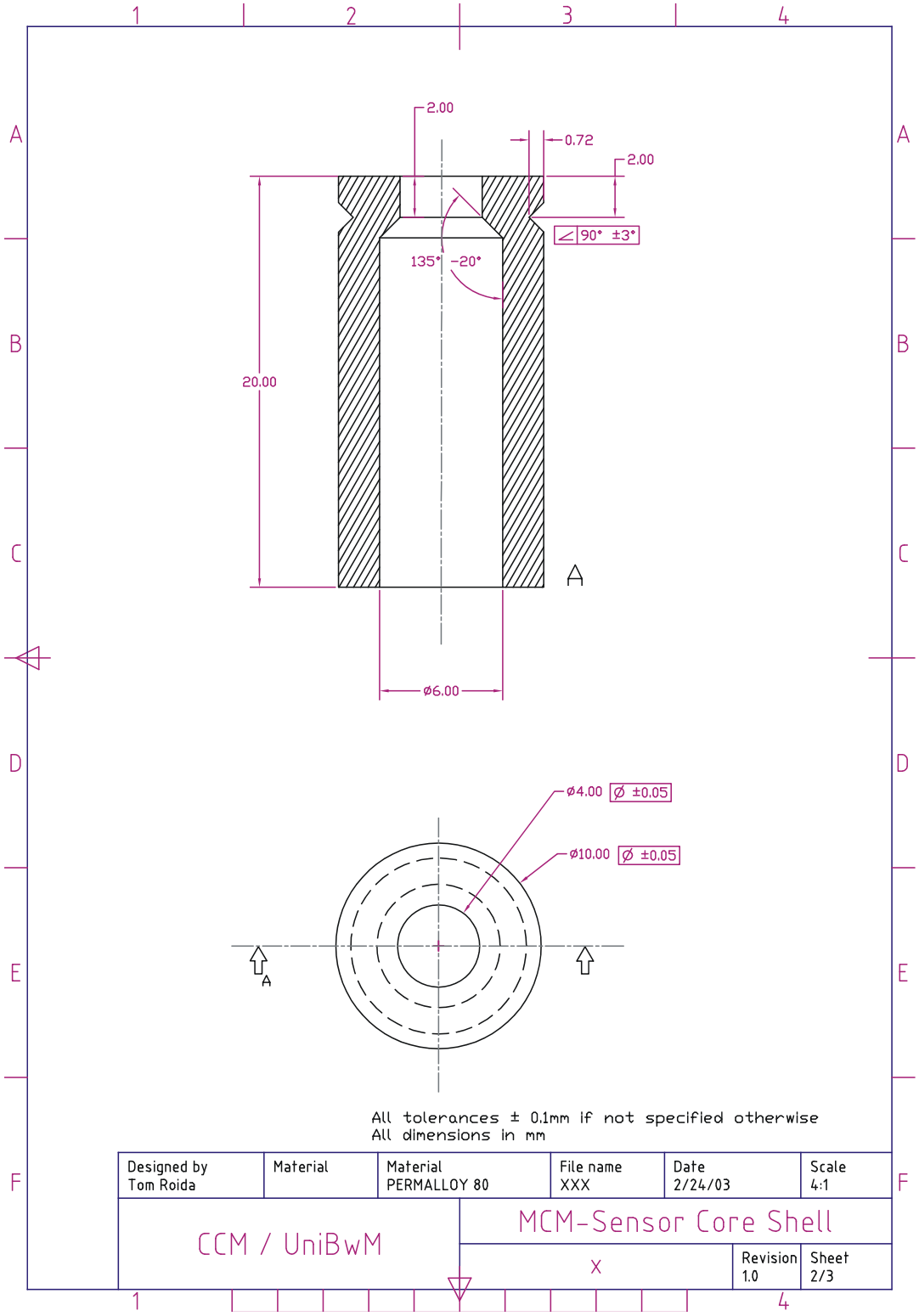
1
2
3
4
A
B
C
D
E
F
2.00
0.72
2.00
90° ±3°
135°
20°
20.00
A
ø6.00
ø4.00 Ø ±0.05
ø10.00 Ø ±0.05
A
All tolerances ± 0.1mm if not specified otherwise
All dimensions in mm
Designed by Tom Roida
Material
Material PERMALLOY 80
File name XXX
Date 2/24/03
Scale 4:1
CCM / UniBwM
MCM-Sensor Core Shell
X
Revision 1.0
Sheet 2/3

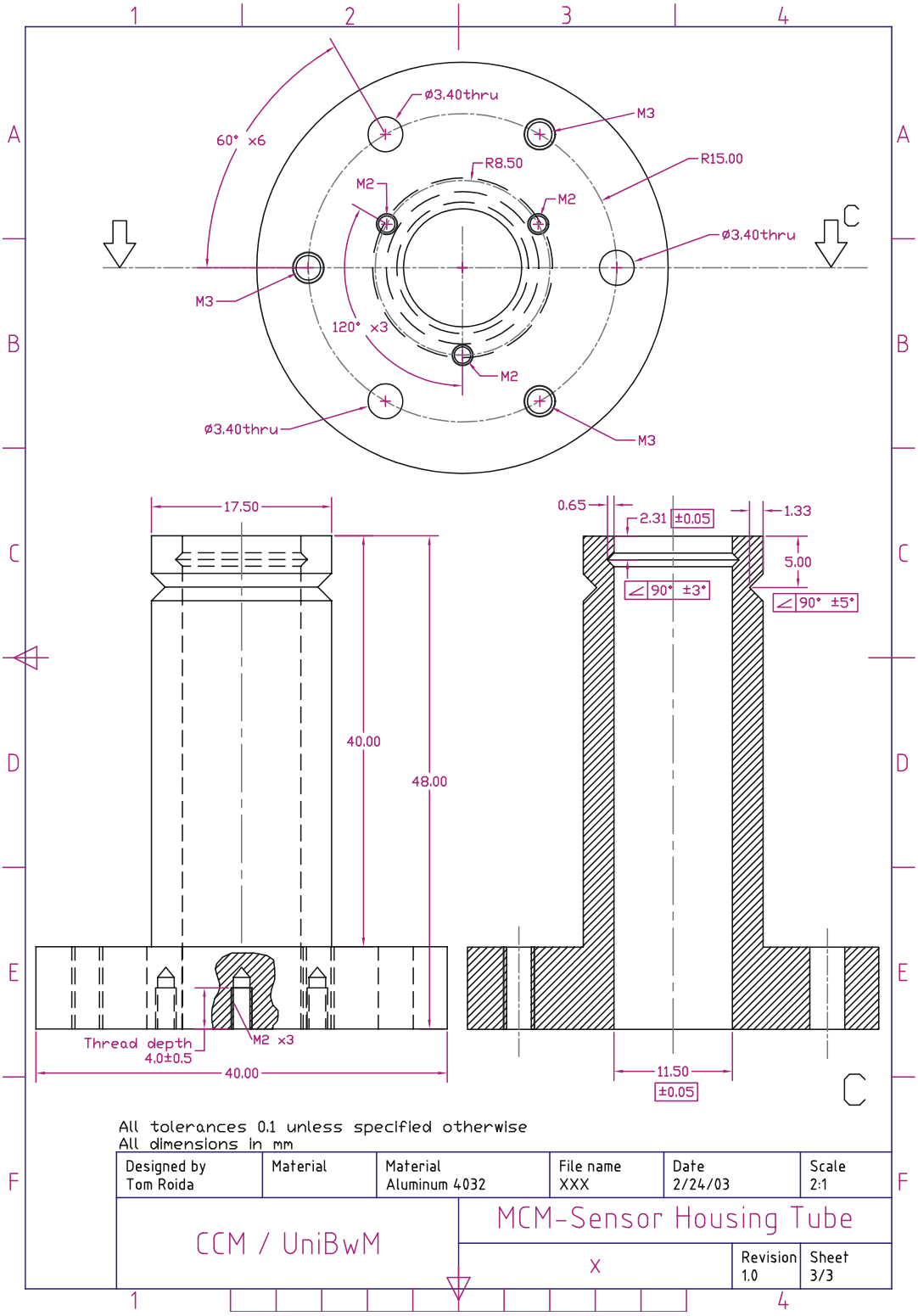
1
2
3
4
A
B
C
D
E
F
ø3.40thru
M3
R15.00
R8.50
M2
M2
ø3.40thru
C
60° x6
M3
120° x3
M2
ø3.40thru
M3
17.50
40.00
48.00
Thread depth
4.0±0.5
M2 x3
40.00
0.65
2.31 ±0.05
1.33
5.00
90° ±3°
90° ±5°
11.50
±0.05
C
All tolerances 0.1 unless specified otherwise
All dimensions in mm
Designed by
Tom Roida
Material
Material
Aluminum 4032
File name
XXX
Date
2/24/03
Scale
2:1
CCM / UniBwM
MCM-Sensor Housing Tube
X
Revision
1.0
Sheet
3/3

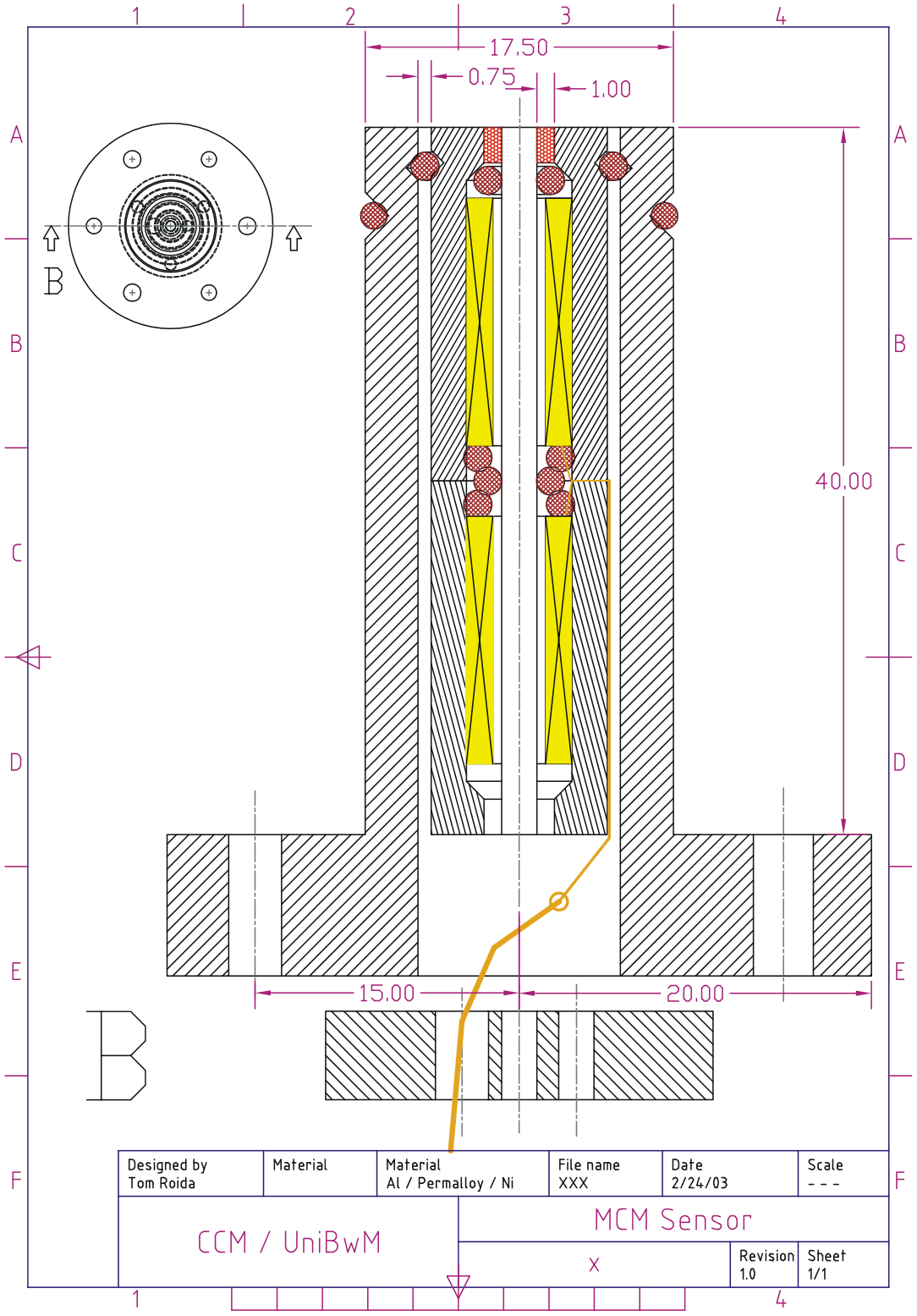
1
2
3
4
A
B
C
D
E
F
17.50
0.75
1.00
40.00
15.00
20.00
B
Designed by
Tom Roida
Material
Material
Al / Permalloy / Ni
File name
XXX
Date
2/24/03
Scale
- - -
CCM / UniBwM
MCM Sensor
x
Revision
1.0
Sheet
1/1

Photos

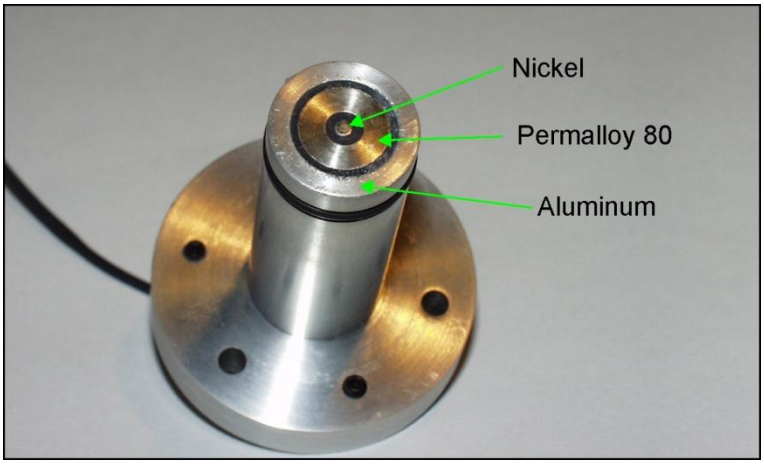

Figure 64: *Assembled sensor, top view*

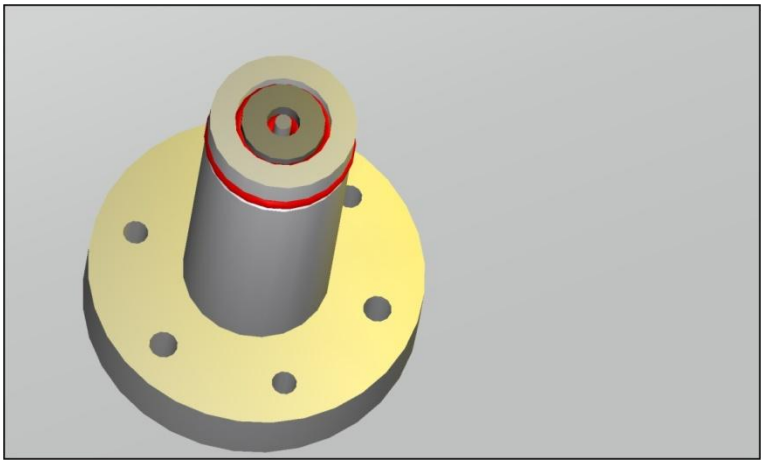

Figure 65: *3D model of sensor (AutoCAD). The technical drawings were created with views (sectional, top, front, etc.) from this solid model.*

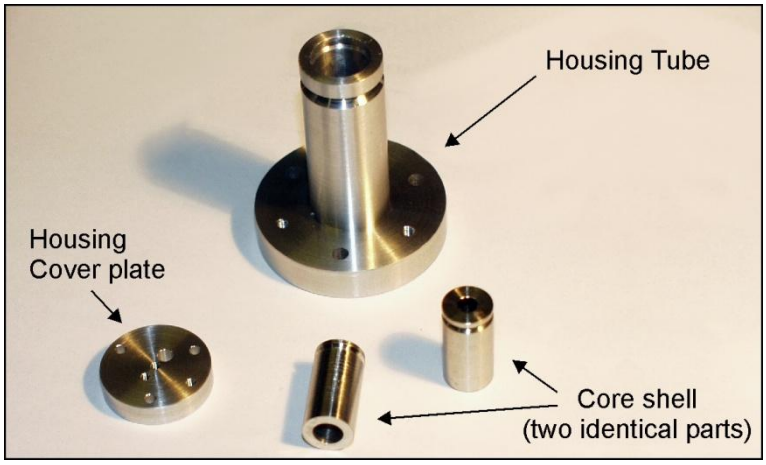

Figure 66: *Metal sensor parts*

VII MEASUREMENTS

This appendix contains some cure measurements and additional measurements of different kinds to support the theoretical sensor model.

VII.1 Cure Measurements

Time independent curing curves

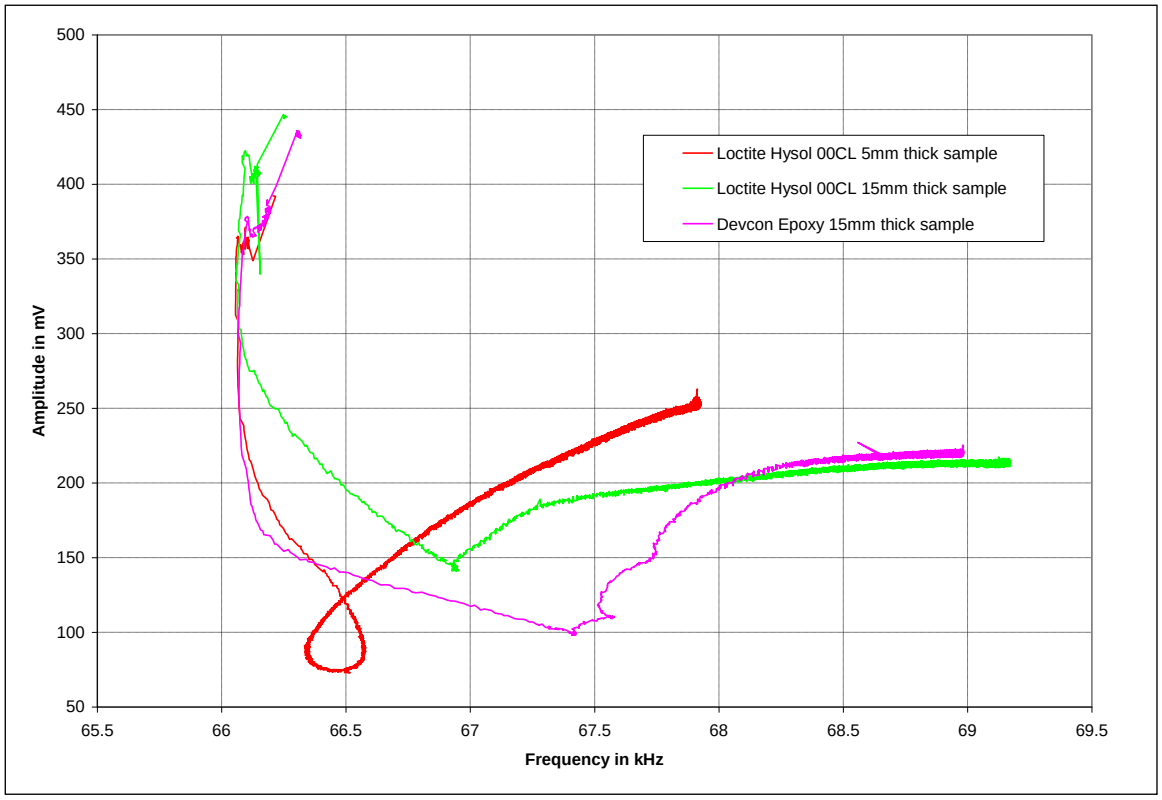

Figure 67: *The resonant amplitude during curing is plotted over the resonant frequency. Curing of two epoxy resins at 22ºC environment temperature.*

Repeatability of measurements

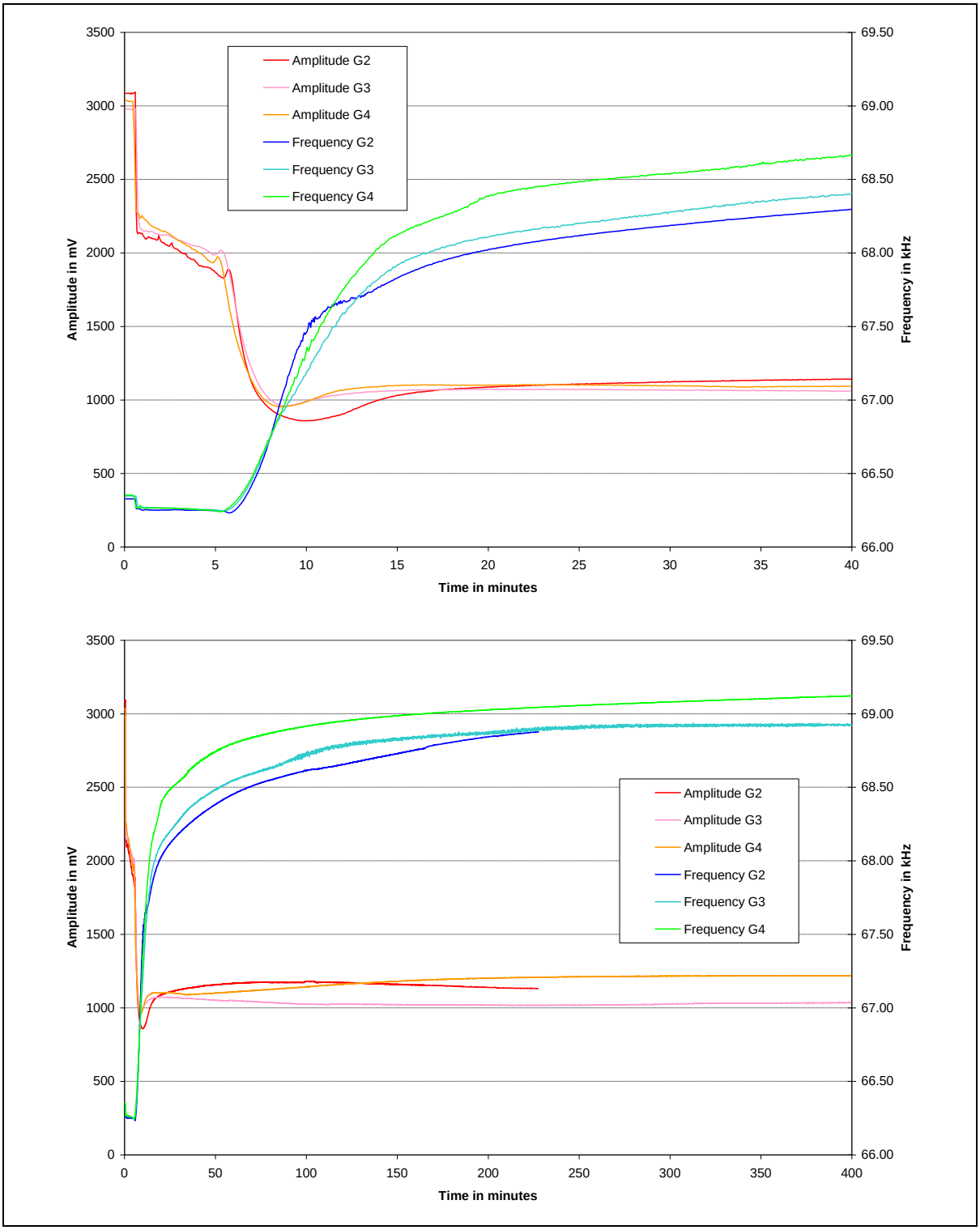

Figure 68: *Three measurements of "DEVCON 5-minute epoxy", under the same conditions (Environment temperature: 22ºC, sample thickness: 12.7±0.1mm, measured with the same MCM sensor). The measurement "G1" was aborted due to a software problem and therefore not shown.*

VII.2 Measuring Magnetostrictive Strain with a Microscope

The following experiment was accomplished to verify the data of magnetostriction of certain materials. The elongation of magnetostrictive materials is hard to measure because of the low strain values. Therefore a microscope was used.

The strain was measured under static conditions with a magnetic field generated by a long solenoid (length: 70mm, inner diameter: 9.8mm, outer diameter: 17.5mm, number of windings: 280) and a 2.5A Power Supply.

It was not possible to measure the strain under dynamic conditions with this setup, although the strain can become much larger (e.g. in the case of resonance) than in the static case. This was because an amplifier for the function generator was not available for this experiment.

Example:

Pure nickel has a saturation strain of approximately:

$$\frac{\Delta l}{l} = -30 * 10^{-6}.$$

At a 4 cm long nickel bar this causes a maximum contraction of about $1\mu m$. With a magnification of 1000 at a microscope this is about 1mm.

Figure 69 illustrates the measurement setup.

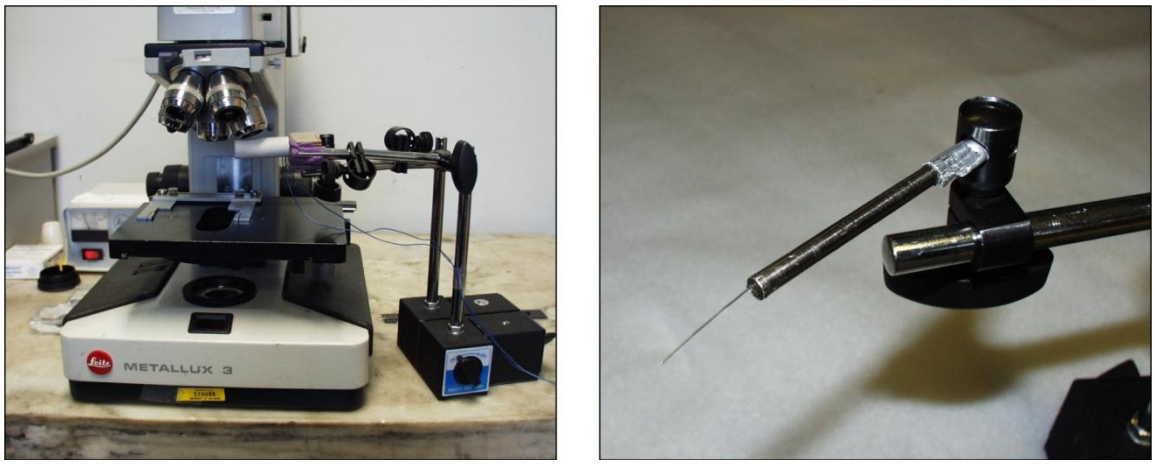

Figure 69: *Measurement setup for measuring static strain.*

Measurement details:

- Ni 200 from McMaster Carr Supply.
- Rod: Diameter d = 4.2 mm, overall length 66.6 mm, length of the part which was not clamped: l= 60mm. Therefore $l = (63 \pm 3) mm$.
- Material was turned on a lathe with no special precautions and had a high surface roughness.
- Room and part temperature during experiment: 22.5ºC
- Used microscope magnification: 500

The measured strain was about $\Delta l / l = -(29.8 \pm 9.6) * 10^{-6}$ at saturation. This is in good accordance to literature values.

Calculation of measurement errors:

The following error sources could be determined:

- Accuracy of the scale reading: $0.5 \mu m$.

  Example: This causes an error of $\pm 25\%$ when the measurement is $2 \mu m$.

- A vibration of the whole setup created a stochastic movement of the rod of approximately $\pm 0.1 \mu m$.

  Example: This causes an error of $\pm 5\%$ if the measurement is $1 \mu m$.

- The non-ideal clamping of the rod allows a certain strain in between the support itself. Example: If the support has a depth of 3mm and the free length of the rod is 50mm, than the effective length of the rod becomes 51.5mm $\pm 1.5 mm$ $(\pm 3\%)$.

The following error sources could *not* be determined quantitatively:

- Coil positioning: The coil around the rod seemed to create a magnetic force onto the rod. Because of the clamping of the rod this caused a movement towards one side. (The clamping was not stiff enough to prevent a slight movement of the rod in between the clamp itself.) This effect superposed with the magnetostrictive effect, but because this effect occurred perpendicular to the magnetostrictive effect it could easily canceled out by repositioning the coil. Therefore it was neglected in the error calculation.
- Attached pin for microscope view: It is assumed that the pin and the glue had no effect on the static experiment because no deformation occurred.

Formula for calculating the strain:

$$\varepsilon = \frac{\Delta l}{l} = \frac{a}{l} \qquad (68)$$

With:

ε: Strain

a: Measured elongation (with microscope) in m

l: Length of the free rod

Determining the error with Gauss:

$$\Delta\varepsilon = \sqrt{\sum \left(\frac{\partial \varepsilon}{\partial x_i}\Delta x_i\right)^2} = \sqrt{\frac{\Delta a^2}{l^2} + \frac{a^2 \Delta l^2}{l^4}} \qquad (69)$$

With this formula the error can be calculated to:

$$\Delta\varepsilon = 9.5 \cdot 10^{-6} \qquad (70)$$

VII.3 Additional measurements

Transfer function of input amplifier

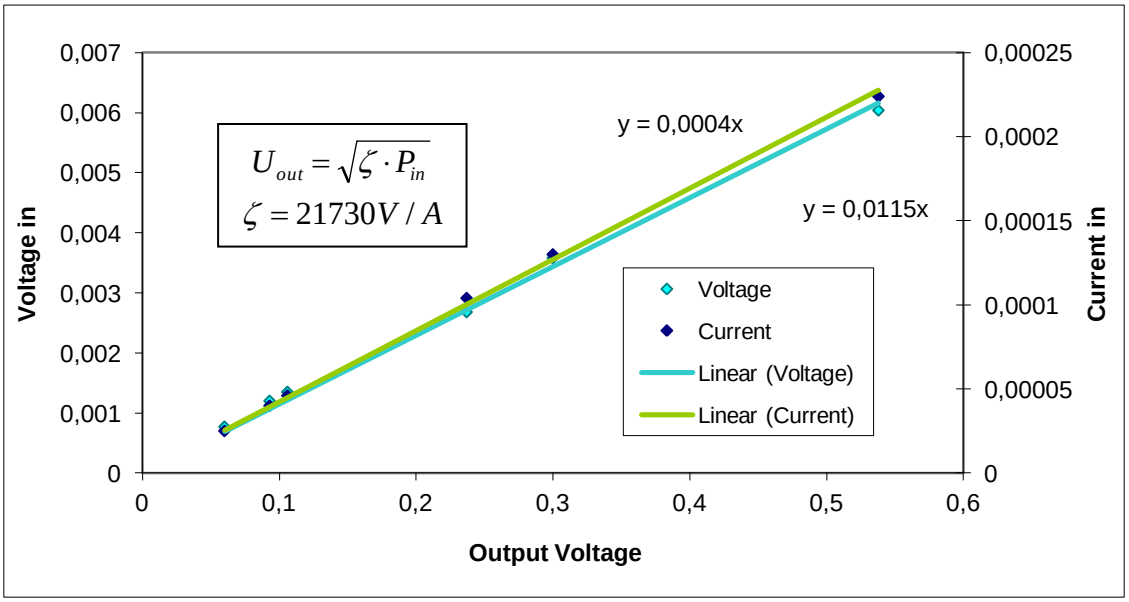

Figure 70: *Measured transfer function of input amplifier. The output voltage is linear to both input current and voltage of the receiving coil; hence the output voltage is proportional to the square root of the input power.*

Sensor frequency response first to third mode

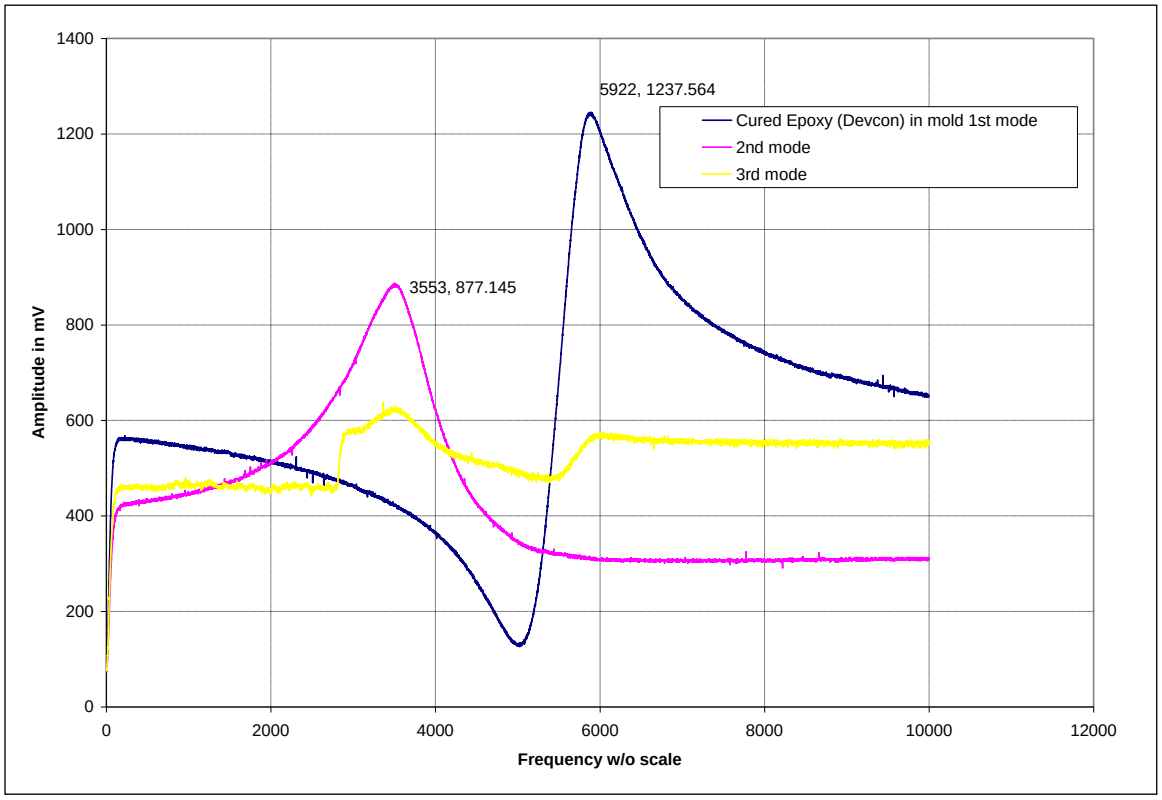

Figure 71: *Frequency response of the sensor with cured epoxy. Shown is the first to the second mode of oscillations (as a result of excitation in different frequency ranges).*

Coefficients for Gladwell's model

The coefficients for Gladwell's model of the contact impedance are given in a table[138]. Actually the values can be calculated as complicated integral functions of the Poisson's-ratio. In the range, which is interesting for MCM sensors these values can also be approximated with polynomial functions.

[138] See Gladwell: Contact Impedance Meter.

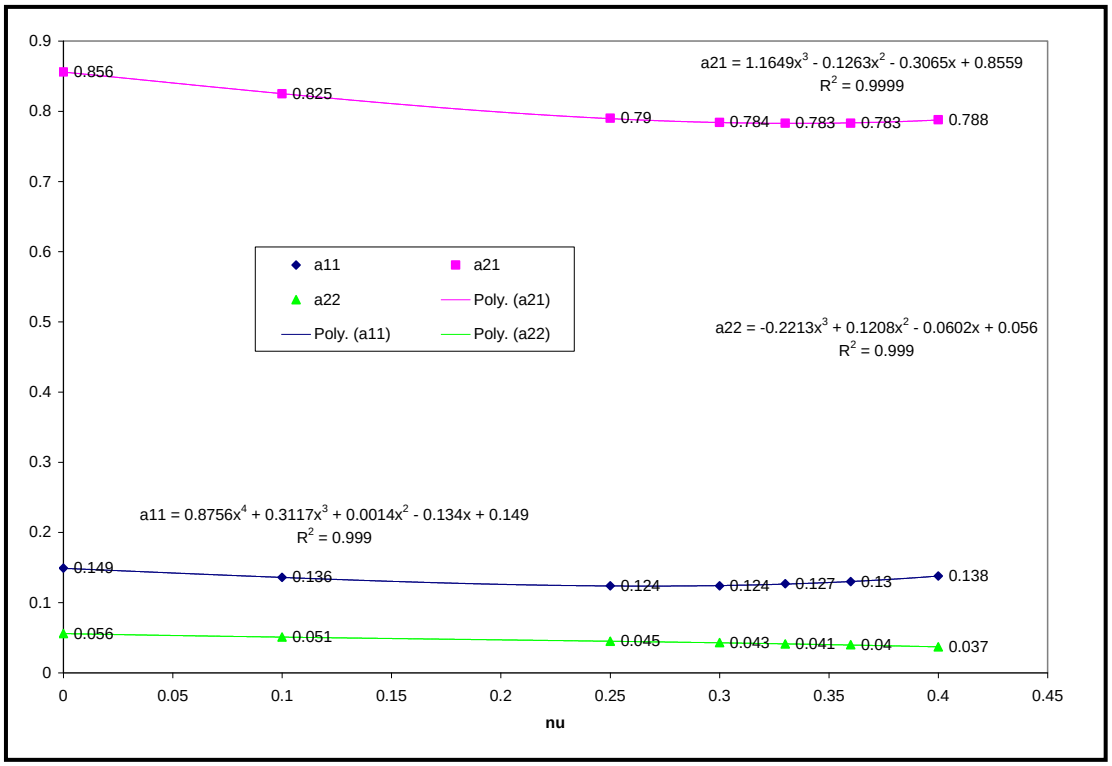

Figure 72: *Polynomial approximation of* a_{ik}.

Voltage transfer function

Table 7: *Measurements to determine the voltage transfer function of the sensor at 75kHz. See chapter 8.1.2 for details*

excitation voltage (RMS) in V	2.192	1.096	0.533	2.732	3.381
measured receiving voltage (RMS) in V	0.00158	0.000805	0.000414	0.001978	0.002515
ideal receiving voltage (RMS) in V	0.681956	0.340978	0.165822	0.849956	1.051867
measured/ideal	0.002317	0.002361	0.002497	0.002327	0.002391
		average	0.002379		

VIII ADDITIONAL RESOURCES ABOUT CURE MONITORING

The following list of literature provides additional resources about cure monitoring, besides the literature that is mentioned in the references:

Challiux, E. et al.: In situ multidetection: application for composite cure monitoring. In: Proceedings of SPIE, Volume 4073, 2000. pp. 290-296

Djordjevic, B. Boro: Ultrasonic Cure Monitoring System. Presentation at the Center for Nondestructive Evaluation, Johns Hopkins University, Baltimore, unknown date.

Dominauskas A, Bansevicius R, Dragasius E.: The Use of Ultrasonic Wave-Guides for Characterization of Composite Materials - Translation from: Implantuotu ultragarsiniu bangolaidziu panaudojimas kompozitiniu medziagu diagnostikoje. Translation:. Kaunas: Technologija, Mechanika-98, Lietuvos mokslas ir pramone, Mechanine technologija XXVI, 1998. pp. 145-148.

Lee, C. William: Composite Cure Process Control by Expert Systems. In: Proceedings of the American Society for Composites, First Technical Conference, Dayton, Ohio, 1986. pp. 187-196

Pelczarski, Noel V. and Huston Dryver: Cure Monitoring of Composite Laminates Used in the Manufacturing of Snowboards. Proceedings of SPIE, Volume 3993, 2000. pp. 228-239

Schlaeger, Stefan: Laboratory Investigations; Development and application of Time-Domain-Reflectometry inversion algorithms for high resolutions moisture profile determination. Online: <http://www.uni-karlsruhe.de/~Stefan.Schlaeger/TDR/Applications/laboratory.htm>, [10/04/2001]

Stark, W. and Doering, J.: Monitoring of Curing Reaction of Polycondensating Thermosets at Press and Injection Moulding. Online: <http://www.ndt.net/article/ecndt98/material/141/141/htm>, [07/20/2001]

Steiner, Karl V. and Don, Roderic C.: Strategies for selection of sensor systems for on-line monitoring and control of the resin transfer molding process. 43rd International SAMPE Symposium, 1998. pp. 949-956

Ton-That, M.-T. et al.: Polyester Cure Monitoring by Means of Different Techniques. In: Polymer Composites, Volume 21, Number 4, 2000. pp. 605-617

IX REFERENCES

The list of references is divided into a list of references about cure monitoring (mainly referred to in chapter 3) and a list with all other references.

References about cure monitoring

Alig, I. et al.: Curing kinetics of phase separating thermosets studied by DSC, TMDSC and dielectric relaxation spectroscopy. In: Thermochimica Acta, 330, 1999. pp. 167-174

Bang, Kyung Geun et al.: Measurement of the degree of cure of glass fiber-epoxy composites using dielectrometry. In: Journal of Materials Processing Technology, 113, 2001. pp. 209-214
Available at <http://www.elsevier.com/locate/jmatprotec>

Bansevicius, R. and Dominauskas, A.: Magnetostrictive sensors with variable boundary conditions. In: Vibroengineering, 2000, No. 1 (2). pp. 7-9

Bartolomeo, P. et al.: Curing of cyanate ester resin: a novel approach based on FTIR spectroscopy and comparison with other techniques. In: European Polymer Journal, 37, 2001. pp. 659-670

Bartolomeo, P. et al.: On the use of WLF equation to study resin curing by dielectric spectroscopy. In: Polymer, 42, 2001. pp. 4385-4392
Available at <http://www.elsevier.nl/locate/polymer>

Bradley, J. E. et al.: On-line process monitoring and analysis of large thick-section composite parts utilizing smartweave in-situ sensing technology. 43rd International SAMPE Symposium, 1998. pp. 254-267

Carotenuto, G. et al.: FT-IR Device for on-line Monitoring of Cure Reactions under Pressure. In: Polymer News, Volume 25, 2000. pp. 172-175

Chailleux, Emmanuel et al.: A fiber-optic sensor for monitoring the polymer cure process. In: Proceedings of SPIE, Volume 4016, 2000. pp. 136-142

Chensha, Li et al.: Two Sorts of Fiber Optic Sensor Monitoring the Cure Process of Composite Laminate. In: High Technology Letters, Volume 6, Number 2, 2000. pp. 61-69

Cusano, Andre et al.: An optoelectronic sensor for cure monitoring in thermoset-based composites. In: Sensors and Actuators, 84, 2000. pp. 270-275
Available at <http://www.elsevier.nl/locate/sna>

Djordjevic, B. Boro and Milch, B.: In-situ ultrasonic cure monitoring sensors. In: 43rd International SAMPE Symposium, 1998. pp. 964-967

Dominauskas, Aurimas and Bansevicius, R.: Magnetostrictive Sensors for On-line Cure Monitoring of Thermosets. In: Mechanika, Number 6 (26), 2000.

Dominauskas, Aurimas and Bansevicius, R.: On-line Cure Monitoring with MCM Sensor and its Characterisation Using DSC and FOS Data. In: Mechanika, Number 5 (25), 2000.

Dominauskas, Aurimas et al.: TDR-line sensor for multifunctional and distributed sensing in LCM. Unpublished edition. Expected publication in: SAMPE Symposium proceedings May 2003, Long Beach, California.

Dominauskas, Aurimas: Spectral Analysis – Composites Cure Assessment Method. Report for INCO-COPERNICUS Project IC 15-CT 96-0727

Don, Roderic et al.: Large scale implementation of flow and cure sensing in a thermoset resin infused composite structure. 43rd International SAMPE Symposium, 1998. pp. 268-275

Dragasius E, Bansevicius R, Dominauskas A: Research and Development of Diagnostic Systems of Miniature Embedded Resonators and Ultrasonic. Translation from: Wave-Guides Schaffen und Forschung der Diagnostischen Systeme mit Hilfe der Implantierten Miniateurischen Resonatoren und Ultraschallwellenleiter. In: Workshop Mechatronik- 3, Brandenburg, 1998. pp. 145 – 150.

Dunkers, Joy P. et al.: A mid-infrared attenuated total internal reflection cure sensor for control of resin transfer moulding of a pre-ceramic polymer. In: Composites: Part A, 28A, 1997. pp.163-170

Dunkers, Joy P. et al.: Fiber optic flow and cure sensing for liquid composite molding. In: Optics and Lasers in Engineering, 35, 2001. pp. 91-104

Fomitchov, A. Pavel et al.: Distributed photoacoustic system for cure monitoring of composites. In: Advanced Nondestructive Evaluation for Structural and Biological Health Monitoring, Proceedings of SPIE, Volume 4335, 2001. pp. 323-329

Gillespie, John W.: Direct Current Flow and Cure Sensing. In: Composite Tech Brief, Number 106, Center for Composite Materials, University of Delaware, 1997.

Giordano, Michelle and Nicolais, Luigi: A Fiber Optic Thermoset Cure Monitoring Sensor. In: Polymer Composites, Volume 21, Number 4, 2000. pp. 523-530

Hager, Nathaniel et al.: Time-Domain-Refrectometry Cure Monitoring. 46th International SAMPE Symposium, 2001. pp. 2251-2263

Karkanas, Panagiotis I. and Partridge, Ivana K.: Cure Modeling and Monitoring of Epoxy/Amine Resin Systems. I. Cure Kinetics Modeling. In: Journal of Applied Polymer Science, Volume 77, 2000. pp. 1419-1431

Karkanas, Panagiotis I. and Partridge, Ivana K.: Cure Modeling and Monitoring of Epoxy/Amine Resin Systems. II. Network Formation and Chemoviscosity Modeling. In: Journal of Applied Polymer Science, Volume 77, 2000. pp. 2178-2188

Kim, Hyoung Geun and Lee, Dail Gil: Dielectric cure monitoring for glass/polyester prepreg composites. In: Composites Structures, 2002. pp. 1-9 Available at <http://www.elsevier.com/locate/compstruct>

Kim, Jin Soo and Lee, Dai Gil: Analysis of dielectric sensors for the cure monitoring of resin matrix composite materials. In: Sensors and Actuators B, 30, 1996. pp. 159-164

Kranbuehl, D. E. et al.: In situ Cure Monitoring for Quality and Process Control. In: ANTEC, 1991. pp. 941-945

Kranbuehl, D. et al.: On-line sin-situ control of the resin transfer molding process. 35th International SAMPE Symposium, 1990. pp. 825-834

Lee, C. William and Rice, Brian P.: Resin transfer molding process monitoring and control. 43rd International SAMPE Symposium, 1998. pp. 231-241

Li, Yan et al.: Monitoring the cure processes of polymer composites and neat resin using an ultrasonic wire waveguide technology. 43rd International SAMPE Symposium, 1998. pp. 937-949

Lin, Mark and Chang, Fu-Kuo: Composite Structures with Built-in Diagnostics. In: Materials Today, Volume 2, Issue 2, 1999. pp. 18-22

Maistros, George M. and Partridge, Ivana K.: Dielectric monitoring of cure in a commercial carbon-fibre composite. In: Composite Science and Technology, 53, 1995. pp. 355-359

Maistros, George M. and Partridge, Ivana K.: Monitoring autoclave cure in commercial carbon fibre/epoxy composites. In: Composites: Part B, 29B, 1998. pp. 245-250

McIlhagger, A. et al.: The development of a dielectric system for the on-line cure monitoring of the resin transfer moulding process. In: Composites: Part A, 31, 2000. pp. 1373-1381
Available at <http://www.elsevier.com/locate/compositesa>

Mijovic, Jovan and Andjelic, Sasa: A Study of Reaction Kinetics by Near Infrared Spectroscopy. 1. Comprehensive Analysis of a model Epoxy/Amine System. In: Macromolecules, 28, 1995. pp. 2787-2796

Murukeshan, V. M. et al.: Cure monitoring of smart composites using Fiber Bragg Grating based embedded sensors. In: Sensors and Actuators, 79, 2000. pp. 153-161
Available at <http://www.elsevier.nl/locate/sna>

Neckers, Douglas C.: The D.C. Neckers Research Program. Online: <http://www.bgsu.edu/departments/photochem/dcneckers/index.html>, [07/20/2001]

Osaka, Katsuhiko and Fukuda, Takehito: Strain monitoring in curing of composites using EFPI sensor. 44th International SAMPE Symposium, 1999. pp.1993-2004

Peinado, C. et al.: Solvatochromic and rigidochromic fluorescent probes based on D-π-A diaryl ethylene and butadiene derivatives for UV-curing monitoring. In: Polymer, 42, 2001. pp. 2815-2815
Available at <http://www.elsevier.nl/locate/polymer>

Perrissin-Fabert, Isabelle et al.: Nondestructive Evaluation of Materials Using an Inserted Piezoelectric Sensor – Correlation with Hardness Measurements. In: IEEE Transactions on Ultrasonics, Ferroelectrics, and Frequency Control, Volume 42, Number 4, 1995. pp. 641-647

Pethrick , Richard A.:Rheological Studies Using a Vibrating Probe Method. In: Collyer, A.A.: Techniques in Rheological Measurement. London, 1993.

Pucic, Irina and Ranogajec, Franjo: DC-electrical conductivity as a method for monitoring radian curing of unsaturated polyester resins. II. Influence of electrical field and dose rate. In: Radiation Physics and Chemistry, Volume 47, Number 6, 1996. pp. 821-825

Pucic, Irina and Ranogajec, Franjo: DC-electrical conductivity as a method for monitoring radian curing of unsaturated polyester resins. III. Evaluation of results. In: Radiation Physics and Chemistry, Volume 54, 1999. pp. 95-108

Rath, M. et al.: Process monitoring of moulding compounds by ultrasonic measurements in a compression mould, NDT&E International, 33, 2000. pp. 123-130
Available at <http://www.elsevier.com/locate/ndteint>

Rose, Hans: In-situ cure monitoring of epoxy resin using fiber optic raman spectroscopy (FORS). 43rd International SAMPE Symposium, 1998. pp. 277-286

Shepard, David D. and Smith, Kim R.: Ultrasonic cure monitoring of advanced composites. In: Sensor Review, Volume 19, Number 3, 1999, MCB University Press. pp. 187-191

Skordos, Alexandros A. et al.: A dialectric sensor for measuring flow in resin transfer moulding. Advanced Materials Department, Cranfield University, England, 2000.
Available at <http://www.flecher.lib.udel.edu>

Su, Hong B. et al.: Monitoring the process of curing of epoxy/graphite fiber composites with a recurrent neural network as a soft sensor. In: Engineering Applications of Artificial Intelligence, 11, 1998, pp. 293-306

Tabellout, M. et al.: The inserted piezoelectric sensor method for monitoring thermosets cure. In: The European Physical Journal Applied Physics, 13, 2001. pp. 107-113

Tayalia, Prakriti: Design and optimization of magnetostrictive sensor for strain monitoring. Master thesis at the Department of Materials Science and Engineering, University of Delaware, 2002.

Theriault, Richard P. et al.: The numerical determination of the TTT-Diagram for epoxy resins. 2nd AVK-TV Conference, Baden-Baden, 1999.

Tuegel, E. J. and Hahn, H.T.: Ultrasonic Cure Characterization of Epoxy Resins; Constitutive Modeling. In: Proceedings of the American Society for Composites; First Technical Conference, Dayton, Ohio, 1986. pp. 129-136

Twardowski, T. E. et al.: Curing in Composite Laminates; Thick Sections and Simulations. In: Proceedings of the American Society for Composites, Sixth Technical Conference, Albany, New York, 1991. pp. 154-163

Urabe, Kei et al.: Cure Monitoring of Matrix Resin with High Frequency Electromagnetic Wave Transmission Line. In: Journal of Reinforced Plastics and Composites, Volume 19, Number 15, 2000. pp.1235-1249

Winter, H.H. and Baumgaertel, M.: A Parsimonious Model for Viscoelastic Liquids and Solids. In: Collyer, A.A.: Techniques in Rheological Measurement. London, 1993.

Willoughby, B.G., Scott, K.W., Jones, S.A.: Understanding cure with the Scanning Vibrating Needle Curemeter; flexible and rigid foams. Rapra Technology Ltd. RTL/3027. Shawbury, UK, unknown date

Additional references

Abramov, O.V.: High-intensity ultrasonics – theory and industrial applications. Amsterdam, 1998

Ackermann, Anthony E., Chen, Liang, Rogers, Craig A.: Dynamic transduction characterization of magnetostrictive actuators. In: Smart Mater. Struct. 1996.

Angus, H.C., Neppiras, E.A.: Nickel-based magnetostrictive alloys for electromechanical transducers. In: Ultrasonics, July 1969.

Bright, Charlie: Better Sonar Driven by new Transducer Materials. In: Sea Technology Magazine, unknown date. Available at <http://www.etrema-usa.com>

Collins, T.H.: Analog Electronics Handbook. Hertfordshire, 1989.

Engdahl, Göran: Handbook of Giant Magnetostrictive Materials. San Diego, 2000

Frederick, Julian R.: Ultrasonic Engineering. New York, 1965

Loctite Datasheets: Loctite Hysol 00CL (05CL, 90CL, 120HP), available at <http://www.loctite.com>, Revision from July 2000.

Loctite European Group: Worldwide Design Handbook. Munich, 1998 (2nd edition), available at <http://www.loctite.com>

Simpson, Ed. J. A. and Weiner, E. S. C.: Oxford English Dictionary; 2nd ed. Oxford, 1989.

Vadel, Hardik: Magnetostrictive Sensor with variable boundary condition (VBC) for Rheological measurements of thermosets: Development and validation of the analytical model. Master thesis at the Department of

Materials Science and Engineering, New York State University, Buffalo, 2003.

White, James L.: Principles of Polymer Engineering Rheology. New York, 1938

X ACCOMPANYING FILE DOWNLOAD

Additional data can be downloaded from the following internet URL:

www.roida.de/science

Content:

- Technical drawings as *Autocad 2000* *.dwg* and *.wmf* files.
- Schematics as a *Protel 99SE* *.ddb* database file.
- *GERBER* files for the printed circuit board (PCB).
- *MATHEMATICA* files for *Wolfram Research MATHEMATICA 4.1* ("<*>" stands for the (latest) version number):
  - Sensor model: "Theoretical model 1 <*>.nb"
  - Inversion of the sensor model: "Reverse determination of Zc <*>.nb"
  - Case studies for the sensor model: "Optimization <*>.nb"
  - Contact impedance model (Gladwell): "Contact Impedance of curing polymers <*>.nb"
- Material data and experimental part data as *Microsoft Excel* files.
- Measurement data.